High Speed Volumetric SCAPE Imaging for Different Model Animals

Wenze Li

Submitted in partial fulfillment of the
requirements for the degree of
Doctor of Philosophy
in the Graduate School of Arts and Sciences

COLUMBIA UNIVERSITY

2019

ABSTRACT

High Speed Volumetric SCAPE Imaging for Different Model Animals

Wenze Li

It is a major challenge to understand functional neuronal circuits across the whole brain. Existing methods for observing neuronal activity represent a major bottleneck in addressing biological problems. In our lab, we developed Swept Confocally Aligned Planar Excitation (SCAPE) microscopy, which offers the ability to image a large 3D volume (e.g. 1000x800x250um) at speeds exceeding 10 volumes per second. Used with different genetically encoded fluorescent indicators, SCAPE enables us to observe neuronal activity across the whole brain of different small animal models, or a much larger volume of intact cortex/tissue compared to traditional approaches. The unique single objective design and flexible system layout of SCAPE makes it simple to image different samples without complex sample preparation and restraint.

During this thesis work, I collaborated with biology and neuroscience labs to develop and optimize a range of novel in-vivo/in-vitro neuroimaging applications using SCAPE microscopy. In particular, my research has focused on using SCAPE to image freely crawling *Drosophila Melanogaster* larvae, intact mouse olfactory epithelium, head fixed behaving adult *Drosophila*, larval zebrafish brain and beating heart, and the neuronal system of behaving *C. elegans*, all in collaboration with experts in these models from Columbia University and other research institutions. I also developed and optimized different sample preparations and experimental procedures to take full advantage of the high-speed 3D imaging capabilities and flexibility of SCAPE microscopy. Finally, I optimized computational and image analysis techniques for large

scale 5D SCAPE imaging datasets, including 3D cell tracking, large scale 3D data motion correction/registration, and cellular level neuronal activity extraction with different dimensionality reduction methods. The experiments I have performed in different animal models have enriched the long-term development of SCAPE by providing valuable feedback for system improvement and dissemination, and pushing the SCAPE design towards a more interchangeable platform with diverse capabilities suitable for routine uses by our collaborators and the wider neuroscience community.

Table of Contents

List of Figures

List of Tables

List of Movies

All movies uploaded as supplemental files for viewing.

Acknowledgement

I consider myself fortunate indeed to have many excellent mentors who inspired and encouraged me to learn and enjoy science and engineering. First and foremost, I would like to express my sincere gratitude to Dr. Elizabeth M. C. Hillman who gave me the opportunity to pursue my research work toward the PhD in her lab, as well as her insightful advice and marvelous support for my research. Her curiosity, obsessions and passions for science will constantly be guiding my future life path as a scientist and engineer. Secondly, I would like to thank Dr. Aurel A. Lazar as my advisor for the first three years and guided me into the neuroscience field. I also want to thank the members of my dissertation committee, Dr. Kenneth L. Shepard, Dr. Christine P. Hendon, Dr. Wesley B. Grueber and Dr. David Schoppik for their insightful expertise, which embellished and refined this dissertation.

I also would like to give many thanks to my colleagues and friends. Venkatakaushik Voleti, who has been my great research partner for the last four years. I learned from him not only about the numerous knowledge of optical design but also the fun part of collaboration. I also want to express my thanks to Citlali Perez-Campos, Hang Yu, Kripa Patel, Ying Ma and Mohammed Shaik and all the other member in the Laboratory of Functional Optical Imaging, who have helped and supported me during the past years.

More importantly, my family has been the strongest comfort to me. I would like to thank my parents for their understanding and unconditional support for my entire life. Finally, my greatest thank you goes to my beloved wife Lu Xu, who has given me unwavering support and a warm home and makes me become who I am now.

Chapter 1

INTRODUCTION

One ultimate goal for neuroscience is to understand how the human brain works. However, it has been a major challenge to understand functional neuronal circuits across the whole brain even in model animals with much smaller brains. The limitations of currently available techniques for observing neuronal activity represent a major bottleneck in addressing biological problems. Taking advantage of Swept Confocally Aligned Planar Excitation (SCAPE) microscopy, developed in our lab, we are now able to image a large 3D volume (e.g. 1000x800x250um) at speeds exceeding 10 volumes per second. Together with different genetically encoded fluorescent indicators, SCAPE enables us to observe cellular level neuronal activity across the whole brain of small animal models, or a much larger volume of intact cortex/tissue than traditional approaches. This thesis documents the progression of how we can use SCAPE to better understand neuronal circuits and is organized as follows:

Chapter 1 provides an introduction of the background and explains the motivation for studying specific model animals and using different approaches. It is followed by a brief introduction to SCAPE microscopy.

Chapter 2 discusses the challenges of, and our solutions to handling high dimensional volumetric data generated using SCAPE microscopy.

Chapter 3 presents the first collaborative work using SCAPE microscopy. Being able to image the freely behaving animals, we were able to understand and decode mechanisms of the *Drosophila* larva proprioceptive system.

Chapter 4 presents a second application of SCAPE microscopy. Taking advantage of the large field of view of volumetric imaging, we observed the non-linear modulatory effects of odor mixing, a crucial aspect of how our olfactory system senses the real world.

Chapter 5 presents a third collaborative application of SCAPE microscopy. By building odor delivery and behavioral monitoring systems for adult, head-fixed *Drosophila*, we were able to develop a new platform to image whole brain activity in the adult behaving *Drosophila*.

Chapter 6 presents new pilot experiments using SCAPE microscopy. We demonstrated the possibility of applying SCAPE microscopy to other model animals, opening up further new research fields.

In the last chapter, several directions for the further development and application of SCAPE are discussed.

1.1 From EE to Neuroscience

Being trained as an electrical engineer, I learned how to build an electronic circuit from different electrical components based on fundamental principles of the circuit and functional properties of the components. Given enough prior knowledge of the circuit principles and its components' model, we are then able to understand the functionality of the whole circuit. Today, with computer assisted design, we are able to build a processor with more than 20 billion transistors and understand its full capabilities. While the number of transistors is approaching the number of neurons we have in the human brain, how much do we really know about how our brain works?

Our brain works as a gigantic network and all ~86 billion neurons are interconnected directly or indirectly though ~1.5×10^{14} synapses. One way to understand a complex system is to dissect it into smaller functional circuit units, characterize the basic components, and then build up the knowledge step by step. However, this is not a trivial task, especially at the scale of the human brain.

Instead, working with model animals is a good alternative. Though we have significantly more neurons than our standard model animals, namely the mouse, zebrafish, fly and worm, many of our basic circuit units, particularly in the sensory system, share the same structure and functional model. This allows us to use these animals to dissect and understand the basic principles of the nervous system, which in turn could help us understand the human brain. Another advantage of working with model animals is that they can be genetically modified with modern genetic technology. As a result, we can manipulate specific experimental variables and test our hypotheses in a controlled way in animals of identical genetic backgrounds.

At the start of my Ph.D. training, I was interested in answering how we encode the complex world around us specifically through smell. It is known that in both insect and vertebrate, there are

only two synapses separation in the olfactory system between the primary sensory periphery to the brain areas for olfaction related memory formation and behavioral output[1]. Specifically, in the *Drosophila* olfactory system the anatomically structure is also very similar to vertebrate. In adult *Drosophila*, there are about 1300 olfactory receptor neurons(ORNs), each expressing one of the 62 odorant receptor exclusively in their antennae[2], which is similar to the sensory structure of the olfactory epithelium in mammals. Then, this sensory periphery input layer project to about 50 glomeruli in the antenna lobe in the fly brain, where the sensory information was integrated and processed with extra local neuron network before sending to the high brain region, which is also functionally and anatomically similar to the olfactory bulb in mammals. Then the projection neurons in the antenna lobe send axons either directly to the lateral horn or indirectly via the calyx of the mushroom bodies, where the higher level olfactory information processing, memory and decision making happen afterward. Again, this is similar to the higher level olfactory processing in mammalian brain. Together with the highly developed genetic tool available in *Drosophila*, it became a great animal model for us to understand the olfactory information processing in the brain. Much of the fundamental research in this field had been done[3, 4], and there was also a strong body of literature that established and solid experimental and theoretical resource available in Bionet Lab, where I started my Ph.D. training, for me to continue working on this field.

1.1.1 Electrophysiology

Following the basic principle of understanding an unknown circuit, it is essential to observe the input and output of the given system properly. Together with anatomic information, we might be able to construct a circuit model of the *Drosophila* olfactory system. My goal in the lab was to

record the neuronal activity in different layers of the fly olfactory system and try to understand and model the information flow of olfactory system in fruit flies.

The classical way of recording neuronal activity is through electrophysiology. To record the neuronal activity of the ORN in the sensillum, we used near field recording instead of patch clamp which is used to record the activity of the projection neurons in the antenna lobe. A sharp tungsten electrode was used as an extracellular probe to record the firing activity of the ORNs of the fly located in the antenna and a grounding reference electrode was inserted in the eye. Using customized spike sorting package developed by my colleague in Bionet lab, we were able to record and separate the neuronal spikes from different ORNs in the sensillum. To understand how single OSN encode the odor in the environment, we used custom built odor delivery system which allows us to deliver the odor at any arbitrary temporal concentration profile. By recording the neuronal spikes of the OSN, we were about to later use computation model, for example linear-nonlinear-Poisson cascade model (LNP model), to identify the computational model of ORNs. Also, I tried expressing ChR2, which is a blue light sensitive channelrhodopsin, in the specific ORN, Or59b here specifically, I could then use optogenetics to decouple this computation path way from the receptor ligand binding to better dissect the sensory functional. The electrophysiology recording results of comparing the light and real odor stimulus are shown in Figure 1. The results show that the ORNs encode both the odorant concentration and the change of the concentration. More specifically, the spiking rate of the ORNs is corresponding to the first order derivate of the odor concentration profile.

Loose patch was used to record the electrical activity of projection neurons (PN). PNs are organized into groups, where each group collects the sensory output of OSNs with the same receptor. In the experiment, we use the fly line with green fluorescent protein (GFP) expressing in

the targeting PNs, which helped us targeting the specific PN subset. While electrophysiology provides a nice, clear readout of the electrical signals of the neurons we record, its primary limitation is that the signal is restricted only to those specific neurons, where the number of the recorded neurons are normally very small limited by the spatial constrain of the recording method. Also, electrophysiology provides no or little spatial information, and it is very hard to discern interactions between different brain regions of a large population of neurons.

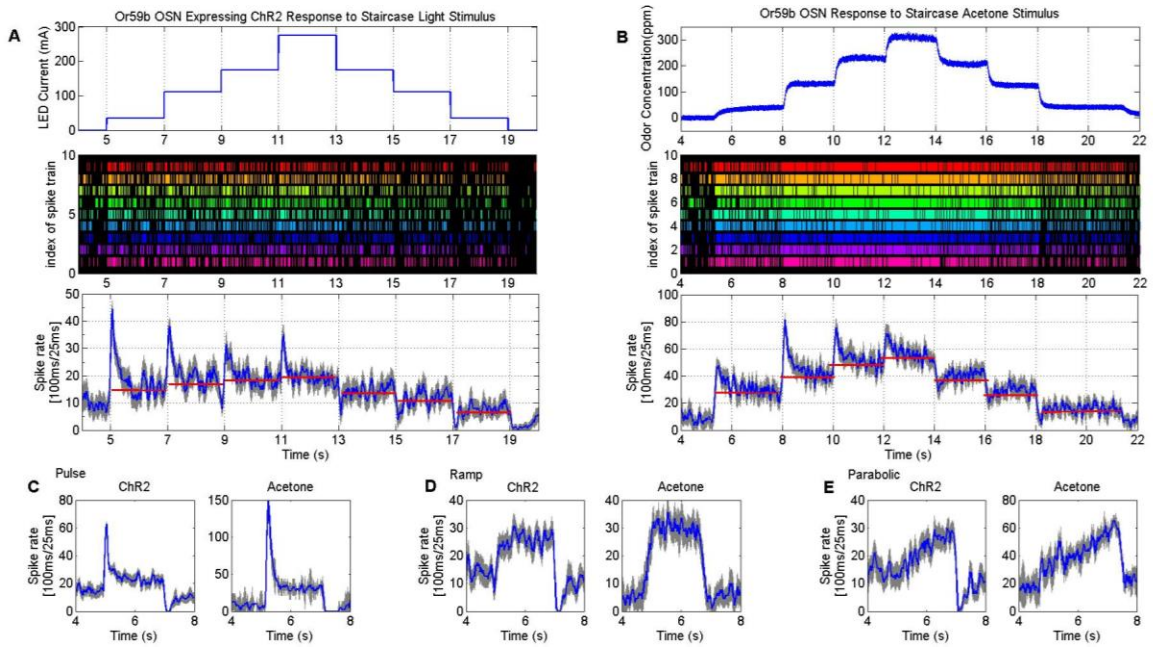

Figure 1 Electrophysiology Result of Or59b OSN Responding to Acetone and ChR2 Induced Stimulus. (A) Intensity profile of the blue LED used to excite the ChR2-expressing Or59b OSN, and the corresponding electrophysiology recording and the converted spiking rate. (B) Concentration profile of Acetone delivered to the fly and the corresponding electrophysiology recording and the converted spiking rate. (C, D, E) Responding spiking rates to differently shaped stimulus profiles.

1.1.2 Optical Recording Using Fluorescent Indicator

The main limitation of electrophysiology is the throughput of simultaneous recording. It is extremely difficult to record more than two neurons in the adult fly brain at one time due to spatial

constraints. Even with multi-electrode arrays, proper interpolation of the information is challenged by the array's poor spatial resolution and its relatively big size comparing with the size of small model animal like *Drosophila* and zebrafish. As a result, we then took an optical approach to image a larger portion of the neuronal circuit. With the development of new fluorescent calcium indicators, we were able to visualize calcium concentration dynamics at a cellular level of a much bigger number of neurons at the same time in a large imaging field of view. Intracellular calcium ion concentration is an important metric of neuronal activity, so by recording fluorescence signal strength, we had a proxy by which to indirectly measure firing activity of individual neuron. Using optical approaches, we can image hundreds of Kenyon cells(KCs) in the mushroom body of *Drosophila* brains, which can reveal the population coding mechanisms of the fly olfactory system in the higher brain level[5]. By observing a 2D imaging plane at a time, a much higher recording throughput could be achieved. More recently, with the development of fluorescent voltage indicators, we are now able to see membrane voltage changes via fluorescence, which could offer similar temporal information as electrophysiology while keeping the higher throughput feature of the imaging approach.

1.2 From 2D Image to 3D Volume

In order to fully take advantage of new fluorescent indicators labelling specific neuronal circuits or even the whole brain, we also needed better imaging techniques. The traditional fluorescent microscopy was optimized for 2D imaging. In order to acquire a 3D volume, a translation or piezo stage is needed to either move the sample or the objectives which restricts our observation of the neuronal circuit to one specific layer or at a lower temporal resolution. But even in model animals, the brain is not flat, the neuronal circuit and the brain in-vivo is always a three-dimensional

structure. So a 3D volumetric imaging system is necessary if we want to record neurons across multiple depths in the brain. Two main approaches have been developed recently to solve the 3D imaging challenge: high speed point scanning microscopy and light-sheet microscopy.

1.2.1 Point-Scanning Microscopy

Point-scanning microscopy techniques, such as confocal or two photon (2P), are done by scanning a small excitation point throughout a volume to form a 3D image[6]. During imaging, either the sample or the objective is moving, and the integration time for each point is very small (normally in μs-ns scale), which makes the fluorescence signal hard to detect. Laser power can be increased to get more signal, but the resulting photobleaching and photodamage is also a big obstacle for in-vivo imaging. Furthermore, the pixel rate of the point scanning method is also limited to the fluorescence lifetime and the laser pulse frequency if 2P excitation is used. Though the field of view is normally quite small in order to preserve the necessary temporal resolution for functional imaging, it is still quite useful for the smaller local circuit such as understanding the landmark orientation and angular path integration of *Drosophila* by imaging the ellipsoid body of a head-fixed walking *Drosophila*[7].

1.2.2 Light-sheet Microscopy

In light-sheet microscopy, a whole plane of the sample is excited instead of a single point and all pixels are exposed during the entire exposure time for each single plane. As a result, light-sheet microscopy images faster and tends to use much less power than point scanning. Previously, light-sheet microscopy is mostly used for embryo development in a slower time domain due to its slower scanning and imaging speed[8]. With the new optical geometry and imaging technology, it is

possible to use light-sheet to image functional dynamics of neuronal circuits. After deciding to switch to an optical approach to observe large scale neuronal activity, I started to build our own light-sheet microscope, based on the Open-SPIM platform[9] as shown in Figure 2.

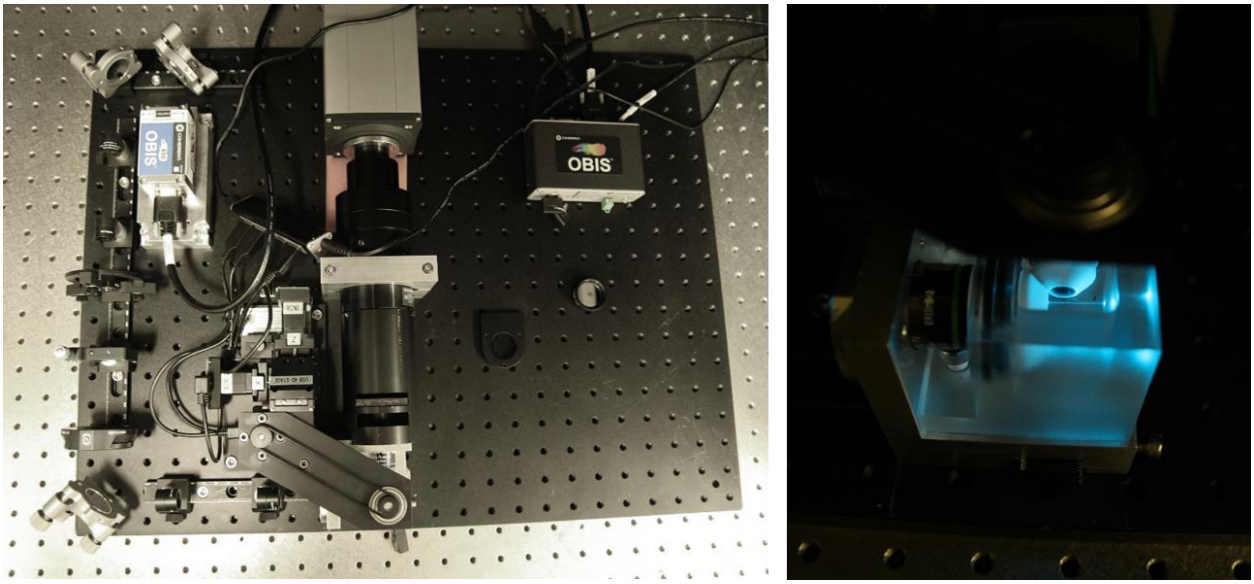

Figure 2 Home-built Open-SPIM based light-sheep microscopy and the sample chamber.

With this simple version of a light-sheet microscope, I was able to perform preliminary volumetric imaging for *Drosophila* larvae. However, speed was still a limitation because of how fast the sample stage could move relative to our scan rate. Furthermore, the need for a full immersion sample chamber, due to its traditional orthogonal objective light-sheet geometry, made it difficult to prepare the sample and impossible for some animals like adult *Drosophila* and mouse.

1.3 From SCAPE to the New Vision of Neuroscience

In 2015, I joined Dr. Hillman's lab, where SCAPE microscopy was being developed and its first demonstration had just been published[10]. We wanted to use this new volumetric imaging method to optically record a larger number of neurons at a high temporal resolution and to help

neuroscientists understand the nervous system in different model animals better with a new vision of volumetric imaging.

1.3.1 Introduction to SCAPE Microscopy

Swept, confocally-aligned planar excitation microscopy (SCAPE) is a high-speed fluorescence imaging technique capable of acquiring three-dimensional images of large fields of view (~0.5 – 1 mm) at rates exceeding 20 volumes/second[10]. By inserting a sheet of laser light off-axis on the back aperture of a high-NA objective lens, an angled sheet of laser excitation is produced within the sample. Fluorescence generated by this sheet within the sample is then collected by the same objective lens and then relayed onto a conjugate image plane, which is then imaged onto a camera chip as shown in Figure 3. By merging the excitation and detection pathways of the system through a single objective lens, SCAPE microscopy provides the benefits of lightsheet-based illumination strategies while maintaining a single objective layout similar to confocal or two-photon microscopy. This innovation addresses the versatility and access problem faced by most light-sheet microscopes. Over the past decade, there have been a number of other groups that have attempted to address this need for greater sample access via alternative single-objective light sheet microscope designs or by optimizing the optical geometry for sample mounting[11].

In its initial implementation, volumetric imaging on SCAPE was achieved by bi-directionally scanning laser light off of one facet of a 12-sided polygonal mirror, which in turn swept the oblique light sheet through the sample as shown in Figure 4a. Fluorescence generated by the sheet traveled back through the same optical path as the laser light and was then de-scanned off of an adjacent facet on the polygonal mirror. As a result, the intermediate image plane of fluorescence remained stationary even as the light sheet was rapidly swept through the sample. By

synchronizing the acquisition of the high-speed camera imaging the intermediate image plane to the polygonal mirror's motion, sequential frames capture planes in an oblique X-Z dimension as shown in Figure 4b. Reconstruction of a fully depth-resolved volume is as simple as reshaping the sequence of frames collected in the proper order as shown in Figure 4c. As a result, the potential volume rate of the system is equivalent to the line rate of the galvanometer. If the galvanometer scans at 10 Hz, the volume rate of the system is 10 volumes/sec. Because galvanometers can scan at kilohertz rates, SCAPE microscopy can theoretically acquire at thousands of volumes per second without bottlenecks stemming from opto-mechanical limitations in system design. Currently, camera frame rates are the main bottleneck to acquisition speed.

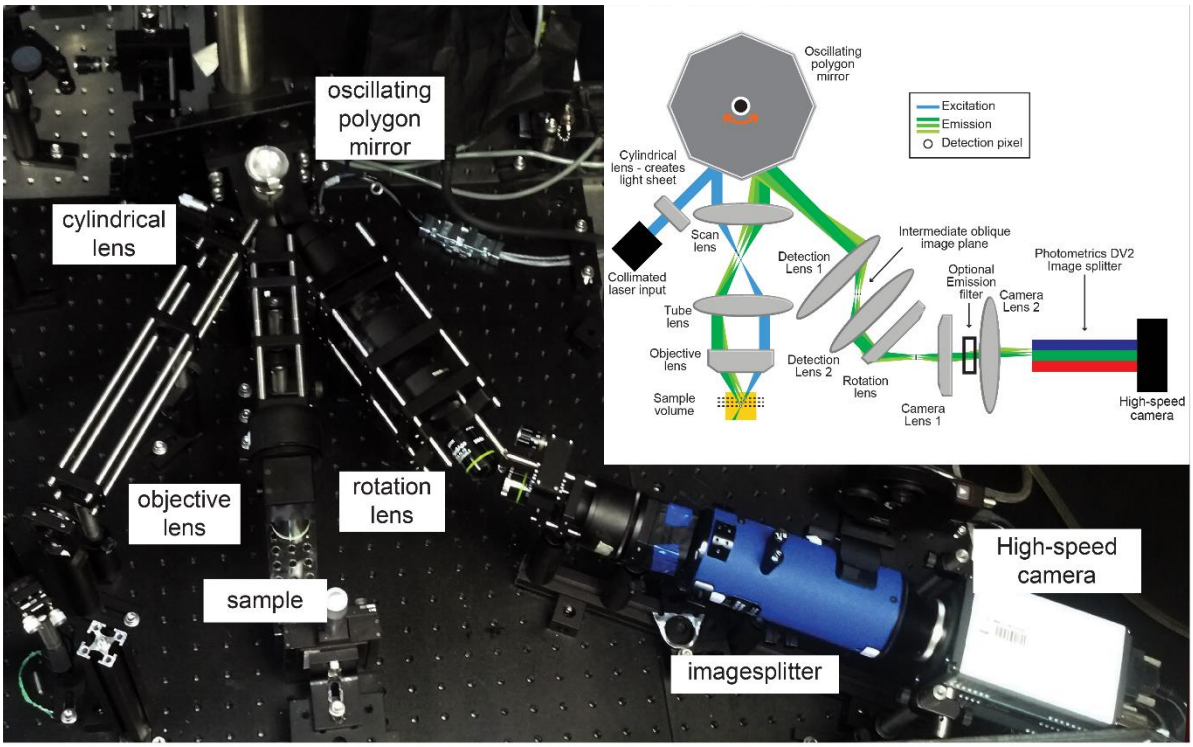

Figure 3 First Generation SCAPE System. System utilized a bi-directionally scanning 12-sided polygonal mirror mounted on a single-axis galvo mirror (6240H, Cambridge Technology), a high-speed sCMOS camera (Zyla 5.5, Andor) and a dual-channel image splitter (DV2, Photometrics). The inset shows a schematic of the system including the locations of conjugate image planes and the directionality of the excitation/detection pathways.

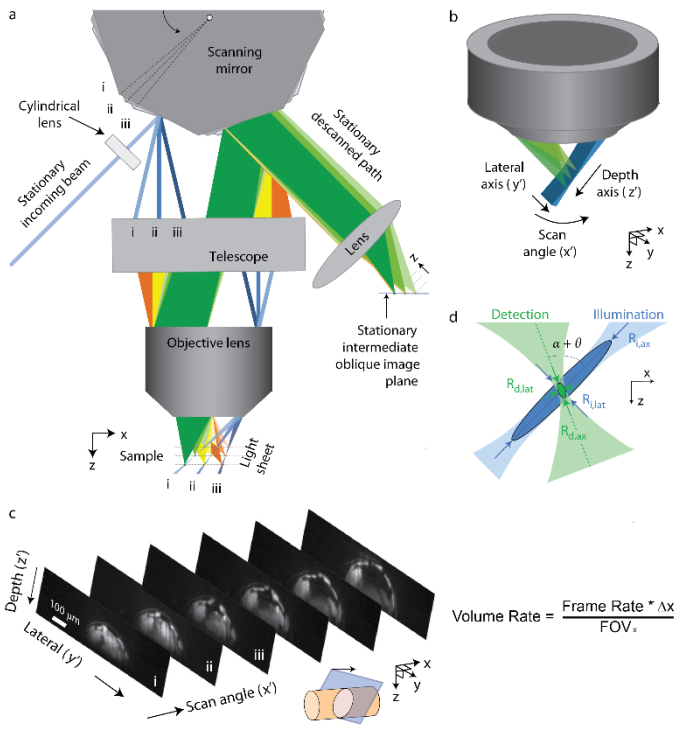

Figure 4 Schematic of SCAPE1 image acquisition paradigm. a. Polygonal scanning results in scanning of excitation and de-scanning of fluorescence similar to confocal microscopy. In SCAPE, the entire plane of the light sheet is de-scanned instead of a single point b. Imaging geometry of SCAPE establishing the scan (X), lateral (Y) and depth (z) dimensions c. Individual frames acquired by camera are reshaped into a volume. The equation shows the relationship between volume rate, frame rate, the field of view in the scanning direction (FOVx) and the step size between adjacent planes in the scanning direction (Δx) d. Resolution of SCAPE is a combination of the detection numerical aperture, the illumination numerical aperture and the crossing angle between the two within the sample.

SCAPE microscopy uses a high-speed, high-sensitivity scientific CMOS (sCMOS) camera for its acquisitions. The sheet dimension that encodes depth into the sample (Z) corresponds to rows on the camera while the length of the sheet (Y) corresponds to columns. Commercially available sCMOS cameras (Andor Zyla, PCO Edge, Hamamatsu Flash) achieve their high framerates via a rolling shutter coupled with an "overlap read-out" exposure. This means that each frame acquisition begins by exposing the rows in the center of the camera chip, followed by the

rows adjacent and so on until the outer-most rows have finished exposing. Acquiring fewer rows or depths on the camera allows one to acquire at higher frame rates. No data reconstruction or pre-processing is needed to preview the 3D volume, all the image frames are sequentially loaded into the 3D stack series.

1.3.2 Evolution of SCAPE Microscopy

The first generation SCAPE system published by the Hillman lab[10] served as a proof-of-principle for the potential applications of high-speed light-sheet based illumination strategies for addressing imaging challenges faced by the neuroscience community. Its single objectives layout allowed access to a wider variety of samples of samples than conventional light sheet microscopes, while the confocal scanning-descanning paradigm elegantly addressed bottlenecks in volumetric imaging speed faced by systems reliant on point or piezo-scanning.

However, a number of important optical design challenges needed to be solved before SCAPE was able to image dense volumes of tissue with the spatiotemporal resolutions necessary to resolve single-cell activity. The first step was to look for an alternative solution to the polygonal scanning mirror, which introduced extra complexity by needing 3 co-aligned optical telescopes. The final solution was a single planar mirror driven by a galvo, which served as the new scan engine. The scan and de-scan telescopes were then oriented at 90 degrees from one another. The new optical layout is shown in Figure 5. The next step was to replace one of the cylindrical lenses with a Powell lense, and replace the second and third objectives with higher NA models. Finally, the camera telescope was redesigned with a new dual-color splitter. We then standardized the newer generation SCAPE design, which offers better uniformity of the illumination profile, better resolution across a bigger field of view, and better light collection efficiency. After testing the

system with fluorescent beads and different biological samples, SCAPE became a valuable tool for imaging large scale neuronal activity with high spatial and temporal resolution.

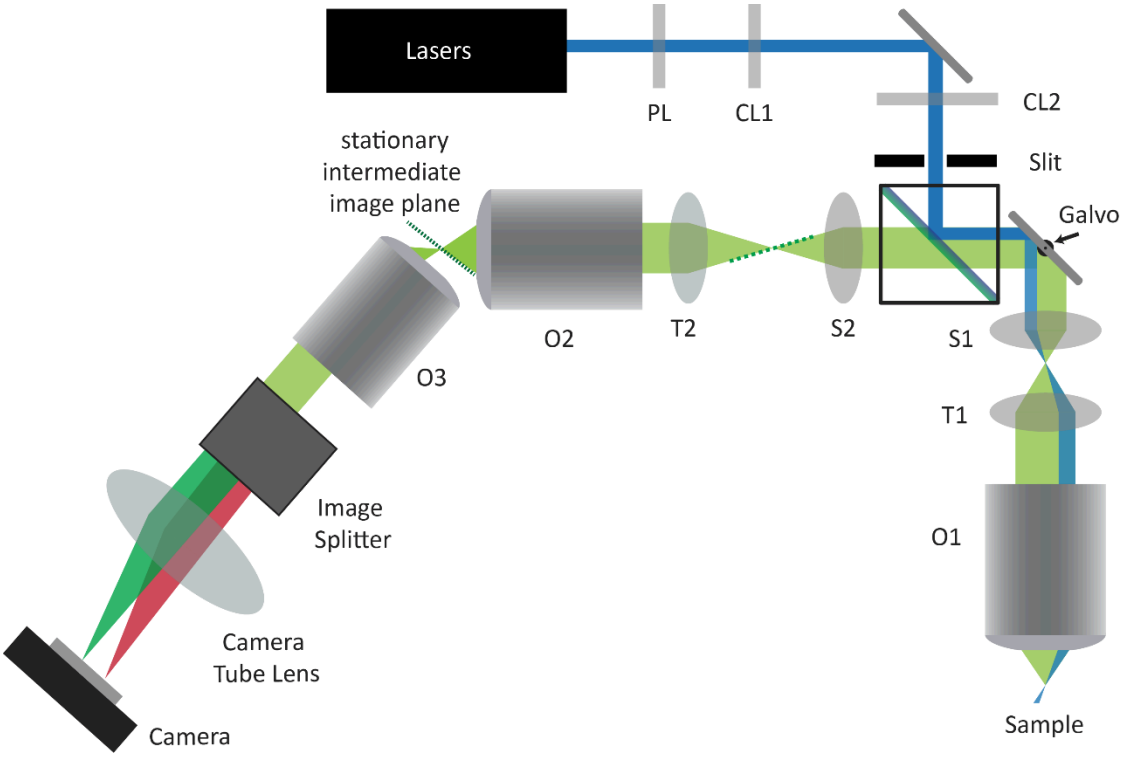

Figure 5 Schematic of The newer generation of SCAPE system. The system is designed in long-pass configuration around a dichroic and galvo mirror. Note the existence of four distinct telescopes. The scan telescope consists of a scan lens (S1), tube lens (T1) and the first objective lens (O1). The de-scan telescope consists of a scan lens (S2), tube lens (T2) and the second objective lens (O2). The camera telescope consists of the third objective lens (O3), a camera tube lens (T3), an optional image splitter and the camera. Finally, the beam shaping optics consist of a series of cylindrical lenses (CL1…4) and a sliding mirror mount. The blue lines represent the excitation pathway from the laser to the sample. The green lines represent the detection pathway of the fluorescence from the sample to the camera.

Chapter 2

ACQUIRING AND HANDLING BIG DATA

From electrophysiology to 2D imaging, to 3D imaging, then to high-speed 3D imaging using SCAPE microscopy, every step brings us a broader view of the fantastic neuroscience world, while at the same time, the data we record dramatically increases with this information explosion. How can we properly understand what we see, what we record, and how can we use this information to decode the brain. The conventional ways to record, store and process data are no longer sufficient for dealing with big data at the TB level. During the past 4 years working with SCAPE microscopy, I have acquired hundreds of TB of data. Handling this data has become a major part of my research work and for different projects and experiments, we need different specific data analysis pipelines. However, how to smoothly get the data from the camera down to the end user, like me and our collaborators, is also an important part of the full imaging system besides the stable optical design. In the past few years, I've worked on building a basic big data pipeline for SCAPE microscopy that will help to bridge this gap between hardware and end user.

2.1 Setup of the Imaging Acquisition System

The first challenge that we encountered was how to smoothly stream images from the camera to the imaging workstation. This is the very first step of the imaging acquisition pipeline and it is not a trivial problem. One of the biggest performance bottlenecks for SCAPE microscopy is the pixel rate of the camera. In our standard SCAPE configuration, we are using the latest sCMOS camera which offers a max 400MHz pixel rate with 16bit pixel depth when using the full width of the camera chip for dual color volumetric imaging. As a result of such a high pixel rate, the maximum data rate of the camera goes up to 800MB/s. Although in a standard experiment, the pixel rate we used for a slightly cropped field of view is about 300MHz for dual color and 160MHz for mono color, this still leads to a data rate of about 600MB/s and 320MB/s, respectively. At this rate, an hour long SCAPE imaging session will have a size of about 2TB for dual color and 1TB for single color, which already requires a special design of the imaging acquisition system.

2.1.1. Setup the Standard Imaging Acquisition Workstation

When we first purchased the sCMOS camera, it arrived with a dedicated high performance imaging workstation, a Dell T7910XL workstation with 1 TB SSD in RAID0 and 32GB RAM. The storage configuration in this system is 4×256GB SATA SSD configured in RAID0 mode which offers more than 850MB/s continuous write speed. This configuration was sufficient for the requirement of the camera running at full speed when it came. However, the speed drop of the SSD drives during daily usage and the potential data writing latency for a RAID volume was not taken into consideration for the initial build of the workstation, especially when the RAID controller used in the system was also a low-end OEM model without onboard cache which could help buffering the input data stream when the drives are handling unexpected data write latency. For these reasons,

during the early stages of SCAPE development and experiments, the data spooling process using the camera recording software was occasionally terminated due to the disk write speed drop during the acquisition and we had to transfer the data out of the SSD raid volume to external USB3 hard drive. The speed drops just became a bigger problem when the SSD volume was close to full. Another issue for this workstation was that the relatively small amount of RAM capacity made it really hard to preview and process the data locally since one-minute of dual color data would exceed the system memory limit. We had to transfer the data to our server and perform the data analysis remotely through Ethernet connections, which did not take advantage of the direct 3D imaging feature for fast data preview after the imaging session without computational reconstruction.

The first challenge I got when I join the lab is to custom build a high-performance imaging acquisition system to address the SCAPE data streaming and preview issue. The ability to preview and check the imaging data during the experiment allows us to optimize acquisition parameters for the later trials with minimum sample exposure, which also helps avoid photobleaching or habituation when we have external stimulus associated with the experiment. Another goal was to have much less system dead-time with sufficient local storage such that no data transfer is necessary during the actual experiment.

When I started configuring the workstation, I considered the following performance metrics:

- CPU: enough PCIe bus lanes for add-on cards including frame grabber for the camera and analog/digital data acquisition card for SCAPE hardware control; registered RAM supported for big RAM capability; high CPU frequency for better computational

performance and data handling; relatively high CPU core number for parallelized data analysis algorithms.

- RAM: registered RAM preferred; large enough to load and process SCAPE imaging data right after every imaging session.
- Motherboard: enough PCIe bus lanes and slots for all the necessary PCIe based add-on cards; enough memory slots for the initial RAM installation and potential upgrade in the future; dual CPUs supports for better performance and expansion capability.
- Network interface: 10Gb Ethernet interface preferred for fast data transfer to the server.
- Storage: two tires structure with one ultra-fast SSD based volume with at least 2TB for the full speed dual color imaging data spooling for a least an hour and one fast HDD based volume with at least 30TB for single color imaging and local data storage.

To meet the requirements above, we initially considered purchasing the computer from an OEM manufacturer for better hardware warranty and support. However, the regular desktop workstation does not meet all the requirements we needed, especially for the 2 tiers storage system, while the only option is to purchase a tower server instead which is very noisy and expensive. Then, I turned to configure and assemble the computer from scratch by myself. For stability reasons, we chose all the components as enterprise/server grade which supports 7×24h running and has a long warranty period. I built the first custom built SCAPE imaging acquisition workstation with the specifications listed in Table 1.

During the stress test of the new workstation, we were able to achieve about 1.4GB/s second continuous write speed for the 2TB SSD volume which is sufficient for the full speed data spooling of the camera until the whole volume is full, while the 35TB RAID5 HDD volume offers about 700MB/s continuous write speed which is also enough for single color SCAPE imaging for

days. The data transfer speed between SSD and HDD volume also reached about 700MB/s, which allowed us to transfer all the data from the SSD volume to the HDD volume in less than 40 minutes. This workstation was also equipped with a high-end graphic card which offered great 3D rendering performance when using 3D visualization software such as Amira.

Parts	Model
CPU	2×Intel Xeon E5-2630 v3, 8 cores, 2.4GHz, 40×PCIe lanes
RAM	8×16GB DDR4-2133
Motherboard	Supermicro X10DAI, 2 CPU sockets, 16 RAM slots, 6 PCIe slots
Network AOC	Intel X540-T2, 2×10 Gigabit Ethernet port, RJ45 interface
SSD	1×Intel 730 Series 480GB, 4×Cruicial MX200 500GB
HDD	8×Seagate Enterprise NAS 5TB Hard Drive
Raid Controller	Areca ARC-1882IX-12, 4GB onboard RAM
Case	Lian Li PC-A75X, 12 hard drive bays
Graphic Card	Nvidia GeForce GTX980

Table 1 System Specification of SCAPE Imaging Acquistion Workstation GEN. 1

After using this system for SCAPE development and some pilot experiments, some issues with the system were found. First, the 128GB memory is good enough for data preview of even long-term imaging data, however, when processing the data with more sophisticated imaging

analysis algorithms that require parallelization, more memory is needed. We then upgraded the memory to 192GB which is the limit for Windows 7 operating system. Second, the SSD volume was set to be RAID0 which sacrificed the reliability to achieve greater write performance. The RAID volume fail did happen once because one of the SSDs was defective, which lost about 600GB of imaging data. After that, I turned to a more expensive but more reliable solution. The high-end data center level PCIe based SSD drive was used in the system instead, which is not RAIDed but still offered about 1.5GB/s read/write speed. After that this workstation has been working without any issue for the past 4 year almost 7×24h.

During this time, I also worked very closely with Andor, the manufacturer of the Zyla (5.5 / 4.2 / 4.2 PLUS) sCMOS camera to debug and improve the data acquisition software, Solis, which is now relatively stable for full speed image spooling.

Based on the experience of the first fully custom-built imaging workstation, I designed and built a better and more stable version of imaging workstations. Since then I have built 5 more SCAPE imaging workstations with different upgrades and with the latest high-performance hardware and taking into account the extra need for storage. The detailed specifications of each system are listed in Appendix A.1. For the latest generation of the workstation, we needed to meet an even higher data spooling speed. The latest high speed camera we purchased requires a continuous write speed of about 2.1GB/s to the disk, while our old PCIe based SSD solution was no longer sufficient and we would regularly suffer constant frame drops, even though the latest model could achieve a burst write speed of about 3GB/s. Taking advantage of the latest SSD storage technology, I found a new solution that worked very well with the new camera without any frame drops and that allows for hours long imaging acquisition.

The new SSD volume for the new high-speed camera data spooling still used RAID0 mode as the first generation SCAPE workstation. However, instead of using the regular SATA interfaced SSD, we used the new NVMe M.2 interfaced SSD. The new SSD interface is based on PCIe x4 link. When using the high end NVMe M.2 interface model alone, we could achieve about 3.5GB/s burst write speed and more than 2GB/s for heavy load data streaming. However, the frame drop still happened constantly. And to raid the M.2 interface drive properly without performance drop and inducing extra I/O latency, I used a HighPoint SSD7101A-1 RAID controller, which has an onboard PLX chip which split the regular 16x PCIe slot into 4 PCIe x4 NVMe M.2 slots. In this case, we are able to configure a 4×1TB NVMe M.2 SSD RAID0 volume with 4TB capacity and continuous write speed of more than 10GB/s, which allows us to spool the new camera data for about an hour. At the meantime, after upgrade the operation system of the software platform from Windows 7 to Windows 10, we were able to install more memory in the system to preview the data generated by the new camera easily.

2.1.2 Setup the Mobile Workstation for SCAPE-in-Suitcase

With the further development of SCAPE microscopy and the increasing need to transport the system to different labs and institutions around the world, we developed a mobile version of SCAPE microscopy. We are now able to fit all the SCAPE parts in a suitcase and then assemble the full system wherever there is an air table. However, traveling with a heavy desktop workstation with a lot of HDDs is not feasible. So, we decided to configure a mobile workstation which could run smoothly with the regular SCAPE system with the sCMOS camera running at full speed.

Thanks to the development of computer technology for mobile workstations, we are now able to install 3 NVMe M.2 SSD in a single laptop and have two of them configured a 2 1TB SSD

RAID0 volume for direct data spooling and use the other one as operation system and software installation. We were also able to replace our traditional PCIe base analog/digital data acquisition card with a USB based module, which could be used to control the galvo mirror and the camera trigger and firing signal while the filter wheel and the laser interact with the computer via a USB interface. The biggest challenge was to properly connect the sCMOS camera to the laptop through the PCIe interfaced frame grabber, since the USB3 interfaced camera is not fast enough for SCAPE to run at full speed.

With a lot of research and working closely with the camera manufacturer, we decided to use the latest Thunderbolt 3 based PCIe expansion enclosure with the new version of frame grabber which offered driver support for the Thunderbolt 3 protocol. In the system configuration, the new frame grabber (Axion-CL, BitFlow) is installed in a 1-slot full speed 16x PCIe to Thunderbolt 3 expansion enclosure (Echo Express SE I, Sonnet) and the camera is able to run without issue under stress test for continuous imaging spooling for over 20 minutes. The main specifications of the mobile workstation are listed in Table 2. In this configuration, there is no extra HDD volume for extra data storage, but we can still use the Thunderbolt 3 interface to connect an external RAID enclosure for the second tier storage when needed. The overall memory in the system is only 64GB, but it is enough for quick preview of the acquired data and entry level data process for demo purpose. Lastly, a high-end graphic card is configured in the system for 3D visualization purposes.

OEM Model	DELL Precision 7720
CPU	Xeon E3-1535M v6, quad cores, 3.1GHz, Thunderbolt 3 support
RAM	4×16GB 2400MHz DDR4 ECC SDRAM

SSD	2×1TB M.2 PCIe SSD, 1×512GB SSD
Graphic Card	Nvidia Quadro P5000, 16GB GDDR5

Table 2 System Specification of Mobile SCAPE Imaging Acquistion Workstation

2.2 Setup of the Big Data Processing and Storage

The second challenge we faced in the imaging data processing pipeline is data storage and analysis. As mentioned, the requirement for data storage and computation power for the imaging processing is increasing dramatically. We could easily take 2TB of data with one SCAPE microscopy system in a day, and sometimes a few TB a day when running long term recording or full series of stimuli protocol. Furthermore, we now have an increasing number of different SCAPE microscopies in our lab, which are also running at the same time. In this case, we decided to use a third tier storage into the SCAPE imaging pipeline which is network attached storage (NAS) and could be accessed by all the SCAPE imaging acquisition workstation as well the servers.

Here, we used the Synology enterprise solution as our NAS solution. The first NAS I configured was Synology DS3615xs NAS unit plus a DX1251 expansion unit, which offered 24×3.5-inch hard drive bays in total. We used 12×Seagate enterprise 5TB NAS drive in each unit and configured a 50TB RAID6 volume in each unit, which offered a 100TB storage space in total and 4 drive fail redundancy for RAID data protection. The NAS was interfaced with all the SCAPE imaging acquisition workstation and the imaging analysis server we have with 10 Gigabit Ethernet, which allowed a network data transfer speed of 800MB/s for data backup and remote access through the imaging workstation and the server simultaneously.

The second NAS I built when the first one is full is also a Synology enterprise system, but it is rack-mountable, which could be installed in the server room with extra cooling and power failure protection. The new storage system was Synology RS3617xs+ NAS unit plus a RX1217 expansion unit, which also offered 24×3.5-inch hard drive bays in total. Here, we used 12×Seagate enterprise 10TB NAS drive in each unit and configured a 100TB RAID6 volume in each unit, which offered a 200TB storage space in total and 4 drive fail redundancy for RAID data protection. This NAS equipped with 10 Gigabit Ethernet with fiber interface, which could be directly connected to the high speed local network in the server room, which offers a high speed data access from all the computers in our institute and also helps us share the data with our cooperator within Columbia.

In addition to the two NAS, there is also a huge need for a high-end server to handle the larger scale data, especially for the new high-speed camera we purchased recently, the size of the imaging data increase from 36GB/min up to 120GB/min. An even larger RAM capacity is needed in the server to analysis this type of data. So, I also configured a high performance data analysis and storage server for the lab last year to meet the requirement of analysis this new type of SCAPE data and also expand our data storage further more.

Working with DELL EMC team, we ended up with a DELL rack-mount server plus a separate storage unit. The main specification for the server is listed in Table 3.

OEM Model	DELL PowerEdge T640
CPU	2×Xeon Gold 6126, 12 cores, 2.6GHz, Thunderbolt 3 support
RAM	12×32GB 2666MHz DDR4 ECC RDIMM

SSD	2×480GB SATA SSD, 1×1.6TB NVMe PCIe SSD
HDD	16×10TB STAT Hard Drive
Raid Controller	PERC H730P+, internal, 2GB; PERC H840, external, 8GB
Network	Onboard 10GbE

Table 3 System Specification of Imaging Analysis and Storage Server.

The server was configured with 24 CPU cores (two CPU, 12 cores each), which is optimal for multi-user application with virtual remote desktops. And an ultra-fast PCIe interfaced NVMe SSD was installed and configured as high speed swap space in the operation system(Redhat 7.6), which makes it possible to handling data even bigger than the RAM capacity (384GB). The HDD storage system in the server was also configured as RAID 6 mode for data protection, which offered 140TB storage. The server could also be upgraded in the future with more memory capacity with half memory slot empty and a delicate GPU could be installed for potential computation need.

The expansion unit we used here is DELL Storage MD 1400 which was equipped with 12×10TB hard drives and configured as RAID6 as well and offered a 100TB volume. This unit is connected to the external raid controller in server directly through mini-SAS HD interface, which offers the same I/O performance as the internal storage unit and could also expanded in the future when more storage is needed.

2.3 Data Analysis Challenge and Imaging Optimization

After we successfully acquire SCAPE data, the next big challenge is handling the big data. Unlike traditional 2D imaging data analysis, analyzing 3D volumetric data generated by SCAPE

microscopy requires 10-100 times more memory and as much time to run the analysis algorithm itself. We have to develop new algorithms and data analysis pipelines which either parallelizes the processing to speed up the analysis or perform dimensionality reduction to reduce the actual size of the datasets we analyze. During the past few years working on different projects, we developed different data analysis pipeline for different model animals and problem sets. Working together with the colleagues in our lab as well as our collaborators, we have standardized some analysis procedures for data pre-processing including data conversion, background subtraction, de-noising, dual-color registration, volumetric imaging de-skewing etc., which makes it easier for us and our collaborators to visualize and analysis the SCAPE data. We are also working closely with a few labs and research institutes to developed different data processing methods and more generalized data processing pipelines.

Another big difference of the SCAPE imaging data is that every single time point acquired is full 3D volume, which is great from data analysis point since we get a more detailed information of the sample in 3D space, but it also makes it much harder to visualize than a regular 2D data set. To render our 3D volumetric time series, we tried commercially available 3D visualization software packages, however, this was also quite challenging because many software packages lacked analytical tools for functional image analysis in high-speed sequential volumes. We have worked closely with several developers for better processing algorithms to visualize 3D functional data.

On the other hand, optimizing the SCAPE experiment itself is crucial to achieve the best spatial and temporal resolution for the sample, use the least amount of resources and minimize the unused pixels in our acquired 3D volume. For SCAPE imaging, we have the temporal and spatial resolution as the following equations:

$$Volume\ Rate = \frac{Frame\ Rate}{Frame\ per\ Volume}$$

$$Scanning\ Step\ Size = \frac{Scanning\ Field\ of\ View}{Frame\ per\ Volume}$$

The camera frame rate is determined by the camera itself, for the regular sCMOS camera we used, it only depends on the number of rows used on the camera chip, which corresponds to the depth of the acquired volume. For other high-speed CMOS cameras, frame rate is determined by both the number of rows and columns of the image. When working with sCMOS cameras, the gold standard is to use as few rows as possible to achieve the highest camera frame rate (at the reasonable photon budget) which helps improves both spatial and temporal resolution. We can achieve the minimum imaging depth by properly positioning the sample. In some case where photobleaching is a limiting factor and a small laser power is required in the experiment, we might have to sacrificed the imaging speed for a better pixel integration time, but it is still better to use less rows to eliminate the unused dark pixels within the imaged volume to minimize the data rate. Meanwhile, the scanning field of view is also determined by how we positioned the sample. It is important to design a proper sample mount/chamber for every sample and also leave extra degrees of freedom to adjust the sample mount to minimize the imaging volumes and achieve the best spatial and temporal resolution.

Chapter 3

IMAGING AND CHARACTERIZING THE PROPRIOCEPTIVE SYSTEM OF BEHAVING DROSOPHILA LARVAE USING SCAPE

Proprioception is the sense of the relative position of one's own body position which is essential for coordinated movement. The proprioceptive sense is built from activity of distinct types of sensory receptors that differ in the specific targeting of sensory endings. The proprioceptive sensing of the position of rigid joints has been described in detail in several systems, however, it is still not known how animals with an elastic skeleton, like worm, encode their body positions and movements. To understand how the proprioceptive system in these animals, we would need a way to observe and measure the structural and functional dynamics of the corresponding proprioceptive neurons in vivo during animal's natural movement. In the past 4 years, I was working with Dr. Wesley Grueber and his PhD student Rebecca Vaadia to develop an imaging paradigm, which took advantage of the high speed volumetric fluorescent imaging using SCAPE microscopy and became the key for us to understand this question. The results of this study were published in [12].

3.1 Introduction to Proprioceptive System of Drosophila Larva

To understand how the proprioceptive sensory activity contributes to the coordinated movement, it is important to reliably monitor the neural activity of the proprioceptive neurons in freely behaving animals. Small invertebrate model systems with an elastic skeleton, well-described sensory systems and complete or near-complete connectomes, such as *C. elegans* and *Drosophila* larvae, are ideal systems in which to uncover fundamental principles of sensorimotor integration. Here, we choose *Drosophila* larvae as our model system which is relatively big and easier to handle and also optically easier to access due to the size and the spiking feature of its proprioceptive neurons. Regular light sheet, confocal, and two-photon microscopy can capture neuronal calcium activity in isolated *Drosophila* brains or immobilized preparations [13-17]. However, none of these methods are able to offer enough volumetric imaging speed with a big enough field of view to observe the body-wide or large proportion of the proprioceptive neural activity across the body in unrestrained or nearly freely behaving larvae.

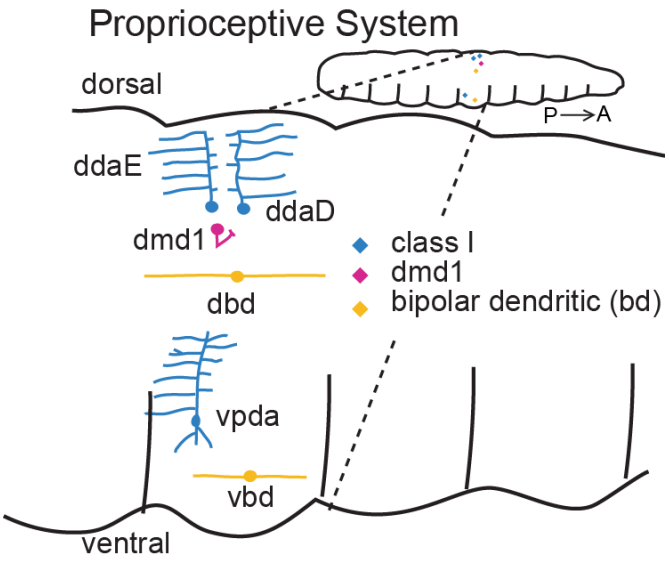

Figure 6 Schematic of the larval proprioceptive system.

SCAPE microscopy is capable of characterizing tissue and cellular dynamics in live behaving animals. Here we used it to characterize the structural and functional dynamics of proprioceptive neuron in freely crawling *Drosophila* larvae. In this study, we focused on multidendritic(md) neurons. They are located just under the larval body wall and extend sensory dendrites along internal structures and the epidermis [18, 19], which are also easily accessible using SCAPE microscopy. A subset of six of these md neurons (Figure 6), extend axons to more dorsal neuropil regions in the ventral nerve cord (VNC) which is important for motor control, suggesting that they are proprioceptors that provide feedback on body position [20, 21]. They are classI neuron: ddaD, ddaE and vpda; bipolar dendritic neuron: dbd and vbd; and another multidendritic neuron: dmd1. This feedback pathway from the body wall region is believed to be particularly important for larvae movement, especially during crawling turning and head exploration [22]. However, as mentioned earlier, studying the structural and function dynamics of these sensory neurons have been limited to dissected preparations due to the speed and field of view limit of the moving larvae. Imaging of axon terminals of these neurons in the isolated central nervous system (CNS) shows that at least some of these neurons are active during muscle contraction [23, 24], while other electrophysiology study has shown activity in one cell type in response to stretch in a dissected preparation [24]. Behavioral studies shown that the crawling behavior was significantly slowed when genetically disabled all or a subset of these six neurons, which suggest that these neurons are proprioceptors that might provide a segment contraction "mission accomplished" feedback signal that promotes progression of the peristaltic wave during the crawling behavior [25]. We were wondering whether these neurons with diverse dendrite morphologies and body wall coverage have redundant functions during crawling behavior or they might have different function in the feedback pathway and reflect different body postures. To

characterize each cell, we would need a reliable measurement of both dendritic dynamic and somatic functional dynamic patterns during natural movement of *Drosophila* larvae, which would further help understanding the synergies and dynamic encoding properties of the larval proprioceptive circuit.

3.2 Experiment Design and Setup for Freely Behaving Drosophila Larva

3.2.1 Experimental Animal and Subject Details

To characterize the spatiotemporal and functional dynamics of this set of *Drosophila* md proprioceptors, we used different fluorescent labels specifically expressed on different neuron subset. And all the *Drosophila* melanogaster strains were maintained on standard molasses food (agar, cornmeal, yeast, molasses, methylparaben, ethanol, propionic acid, penicillin, streptomycin) at 25ºC, 60% humidity. Fly lines were obtained from the Bloomington (BL) *Drosophila* Stock Center or published sources as noted below.

For dendritic structural dynamics, we chose to image bright static fluorescence expressed on the neuron subset which shows a very clear signal along the full dendrite and axonal projection, and for functional dynamic, we imaged the proprioceptive neurons co-expressing GCaMP and tdTomato, which could be used for ratiometric calcium signal extraction for moving subject.

Specifically, for class I da neuron (ddaD, ddaE and vpda), we used 221-Gal4[30], UAS CD4-tdGFP (BL#35839) and IT.410-Gal4 (BL#63298), 20XUAS-IVS-GCaMP6f (2 copies, BL#52869 and BL#42747), UAS-CD4-tdTomato (BL#35841); for the dorsal proprioceptor clusters (ddaD, ddaE, dmd1 and dbd), we used GMR10D05-Gal4 (BL#48438), 20XUAS mCD8::GFP or GMR10D05-Gal4, 20XUAS-IVS-GCaMP6f (2 copies), UAS-CD4-tdTomato; for vbd we used

IT.1129-Gal4 (BL#65461), 20XUAS-IVS-GCaMP6f (2 copies), UAS-CD4-tdTomato. We also image the functional dynamic of GFP and tdTomato co-label as a control, which we used IT.410-Gal4, 20XUAS mCD8::GFP (BL#32194), UAS-CD4-tdTomato.

3.2.2 Experiment Design and Sample Preparation

In this project, there are 3 important milestones for which we developed different imaging procedures and animal preparation.

The first stage is project validation, which gave us a general idea of whether SCAPE microscopy worked for freely moving *Drosophila* larva. This is important since the tissue scattering is different for each animal sample and the resolution and SNR requirements are also different. So we started with a simple preparation, where we embedded the larva within 1.5% low gelling point agarose in a glass bottom petri dish which was also covered by cover glass to prevent the larva from escaping. The cover glass was pushed down so that the space between the cover glass and the glass bottom is less than the larva body diameter. In this case, the larva is partially immobilized, which is useful for us to characterize our imaging resolution and depth field of view. As mentioned in Chapter 1, the field of view of SCAPE is about 1000μm×800μm×200μm, so a 2nd instar larva was used in our imaging prep so a nearly full body or a big proportion of body including multiple segments can be imaged at once. Based on the measurement of immobilized larvae, we validated that SCAPE offered sufficient spatial resolution to resolve the calcium activity of proprioceptive neurons as well as their dendritic trees and axonal bundle. Also, by slightly releasing the cover glass on top of the agarose, the larva could start moving in the agarose media, which also help us define the 10 volume per second as a proper volumetric scanning speed without getting motion induced blurry effect when imaging moving samples.

However, during the preliminary imaging, we found that because of the gut and the body fat in the larva body is very scattering, which dramatically affected the light-sheet quality when imaging the proprioceptive neurons on the other side of the body throughout the body. The spatial resolution as a result dropped down to around 5-10μm, which is not ideal to resolve the cellular calcium activity and also impossible to see the dendritic structure as well. In this case, taking advantage of the flexibility of SCAPE microscopy objectives configuration, we decided to use inverted configuration to image the proprioceptive neurons in the ventral side from below and use the up-right configuration to image the proprioceptive neurons in the dorsal side from. Though we cannot image the full proprioceptive system of the larva on both side at once, the proprioceptive activity of the full system during the stereotyped crawling behavior can still be resolved by properly normalizing the observation from different imaging session.

After collecting the first set of the preliminary data, we start to design the proper experiment procedure and animal preps to characterize the full proprioceptive system. As mentioned in chapter 2, it is important to design the sample preparation for SCAPE imaging to achieve the maximum spatial and temporal volumetric resolution. We would like to characterize two type of behavior patterns in this project: forward crawling and head exploration. We tried several different animal mounting methods until we found the ones that works the best.

There are a few important criteria for the larva preparation. First, the larva can be freely behaving in the mounting media, so the mounting media could be air, water or low concentration agarose. Considering the reflection index match criteria for the water immersion objectives in SCAPE microscopy, we have to submerge the larva in either water or low concentration agarose (1-1.5%). Second, the larva should be mounted on a flat platform and constrained in a certain depth space which is the same or slightly smaller then and body diameter, so the larva can only crawl in

two-dimensional space, but not swim or dig up and down too much within the submerging media. Third, the larva cannot be restrained or squeezed which will affect the normal crawling behavior or crawling speed. Forth, since we would like to image from both ventral and dorsal side of the larva, it is better that the prep is optically accessible from both side, such we could easily image both ventral and dorsal side of the proprioceptors without mounting the animal up-side-down, which might also affect the normal crawling behavior of the larva. To meet all the criteria described above, I have designed two different larva preparation to image the forward crawling head exploration/turning behavior.

To image forward crawling behavior, 2nd instar larvae with the body length about 1-1.5mm were chosen to image multiple segments at once. The idea here is to make a narrow channel with the width similar to the larva body width, so the larva can only crawl forward or backward and there is not space for turning and other complex head behavior. Different materials are tried to make this channel including glass/plastic cover slips, different concentration agarose, microfluidic chip and FEP sheet. The difficulties here are: the channel needs to be adjustable to fit the larva with slightly different size since their body is quite flexible, a tight fit is necessary to eliminate the turning behavior without adding extra constrain which might affect the crawling; also the reflection index of the material at the edge of the channel need to be the same or close to the immersion media in the channel, so the light sheet will not bend when scanning through the edge of the larva body. After a few attempts with different materials with water and low concentration agarose channel filling media, we chose FEP as our best candidate for the channel bounding material since its water-matching reflection index and availability of different thickness for different size of larva. We ended up with making a 300μm wide water-filled channel bounded by two hand crafted FEP spacers covered by a 40mm × 24mm cover glass. When imaging the ventral side, the channel was

positioned on a 50mm × 24mm cover glass, when imaging the dorsal side, the channel was positioned on a glass slide for better stability as shown in Figure 7. The sample was positioned on a XYZ 3-axis linear translation stage while the channel was aligned with the light sheet. In this case, the SCAPE microscopy only needs to scan through the width of the larva body to image the full volume containing the targeting proprioceptors which allowed us to achieve as high as 10 volumes per second to capture the dynamic activity during the larva locomotion. During each trial, we also manually adjust the translation stage along the FEP channel axis which help to keep the larva in the field of view for longer acquisition based on the live preview of the sCMOS camera.

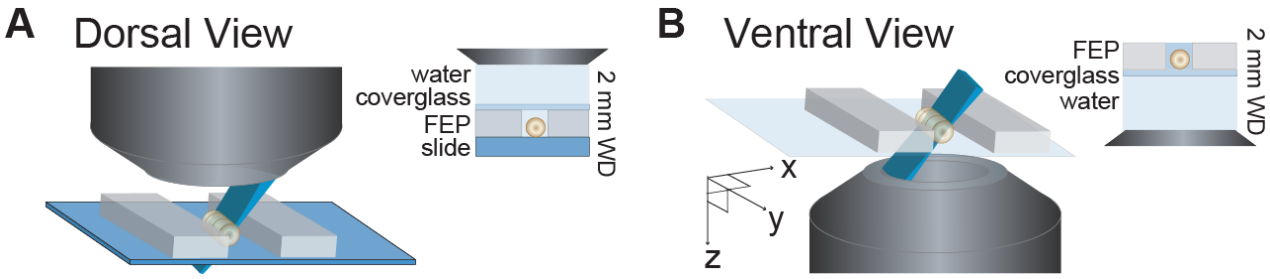

Figure 7 Schematic of larval imaging platform for SCAPE microscopy. (A)An upright configuration is used to image the dorsal side of the larva. (B) An inverted configuration is used to image the ventral side. The cover glass on top of the channel is not shown for better visulation.

To image the complex head movements (turns and retractions) during head exploration behavior, unlike the forward crawling case, we would need the larva to stay in small arena which is wide enough for the larva to move its head around but not long enough to crawl forward or backward. The desired size of the arena should be around 1-1.5mm long and about 500μm wide. In this case, it is very challenge to use FEP due to its hydrophobic surface and the extensibility make it very hard to hand craft the small and flat feature with water filled. However, in this situation, the larva won't be very close to the edge of the bounding material, we could actually use other materials with unmatched reflection index with water. We then try constraining the 2nd instar

larvae in a small water-filled arena bounded by 10% agarose, with a coverslip on top. The size of the arena is about 1-1.5mm by 500μm and it was made on a ~200μm thick agarose pad. The agarose pad was made using glass slide and tape spacer and the arena was made by manually etching and removing a small rectangular agarose with #5 forceps.

3.3 Characterizing the Dendrite Deformation

Using the animal preparation described above, we are able to image proprioceptors of *Drosophila* larva with enough spatial and temporal resolution to resolve the dendrite dynamic during the natural movement. We are able to image the larva for more than 10 minutes without serious photobleaching and noticeable photodamage from the laser sheet excitation. The next challenge is to properly extract the neuronal activity of each proprioceptive neuron in the moving larva.

As mentioned above, to characterize the proprioceptors in the *Drosophila* larva, we would like to have both dendrite dynamic and functional dynamic of the soma, which we use calcium ion dynamic here as an indicator reveled by GCaMP, for each proprioceptive neuron while freely behaving. Taking advantage of high spatial temporal volumetric speed of SCAPE microscopy, we could easily observe and characterize the dendritic dynamic of each neurons with very bright static fluorescent label, GFP and tdTomato specifically here in our research.

For the visualizations of SCAPE images of dendritic structure, raw camera 16bit data was square root scaled to enhance the visible dynamic range to avoid display saturation and to make all components (soma and dendrites) more visible, since the fluorescent expression level in soma and dendrites varies in an order of 10 or more. Resulting pixel values are then shown on a linear gray, red or green colorscale without further adjustment. SCAPE data was interpolated to uniform voxels with spline smoothing when making static figure or movies when characterizing the

neuronal dynamic, and sharpened using the imageJ function ‘unsharp mask’ (radius:1.5, weight:0.4) to enhance dendrite visualization

3.4 Cell Tracking and Ratiometric GCaMP Activity Analysis

To quantitatively characterize the functional calcium activity of each neuron however, it is not trivial to extract the GCaMP dynamic of a neuron which is moving around in 3D space inside the biological sample. First of all, we need to be able the track the neuron in 3D space.

When we start to explore the proper method for cell tracking, we explored a few currently existing methods including the tracking plug-ins in Fiji and 3D visualization software like Arivis and Imaris. However, they are not working very well because: one, we sacrificed some spatial resolution to achieve as high as 10 volumes per second for a large FOV, so each neuron is relatively small in our FOV, which is about 8-10 pixel in each depth plane, and also during the body contraction phase of the larva, the neighboring proprioceptive neurons will be squeezed and pushed very close to each other, which makes it very hard for the algorithm to separate them as two objects and fails the tracking. So we decided to make our own supervised cell tracking algorithms using Matlab, which allows us to manually correct the incorrect tracks during the cell tracking.

The tracking algorithms is based on the local maximum intensity, which works very well in the raw red channel of tdTomato fluorescent imaging to identify the center of each neuron. Each neuron was first manually selected from the top and side maximum intensity projection of the tdTomato image in logarithmic scale, which helps boost up the dynamic range for visualization. After the initial selection, we interpolated a 3D volume centered at the selection point based on a previously determined 3D window and then used local maximum to correct the actual center of

the neuron from the manually selection point. After this, for the next time point, we will look for the new local maximum point within another skewed predefined 3D window and set it as the new center position of the tracked neuron. The skewed window is set to extended in the direction of the desired moving direction of the neuron. For example, for the forward crawling trials, the tracking window is extended more in the anterior direction as we know that the neurons are more likely to move forward than backward, which helps reduce the tracking error a lot. And we also have extra constrains for local maximum, which should be within a ±25% change of the intensity value of the previous time point, since the static fluorescent change within the 3D volume due to the nonuniformity of the excitation sheet profile and the tissue shadowing should not be dramatic in most of the case. If the condition was not meet, then the tracking algorithm would jump out of the automatic tracking loop and switch to manual mode, which we could manually select the neuron again and continue. The new tracked result of each time point was also shown on the screen so we could also interrupt the auto-tracking loop anytime if we found any tracking error.

After getting the centroid position of each neuron, for fluorescence signal extraction, tracking regions of interest (ROIs) were defined as the smallest rectangular 3D cube around the tracked cell that encompassed the entire cell body. Average fluorescence intensity values of GCaMP6f and tdTomato were then extracted from these ROIs for each time point. A ratio between GCaMP6f and tdTomato was calculated after subtraction of background signal to account for the motion induced intensity change for each frame (yielding the green-to-red ratio R). The average of the lowest 10% ratio values was used as the baseline (R0) for each ROI. The GCaMP signal reported as neural activity at each time point then corresponds to the change in this ratio from baseline ($\Delta R/R0$). In addition, control measurements are shown that applied the same analysis to larvae co-expressing tdTomato and static GFP. In the GFP case, dynamic changes in $\Delta R/R0$ were

insignificant, confirming the sensitivity of our (ΔR/R0) measure to the intracellular calcium-dependent fluorescence of GCaMP. To demonstrate this process, raw red, green and ratiometric signals are shown in Figure 8A, B. The ratiometric activity of tracked neurons between the resting and contraction phase are evaluated with two-tailed paired t-test in Figure 8, showing reliable neuronal activities could be extracted.

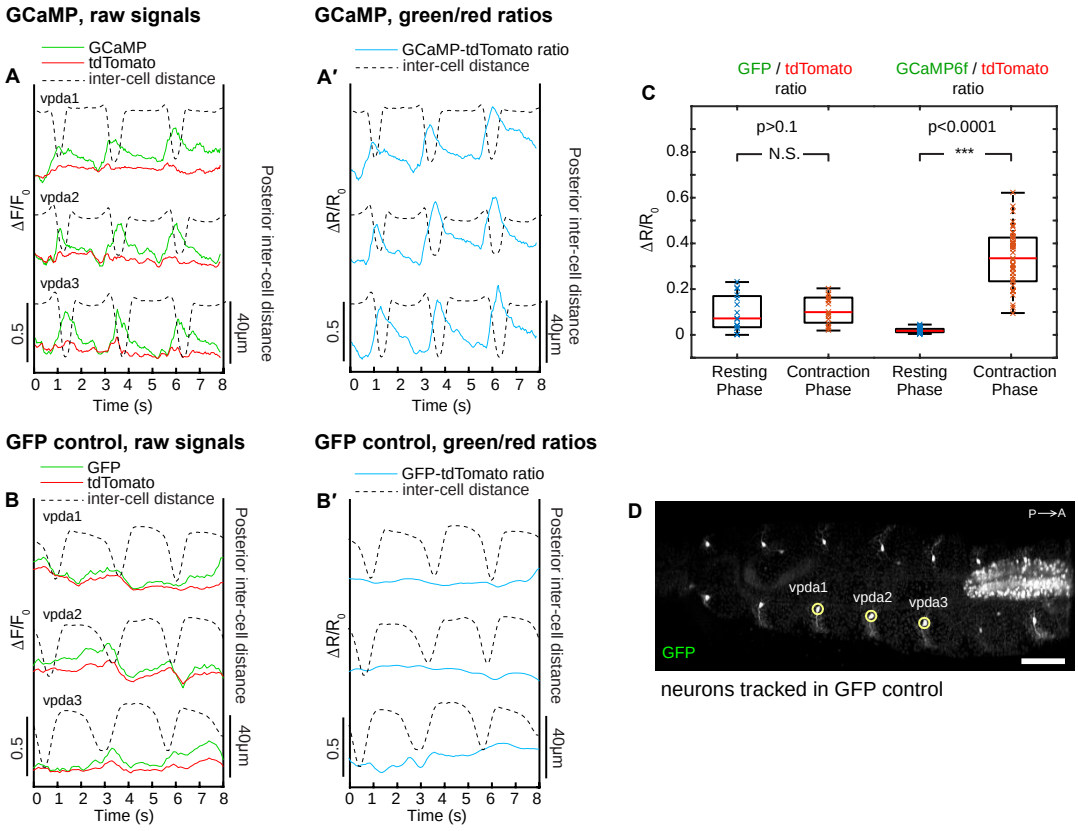

Figure 8 Ratiometrically measured calcium dynamics properly control for motion artifacts. (A) Change in fluorescence from baseline ($\Delta F/F_0$) in GCaMP6f (green) and tdTomato (red) during crawling in vpda neuron somas. Segment contraction is depicted with inter-cell distance (dashed lines). **(A´)** Change in ratio of GCaMP6f to tdTomato fluorescence ($\Delta R/R_0$, blue). Increases can be seen during segment contraction. **(B)** Change in fluorescence from baseline ($\Delta F/F_0$) in GFP (green) and tdTomato (red) during crawling in vpda neuron somas. Segment contraction is depicted with inter-cell distance (dashed lines). (**B´**) Change in ratio of GFP to tdTomato fluorescence ($\Delta R/R_0$, blue). No increase is associated with segment contraction. **(C)** Comparison of GFP-tdTomato and GCaMP6f-tdtomato ratios

between resting and contraction phases. For GFP-tdTomato analysis, n= 2 animals, 7 cells, 14 events, for GCaMP6f-tdtomato analysis, n=3 animals, 22 cells, 26 events. Note that there is no difference between GFP-tdTomato ratios in the resting versus contraction phases, while there is a significant increase in GCaMP6f-tdTomato ratios during contraction ($p<0.001$, as measured by two-tailed t-test). **(D)** SCAPE imaging of *410-Gal4, 20XUAS mCD8::GFP*, *UAS-CD4-tdTomato* animals during forward crawling, Ventral side. Imaging shows vpda neurons. GFP channel is shown. Posterior is to the left. Images are shown on a square root grayscale to reduce dynamic range for visualization of both cell bodies and dendrites. Scale bar=100µm.

3.5 Understanding Different Proprioceptive Neurons and the Distinct Activity Patterns

3.5.1 Characterization Proprioceptive Domain on the Larva Body Wall

Forward locomotion in *Drosophila* larvae involves periodic strides driven by muscle contractions progressing from posterior to anterior segments [22]. Proprioceptive feedback is especially important for monitoring the status of this peristaltic waves of contraction that drive locomotion [25]. Sensory dendrites grow in close proximity to epidermal cells, and prior studies indicate that guidance cues can be passed from epidermis to dendrites [26]. Each segment of the embryonic and larval epidermis is comprised of anterior (A) and posterior (P) compartments. To determine whether the P compartment might function as a proprioceptive "domain", we used SCAPE microscopy to examine body wall dynamics in crawling larvae with GFP-labeled epidermal cells driven by engrailed-Gal4. SCAPE imaging was performed either from above to capture optimized dorsal side dynamics, or from below to capture optimized ventral side dynamics as shown in Figure 7.

Volumetric SCAPE imaging revealed that during peristalsis the P compartment showed repeated contraction and extension; contraction as a peristaltic wave entered a segment, and extension as the wave moved to anterior segments (Figure 9A-A', Movie 1). When viewed in a virtual cross section down the midline of the larva, the dorsal P compartment folded in two domains, which led to shortening of Engrailed stripes during segment contraction and extension of the stripes during segment relaxation (Figure 9B-B'). By contrast, the ventral Engrailed domain showed hinge-like dynamics, sweeping across an approximately 90˚ angle during each peristaltic contraction (Figure 9C-C', Movie 2). vpda and ddaE dendrites extend across these dynamic regions so are ideally positioned to sense changes in body wall folding during segment contraction or compartment stretching during segment extension.

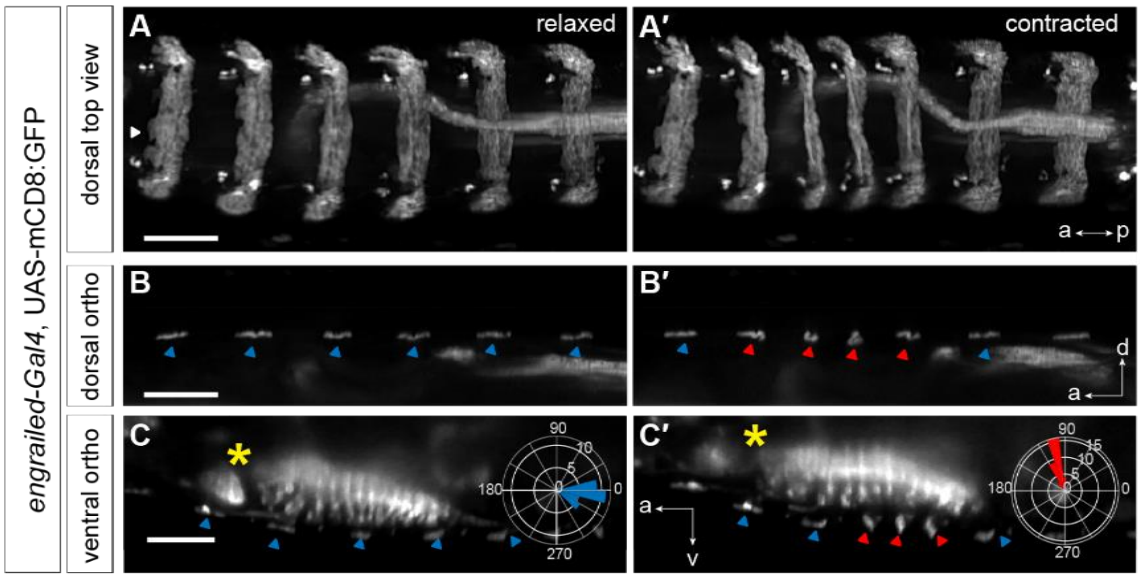

Figure 9 Analysis of epidermal deformation during locomotion using SCAPE. (A-A´) SCAPE imaging of the dorsal body wall of a larva labeled by *en-Gal4, UAS-mCD8::GFP* in relaxed and contracted state. Images show a top-down (x-y) maximum intensity projection (MIP) over a 100 µm depth range from a 137 µm deep volume (excluding gut autofluorescence). Data acquired at 10 volumes per second (VPS). (B-B´) Single virtual cross section down the dorsal-side midline of the larva (plane indicated by white arrowhead in C). Colored arrowheads indicate segmental labeling in relaxed (blue) and contracted (red) states. Movie 1 shows this dynamic dataset from 2 views (C-C´) SCAPE

imaging of the ventral body wall and ventral nerve cord (yellow asterisk) of a larva labeled by *en-Gal4, UAS-mCD8::GFP*, single virtual cross section down the midline of the larva (imaging at 10 VPS). Colored arrowheads indicate segmental labeling in relaxed (blue) and contracted (red). During mid-body contraction *en-Gal4*-positive epidermis swings to a vertical arrangement (indicated by red arrowhead in C´). Movie 2 shows this dynamic dataset from 2 views. (C, insets) Distribution of epidermal angles, ventral side, where 0˚ is a horizontal orientation, in relaxed segments (blue; n=31 relaxation phases in 6 segments from A2-A7, 1 animal) and contracted segments (red; n=33 contractions in 6 segments from A2-A7, 1 animal). a is anterior, d is dorsal, v is ventral. SCAPE images are shown on a square-rooted grayscale to reduce dynamic range and permit visualization of both the ventral nerve cord and epidermis. Scale bars = 100μm

3.5.2 Functional Characterization of All Different Types Proprioceptive Neurons

To characterize proprioceptor dynamics as larvae crawl, we started with the ventral class I neuron vpda (Figure 10) since it is sparsely spread in the ventral side of the larva body, which makes it easy to track. Class I neurons spread sensory dendrites along the body wall epidermis, suggesting that these cells may detect cuticle folding as shown in Figure 9. To investigate how vpda sensory terminals deform during forward crawling, we first characterized dendrite dynamics by imaging the cytosolic labelled GFP expressed in the vpda neuron with SCAPE from the ventral side at 10 VPS as a 2nd instar larva crawled within a linear channel prep on the large cover glass.

During forward crawling, peristaltic muscle contractions move from posterior to anterior along the animal [22]. vpda proprioceptors showed repeated folding and extension; folding as a peristaltic wave entered a segment and extending as the wave moved to anterior segments (Figure 10, Movie 3). Viewed from the side of the acquired volume, vpda dendrite tips flexed from distal to proximal, eventually angling at more than 90˚ during each peristaltic contraction (Figure 10C). This dendrite deformation also matched the results of the P compartment of the epidermis on the ventral side (Figure 9C'). Since class I dendrites are positioned along the basal surface of the

epidermis [27], vpda dendrite dynamics likely reflect body wall dynamics. Our data indicates that vpda dendrites are positioned to respond to repeated deformation of the body wall that occurs during forward crawling.

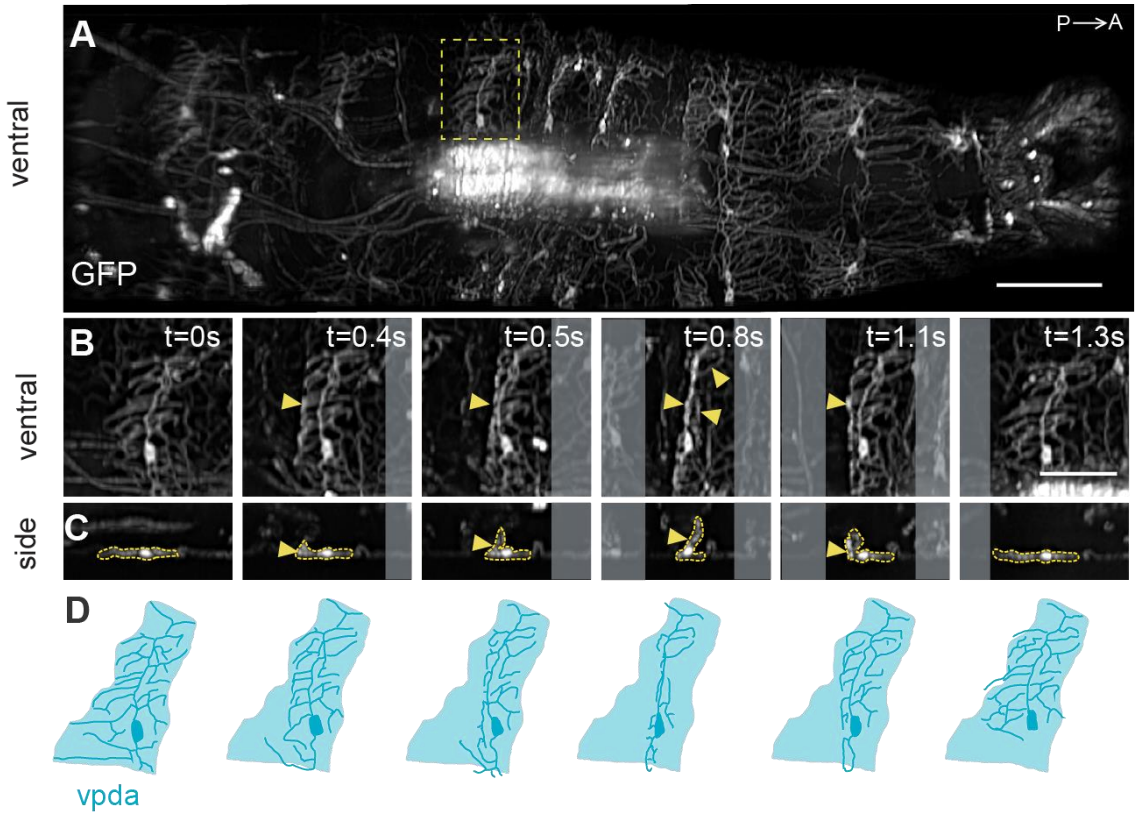

Figure 10 SCAPE imaging at 10 VPS from ventral side during crawling. Maximum Intensity Projection (MIP) over a 95 µm depth range from a 160µm deep volume (to exclude some fluorescent signal from other structures for better visualization, including the gut and part of CNS). Yellow box indicates neuron examined in time lapse in B-C. (B-C) vpda in ventral view (B) and side view (C) in successive time lapse frames during forward crawling. vpda dendritic arbors and cell body are outlined in yellow. Other arbors are from cIV neurons. (D) Tracing of neurons in B. Shaded areas represent dendritic field territory at t=0s before folding. Scale bar=100 µm in A, Scale bars=50 µm in B.

Next, we sought to reveal if and how the activity of these neurons changes as the dendrites fold during segment contraction of forward crawling. We imaged a dual-expression line of larvae

to label targeted proprioceptive cells with both calcium-sensitive GCaMP (green) and static tdTomato (red) and used the tracking algorithm described above for fluorescent signal extraction. We used the inter-cell distance between the measured neuron and a neighboring homologous neuron in the posterior or anterior segment as our measure of segment contraction and extension since the tracked soma is relatively static to the epidermal cuticle within each segment. We observed consistent rises in GCaMP fluorescence (ratiometrically measured as described above) in vpda neurons during each segment contraction (Figure 11A-D). Calcium signals subsided as the peristaltic wave progressed to adjacent anterior segments (Figure 11B, D; Movie 4). Dynamic calcium responses were also visible in dendritic arbors and axons (Figure 11C-C´, arrowheads and arrows, Movie 5). Note that because of variability in calcium signal amplitude across contraction events (Figure 11B), signals were normalized for the averages shown in Figure 11D. Together with the control experiment with GFP and tdTomato co-expressed larva line shown in session 3.4 and Figure 8, our results indicate that vpda neurons respond to body wall folding during segment contraction.

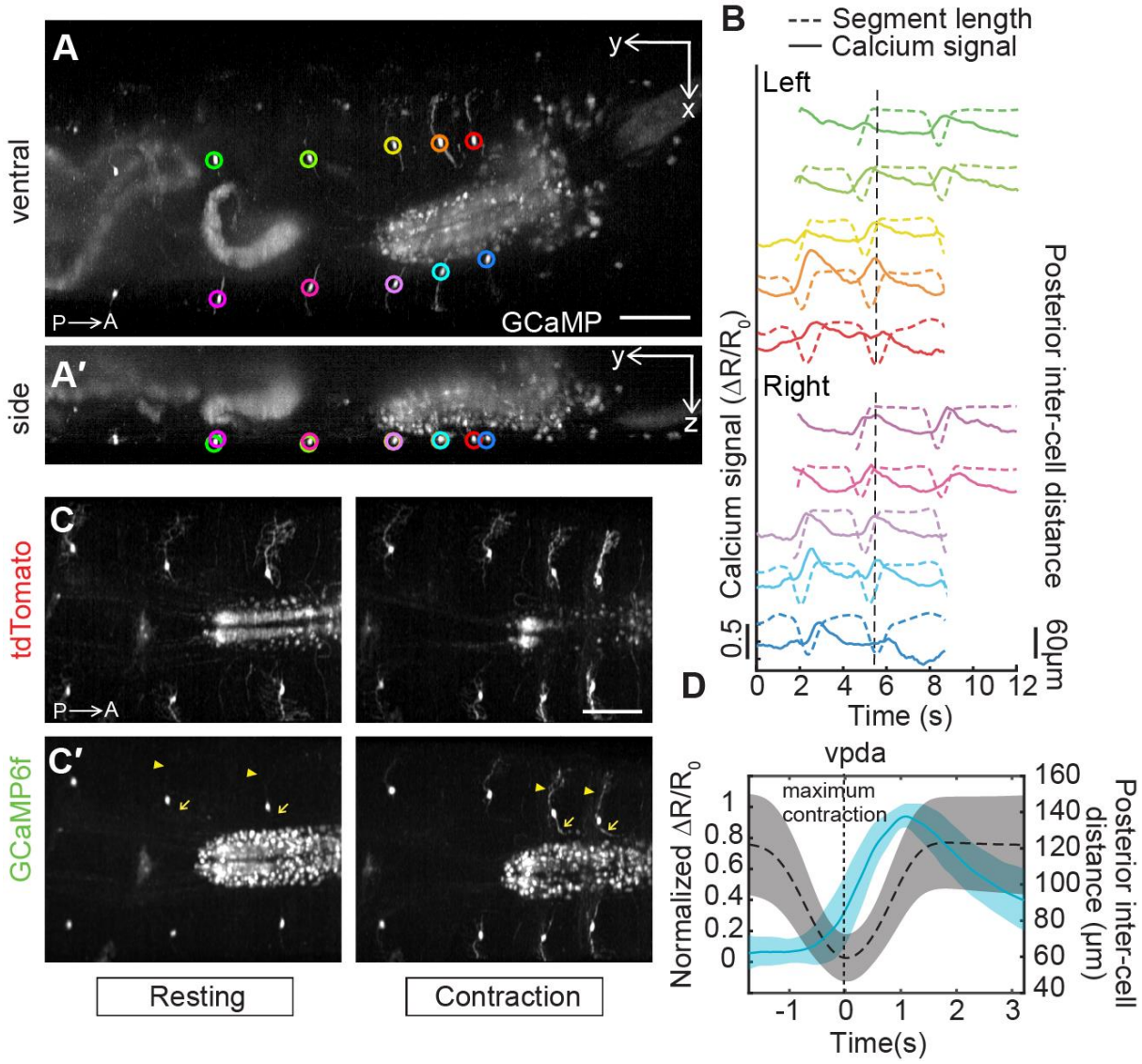

Figure 11 Dual-color SCAPE imaging of proprioceptor activity dynamics in crawling larvae. (A-A´) SCAPE imaging of a *410-Gal4, 20XUAS-IVS-GCaMP6f* (x2), *UAS-CD4tdTomato* larva, ventral side, during forward crawling. Images are MIP of a full 168µm deep imaging volume (square root grayscale). (A) shows a ventral view (x-y) and (A´) shows side view (y-z). GCaMP signal was extracted from the segmentally repeated vpda neurons indicated by circles. (B) vpda somatic response for the neurons tracked in (A). The distance between the measured neuron and the posterior neuron (posterior inter-cell distance) is plotted in dashed lines and the GCaMP6f response is plotted in solid lines. Dotted vertical line refers to time point shown in A. (C) Representative tdTomato and (C´) GCaMP6f images showing increased activity in dendrites (arrowhead) and axons (arrow) during contraction. Images cropped to show region of interest and are MIP of a 70 µm depth range from a 160 µm deep volume (square root

grayscale). (D) Mean calcium response (solid line) ± standard deviation (s.d., ribbon) of vpda soma (3 animals, n=22 cells) during segment contraction, represented by mean posterior inter-cell distance (dashed line) ± s.d. (ribbon). Maximal segment contraction is set at 't=0s' for each event. $\Delta R/R_0$ amplitude was normalized for each event. Posterior is to the left for all images. Scale bars=100 μm.

Based on this pipeline for both dendrite dynamic and cellular functional dynamic characterization of vpda, we used the same method to characterize the structural and functional dynamics of the remaining proprioceptive cell types, each of which has unique dendrite morphologies and positions (Figure 6). Two additional class I neurons besides vpda project secondary dendrites along the dorsal side of the body wall (ddaD anteriorly and ddaE posteriorly within each segment) [19]. These neurons are poised to detect cuticle folding on the dorsal side of the animal similar to vpda. In addition, dorsal and ventral bipolar dendrite md neurons (dbd and vbd, respectively) extend in an anterior-posterior direction and it is known that at least dbd extends along internal connective tissue [28]. By contrast, neuron dmd1 extends an atypical thick dendrite from the body wall to the internal intersegmental nerve [29], which lies along the muscle layer, suggesting that this proprioceptor could be poised to detect muscle dynamics verse the cuticle dynamic.

Imaging of dorsal class I neurons revealed that ddaE and ddaD dendrites deform as the peristaltic wave enters each segment and flatten as the wave passes (Figure 12A-A´´; Movie 6). While there is some variability in the degree of dendrite deformation, we consistently see folding in both cell types, with ddaE folding before ddaD (Figure 12A´´-B) in synchrony with the posterior to anterior progression of peristaltic waves. Like vpda, calcium dynamics revealed increases in dorsal class I activity during segment contraction (Figure 12C-F). When comparing paired ddaE and ddaD cells within the same segment, responses of posterior ddaE and anterior ddaD neurons occurred in succession during segment contraction, with ddaE responding just before ddaD (Figure

12A, C), corresponding to the lag in dendrite folding. These data suggest that cellular calcium activity is a result of dendritic folding in all class I neurons. As a control, the same larva line was also imaged under compression with a glass coverslip. In this prep, larvae were constrained in a linear channel with the inner diameter smaller than the body width and filled with mineral oil, which prevented physical folding of the anterior compartment of epidermis and the ddaD dendrites underneath during forward crawling (Figure 13). In this case, no increases in ddaD calcium activity were seen during forward crawling, consistent with dendritic folding driving calcium activity. This same compression did not prevent dendritic folding in ddaE neurons, and accordingly this cell type continued to show activity during crawling. The difference between these normal and compressed preparation shows the importance of imaging freely crawling larvae for characterization of locomotion, since physical restraint itself appears to influence proprioceptive signaling.

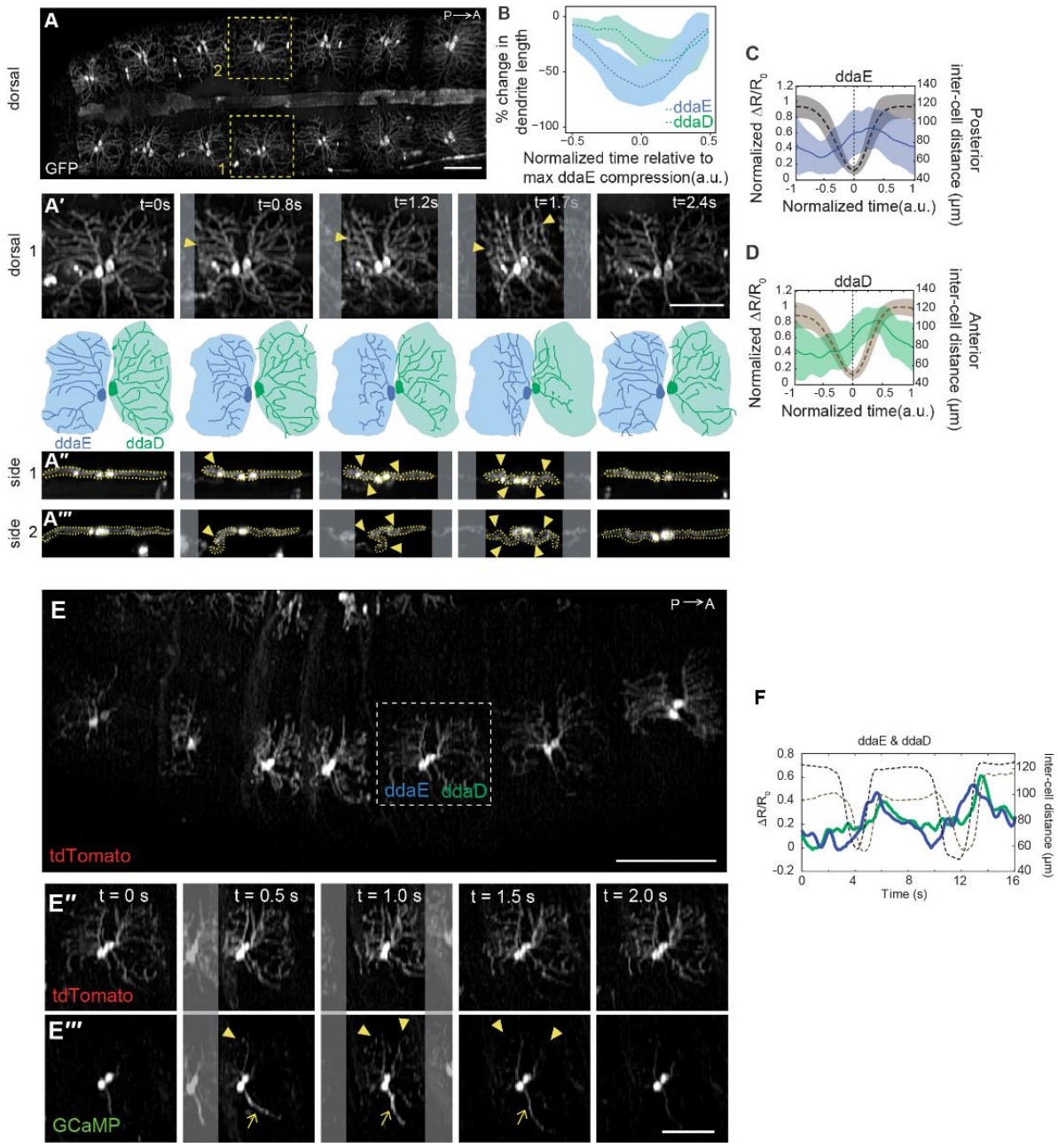

Figure 12 Dorsal Class I Neruon Dynamic and the Activity Patterns. (A) Single frame from SCAPE movie of larva during crawling with ddaD and ddaE neurons visible on the dorsal side. Neurons were labeled using *221-Gal4*, *UAS-CD4tdGFP*. Yellow box indicates neurons examined in time lapse sequences below. (A´) Top: enlarged dorsal view of right-side neurons (1). Arrowheads indicate regions of dendrite folding. Bottom: tracing of neurons in A´. Shaded areas represent dendritic field territory before folding. (A´´- A´´´) Side view of right-side neuron (1), and left side neuron (2) during segment contraction. (B) Mean (± s.d.) percent change in dendritic length along the

anteroposterior axis (a measure of dendritic folding) of ddaD (green; n= 10 cells) and ddaE (blue; n= 10 cells) during forward crawling. (C, D) Mean (± s.d.) calcium response (solid line) of ddaE and ddaD soma during segment contraction. In (D), we plotted anterior inter-cell distance between the measured neuron and the homologous neuron in the anterior segment, since this was a better proxy for ddaD dendrite folding. (E-E´´´) SCAPE imaging of *410-Gal4*, *20XUAS-IVS-GCaMP6f* (x2), *UAS-CD4-tdTomato* larva. Arrowheads indicate increases in dendritic GCaMP6f, arrows indicate increases in axon bundle (containing both ddaD and ddaE axons). Note ddaE dendrites are active before ddaD. (F) Examples of single cell calcium activity dynamics during forward crawling for ddaD and ddaE. The calcium response is plotted in solid lines (quantified as $\Delta R/R_0$). The distance between the measured neuron and the posterior neuron (posterior inter-cell distance) is plotted in black dashed lines. The distance between the measured neuron and the anterior neuron (anterior inter-cell distance) is also plotted in brown dashed lines on the ddaD plot, since this is a better proxy for dendrite folding.

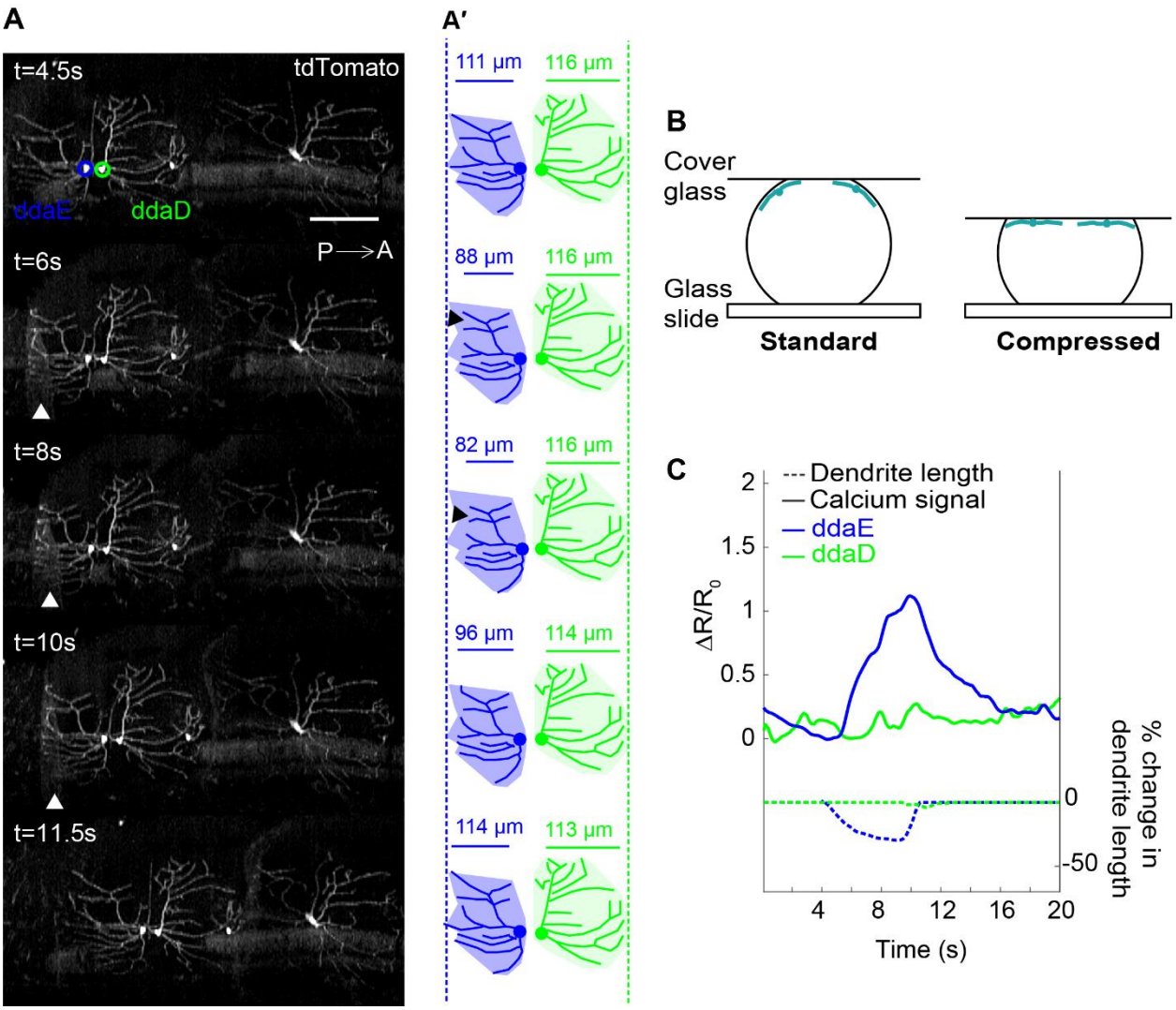

Figure 13 Sensory activity does not occur in the absence of dendritic folding. (A) Time lapse of SCAPE imaging of dorsal class I neurons labeled with 410-Gal4, 20XUAS-IVS-GCaMP6f (x2), UAS-CD4-tdTomato, in a compressed preparation, which prevents dendritic folding in ddaD. TdTomato channel is shown to depict dendrite dynamics. Larva is 3rd instar. Posterior is to the left. (MIP) over a 50µm depth range from a 160µm deep volume. (A´) Tracing of time lapse data shown in (A), posterior cells. ddaE is blue and ddaD is green. Dotted lines and shaded areas represent extent of arbor in a relaxed segment. Measurements represent dendrite length (µm), a measure of dendrite folding. Arrows denote frames with dendrite folding. Note that ddaE dendrites fold, but not ddaD. (B) Schematic of compressed preparation. (C) Calcium responses (ΔR/R0, solid lines) and % change in dendrite length (dotted lines) in a compressed preparation of ddaE (blue) and ddaD (green) during segment contraction. Activity correlates with dendrite folding. Scale bar=100µm

The remaining three proprioceptor types are located further inside the body with different dendrite end compared with class I neurons, and also showed more complex 3D motion paths during crawling. We leveraged SCAPE's high-speed volumetric imaging capabilities to capture the distinct 3D movements and activity dynamics of these dmd1, dbd, and vbd proprioceptors during forward crawling. Different GAL4 promoters were used in the larva lines here to specifically express the fluorescent indicators in different subset of the proprioceptors. We then also characterize both dendrite structure and somatic functional dynamic of these three proprioceptor types with the same processing pipeline described above.

Proprioceptor neuron dmd1 extends its dendrite from the body wall to the muscle layer, its dendrites were slack and coiled in resting phase and prior to the contraction wave, then as the segment contracted, the dendrite bundle stretched anteriorly and was then pulled deeper into the animal (Figure 14A´-A´´´, Movie 7). As the segment extended, the bundle swung posteriorly and then returned to the coiled position. GCaMP imaging of the dendrite bundle and the extracted somatic ratiometric measurement revealed increases in calcium activity in dmd1 during segment contraction, as the dendrite bundle stretched (Figure 14C-G).

Both dbd and vbd have their bipolar dendrites folded as the segment contracted (Figure 14A´ arrowhead for dbd, Figure 15A-A´´ and Movie 8 for vbd). For dbd, GCaMP fluorescence peaked during segment stretch (Figure 14D, G), consistent with previous electrophysiology results in a dissected prep [24]. However, in contrast to dbd, GCaMP fluorescence in vbd peaked during segment contraction (Figure 15B, D). Both neuronal activities could be seen from the GCaMP imaging and the extracted somatic ratiometric measurement. Thus, two proprioceptors with similar morphologies and dendrite dynamics can show distinct responses during crawling.

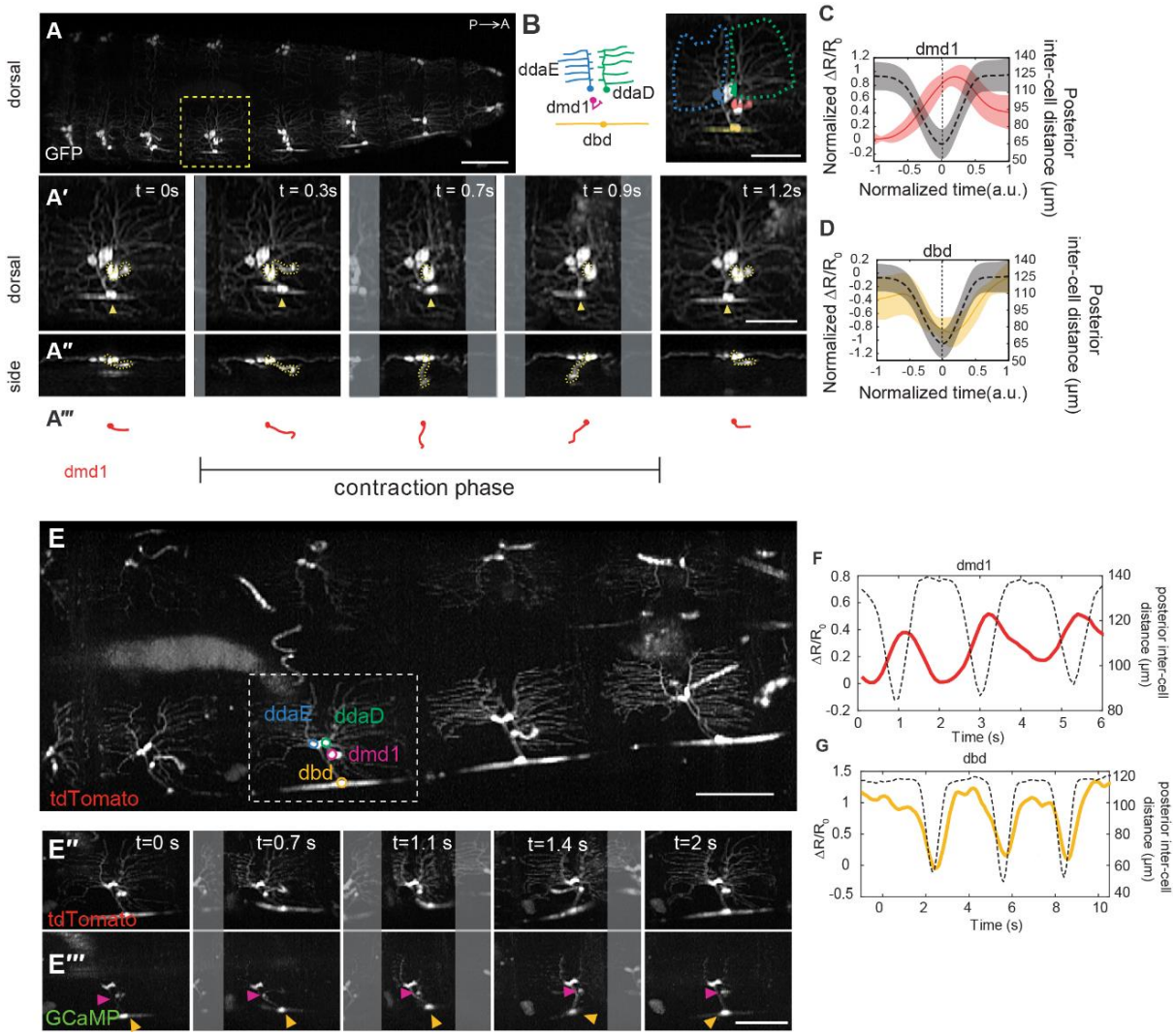

Figure 14 Dorsal Cluseter Neruons dmd1 and dbd Dynamic and the Activity Patterns. (A) SCAPE imaging of GMR10D05-Gal4, UAS-CD4tdGFP larva during crawling showing dorsal cluster dendrite dynamics. (A´-A´´) dorsal and side views in which dmd1 soma and dendrite bundle are traced with a dashed yellow line – tracing shown in A´´´. dbd noted with arrowhead. (B) Schematic and inset image showing neurons imaged together in A. Inset image shows pseudo-colored neurons. ddaE (blue), ddaD (green), dbd (yellow), dmd1 (pink). Dashed line represents outline of ddaE and ddaD dendritic fields. (C,D) Mean (± s.d.) calcium response (solid line) of dmd1 and dbd soma during segment contraction (quantification and representation is same as in **Figure 12** above). (E-E´´´) SCAPE imaging of GMR10D05-Gal4, 20XUAS-IVS-GCaMP6f (x2), UAS-CD4-tdTomato larva. Orange arrowhead marks dbd cell body, pink arrowhead marks dmd1 cell body. (F,G) Examples of single cell calcium activity dynamics during forward crawling for dmd1 and dbd.

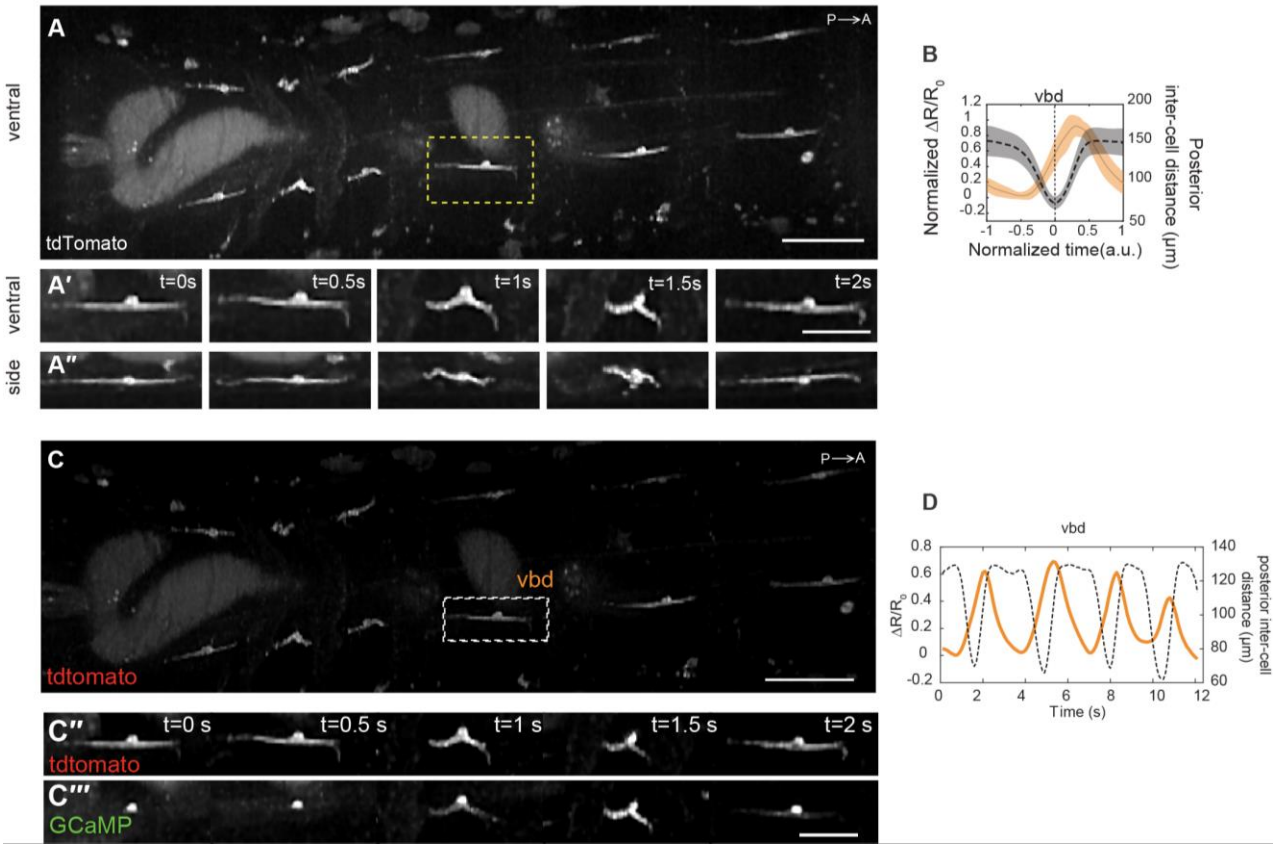

Figure 15 Ventral Bipolar Dendrite Neruons vbd Dynamic and the Activity Pattern. (A) SCAPE imaging of *1129-Gal4*, *20XUAS-IVS-GCaMP6f* (x2), *UAS-CD4-tdTomato* larva ventral side during crawling. Yellow box indicates neuron examined in (A´-A´´) dorsal and side views. (B) Mean (± s.d.) calcium response (solid line) of vbd soma during segment contraction (quantification and representation is same as in **Figure 12** above). (C-C´´´) SCAPE imaging of 1129-Gal4, 20XUAS-IVS-GCaMP6f (x2), UAS-CD4-tdTomato larva. (D) Example of single cell calcium activity dynamics during forward crawling for vbd.

3.5.3 Sequential Activation of Dorsal Cluster during Forward Crawling

Then we examined the dorsal proprioceptor cluster (ddaD, ddaE, dmd1 and dbd) together to directly compare the timing of their activity during forward crawling and try to unveil the potential functional relationship among them. We found that each cell type actives sequentially during segment contraction of forward crawling (Figure 16) when align them together based on the

normalized posterior inter-cell distance. dbd is most active in a stretched or relaxed segment. Then as the segment contracts, dmd1 activity increases first, followed by the class I neurons (ddaE and ddaD) as the cuticle folds during segment contraction (Figure 16A). Using the normalized time at half-maximum calcium activity as an onset metric confirmed that ddaD activity was significantly delayed relative to ddaE during forward crawling (Figure 16C; p=0.01 by single tail paired t-test) and that ddaE activity occurs significantly later than dmd1 activity during forward crawling (Figure 16B, p=0.0078 by single tail paired t-test). These results suggest that different dorsal proprioceptor respond at different times during a peristaltic wave of forward crawling. These activities could provide a continuum of cell-type specific encoding during movement.

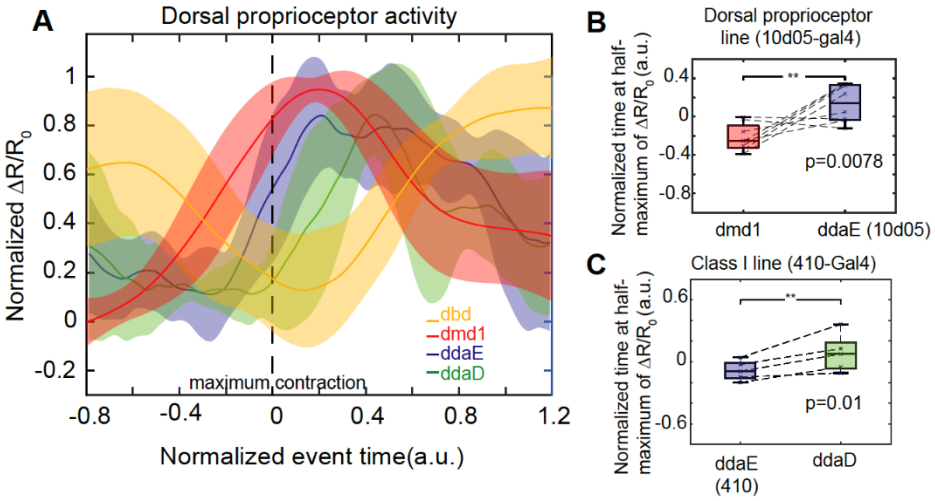

Figure 16 Each dorsal proprioceptor type is activated sequentially during segment contraction. (A) Mean calcium response (± s.d.) of dbd, dmd1, ddaE, and ddaD during segment contraction. Dmd1 and dbd data is same as shown in Figure 14 C-D**.** This plot includes a subset of ddaE and ddaD activity data shown in Figure 12C-D from paired cells within a segment (n= 4 animals, 5 cells, 5 events). Data is aligned using time at maximum contraction (as measured by distance between ddaE and homologous ddaE in posterior segment), which is set at 't=0s' for each event. The time window and the amplitude of $\Delta R/R_0$ of each trace were normalized and interpolated across events (see methods). **(B)** To test the lag between dmd1 and ddaE activity, we compared the time at half-maximum calcium activity from paired cells within a segment in GMR*10D05-Gal4, 20XUAS-IVS-GCaMP6f* (x2), *UAS-CD4-tdTomato*

larva (n=4 animals, n=8 cells, 8 events). ddaE activity occurs significantly later than dmd1 activity (p=.0078) by single-tailed paired t-test. **(C)** To test the lag between ddaE and ddaD, we compared the time at half-maximum calcium activity from *410-Gal4, 20XUAS-IVS-GCaMP6f* (x2), *UAS-CD4-tdTomato* animals (n=4 animals, n=5 cells, 5 events). Data are from the same cell pairs as analyzed in panel **A.** ddaD activity occurs significantly later than ddaE activity (p=0.01) by single-tailed paired t-test.

3.5.4 Combinational Coding for More Complex Behavior: Head Exploration

In addition to characterizing the forward crawling of larvae, we could also image more complex movement of their head using SCAPE microscopy. To further evaluate how proprioceptive activity might provide feedback during complex movements, we mounted the larvae in a small arena bounded by agarose. With this setup, we were able to track and extract dorsal sensory activity of class I neurons during the exploratory head movements.

During the head exploratory movement, we observe the turning behavior happened together with the head retraction in many cased. (Figure 17A-A´´). These behaviors are not always synchronized, which can lead to a complex motion path for each neuron and segment compared to linear forward crawling behavior. However, SCAPE recordings confirmed that even for this less-stereotyped motion, class I neuron activity is still reliably associated with segment contraction. In the dataset shown in Figure 17, we focused on ddaD and ddaE within thoracic segment T3 (termed D1 and E1), and ddaD within abdominal segment A1 (termed D2), since these cells were dramatically deformed by the observed exploratory movements and also stay within the imaging field of view during the whole behavior period. Ratiometric measurement was used to indicate the neuronal activity of these cells and showed correlation with the distance between ipsilateral D1 and D2 neurons (termed inter-cell distance) (Figure 17B, Movie 9). In this example, calcium signal changes in ddaD neurons were greater than those in ddaE, consistent with greater measured

changes in dendrite length for ddaD than for ddaE neurons during these turning and retraction events (32% ± 25% s.d. for ddaD; 10% ± 6.6% s.d. for ddaE).

We then examined whether the complex inter-cell distances and calcium signals could be interpreted in terms of the larva's combined turning and head retracting behavior. When examining the physical properties of the larva's segmental structure and its moving pattern, we noted that head retraction and turning are distinct in that retraction is symmetric and head turning is asymmetric, which could be further derived as comment and differential components. Subtracting the D1-D2 inter-cell distance on the left side of the larva from the D1-D2 inter-cell distance on the right-side neuron pair should thus cancel out the effect of symmetric head retraction. This differential distance was found to closely match the calculated angle of the segment which could be used as a turning metric. Furthermore, when assuming rigid coupling between the left and right cells, we found that adding the left D1-D2 inter-cell distance to the right D1-D2 inter-cell distance cancelled out the effect of turning providing a measure consistent with the timing of the larva's head retractions which could be used as a retraction metric. Even more interestingly, the difference between calcium signals on the left versus right side was found strongly correlated well with turning metric, especially for ddaD cells (Figure 17C). Similarly, the sum of the calcium signals from the left and the right sides correlates strongly with our retraction metric for each cell type (D1, E1, D2) (Figure 17D).

These results indicate that proprioceptor activity during exploration can represent simultaneous head turning and retraction and the linear combination of calcium signals from left and right neuron pairs could provide independent metrics of turning and head retraction.

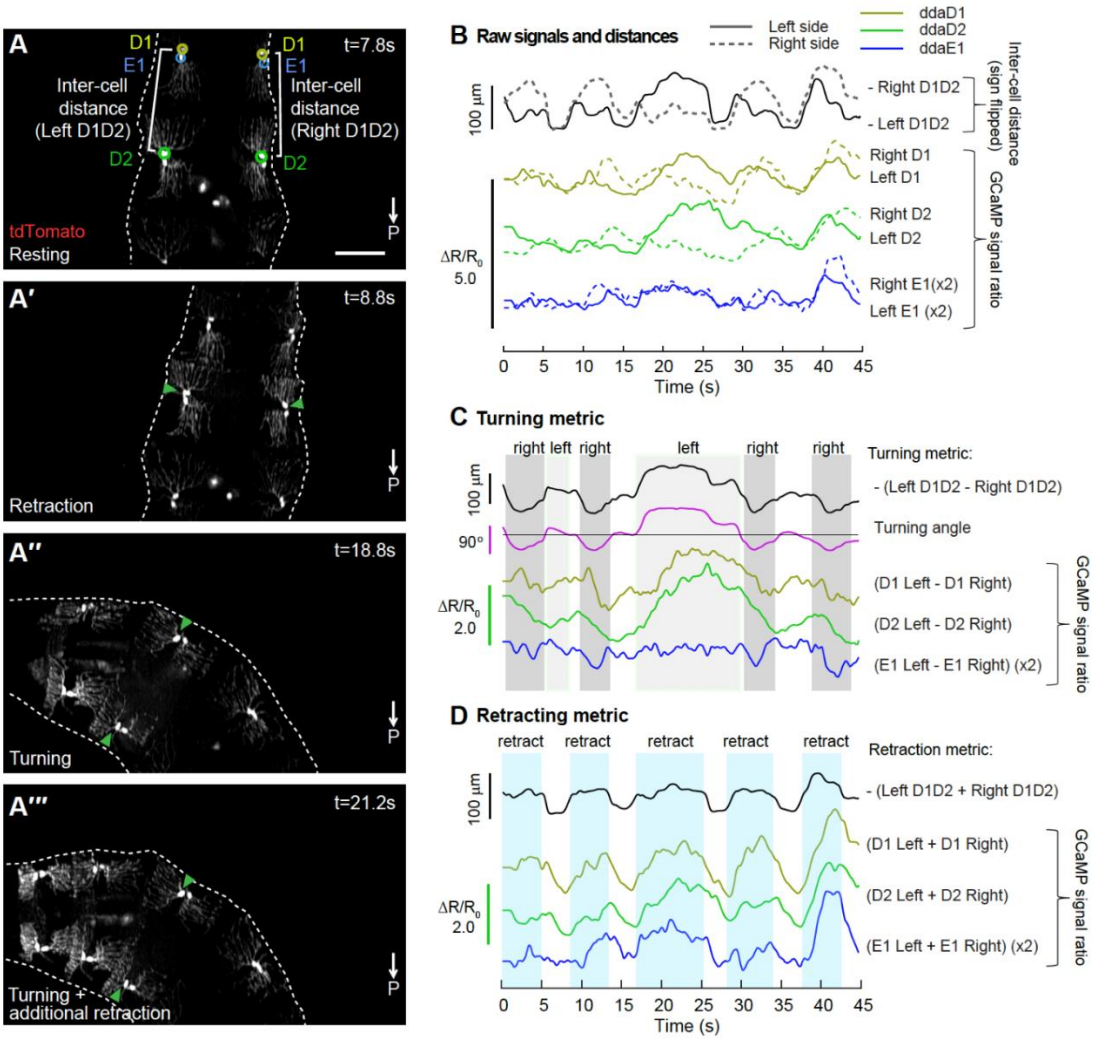

Figure 17 Dorsal proprioceptor activity can simultaneously code for head turning and retraction.SCAPE imaging of dorsal class I neurons labeled with *410-Gal4, 20XUAS-IVS-GCaMP6f* (x2), *UAS-CD4-tdTomato*, during exploratory behavior. Posterior is to the bottom of all images. TdTomato channel shown. MIP over an 80µm depth range from a 140µm deep volume (square root grayscale). GCaMP fluorescence was quantified from circled neurons, ddaD (D1, yellow-green) and ddaE (E1, blue) in segment T3, and ddaD (D2, green) in segment A1. Inter-cell distance (white brackets) is quantified as distance between ipsilateral D1 and D2. Representative behaviors are shown including resting (A), retraction only (A´), and turning (A´´-A´´´). (B) Calcium activity (measured as the ratio of GCaMP to tdTomato fluorescence) in left (solid) and right (dashed) D1, D2 and E1 neurons are compared to inter-cell distance (black). The sign is flipped on inter-cell distance measurements, so larger values represent shorter distances. ddaE activity was smaller than ddaD activity, so E1 data is shown at 2X. (C) Plots of the difference in

calcium activity between contralateral cells compared to the difference in contralateral inter-cell distances (our turning metric) and the calculated angle of the D1 segment. (D) Plots of the sum of calcium activity between contralateral cells and the sum of contralateral inter-cell distances (our retraction metric). Movie 9 shows this dataset. Scale bar=100 μm.

3.6 Discussion

This study demonstrates that SCAPE microscopy could be used for in-vivo volumetric imaging of sensory activity in freely behaving animals [10, 11]. We were able to characterize the activity patterns of a heterogeneous collection of proprioceptive neurons of *Drosophila* larvae during forward crawling, as well as during more complex movements such as head exploratory behavior, to determine how larvae sense body shape dynamics. We are able to image different proprioceptive dendrites deformation during movement in 3D space with high temporal with simultaneously GCaMP activity extracted from the somatic area. Our results for ddaD and ddaE dorsal proprioceptors are also consistent with a complementary study [30]

By examining the full set of proprioceptors in unconstrained behaving larvae revealed that all class I neurons, dmd1 neurons and vbd neurons increase activity during the contraction phase of forward crawling while dbd neuron showed decreased activity during this phase, which is also consistent with previous electrophysiological recordings of dbd in a dissected preparation [24]. The relatively high temporal resolution afforded by high-speed SCAPE microscopy imaging further revealed that different proprioceptors exhibit sequential onset of activity during forward crawling. This timing sequence associated with distinct dendrite morphologies and movement dynamics, suggest that proprioceptors monitor different features of segment deformation. These results indicate that this set of proprioceptors function together to provide a continuum of sensory feedback describing the diverse 3D dynamics of the larval body.

Here, we also provide an example of how high-resolution, high-speed volumetric imaging enabled investigation of the previously intractable question of how different types of proprioceptive neurons encode forward locomotion and exploratory behavior during naturalistic movement. Experiment could readily be extended to explore a wider range of locomotor behaviors and other sensory modalities such as gustation and olfaction Waves and even cellular activity in central neurons within the ventral nerve cord can also be observed when needed. We expect that the *in vivo* SCAPE microscopy platform utilized here could ultimately allow complete activity mapping of sensory activity during naturalistic behaviors throughout the larval CNS.

Chapter 4

HIGH THROUGHPUT IMAGING AND SCREENING OF THE INTACT MOUSE OLFACTORY EPITHELIUM

How the brain interprets peripheral chemosensory stimulation remains an enduring puzzle. Unlike vision and auditory senses, the input for the olfactory system is a combination of discrete chemical compounds. There is a large number of different receptors in mammalian olfactory system and expressed exclusively in each olfactory sensory neuron (OSN). However, most of the time, we focused on the response profile of different OSN to single odorant input while in the real world we always face a huge variety of odor mixtures in the environment. To understand how our complex olfactory system encodes this complicated input, it is important to have a platform with high throughput to observe the olfactory sensory system responding to different mixture input. Working with Dr. Stuart Firestein and his Ph.D student Lu Xu over the past 4 years, we together developed a SCAPE based experiment platform for high throughput screening of the intact mouse olfactory epithelium to try to understand the computational mechanisms behind the peripheral sensing of odor mixtures.

4.1 Introduction to Mouse Olfactory Epithelium and Odor Mixture

When modeling the olfactory sensory input, the combinatorial additive coding mechanism is one of the most commonly accepted model based on early studies on the peripheral receptor in different animal models [31]. This model would be analogous to color vision where a few receptors of overlapping wavelength sensitivity covering the visible light spectrum are sufficient to encode millions of hues. Despite the olfactory stimulus being discrete (i.e., not continuously varying along a physical parameter like wavelength or frequency) the much larger number of receptors (c. 500-4000, depending on the species) seemed sufficient to provide a "molecular basis" for olfactory discrimination [32-36]. However, the olfactory system in the real world must handle a far more complex input than monomolecular stimuli. Most of what we and other animals smell are blends or mixtures of a big number of different odors, not individual chemical compounds. Some of these blends can be complex and may consist of tens to hundreds of individual chemical components. Even in the simple case of two odors there are numerous instances in which the combined odor is perceived as distinctly different from the individual odors, often as if one were masking the other [37-42].

Here, we utilized a new approach to high-speed 3D imaging of intact olfactory epithelium with SCAPE microscopy, which allows to image single-cell responses to multiple odor injections thanks to both low phototoxicity and high signal to noise throughout the 3D volume [43, 44]. We were able to monitor the intracellular calcium activities of large numbers of individual intact olfactory sensory neurons (OSNs) expressing GCaMP6f with SCAPE microscopy. To maximize the field of view with sufficient spatial resolution for single cell segmentation, the volumetric imaging data was acquired at 2 to 5 volumes per second, over large volume (~ 1mm x 800μm x 220μm), capturing single-cell activity throughout the epithelial layers overlying the curves of

intact nasal turbinates within a novel mouse hemi-head perfused preparation. This significant parallelization of olfactory read-outs enabled large-scale single-cell analysis far exceeding that possible with previous imaging methods or electrophysiological recordings of activity in single sensory neurons in isolation or population responses as field potentials.

By tracking the response of the same cells to sequences of pure and mixed odors, we were able to observe how the OSNs response to the odor mixtures differently with pure odors, and whether any suppression effects exist across odorants in the mixture responses in this peripheral sensory level. Though antagonism has been reported by several laboratories [45-47] at the single receptor level, these studies were limited within a few single odor receptors and a limited number of related monomolecular stimuli. Our results draw into question the notion of a simple combinatorial code for discrimination of odors or odor mixtures.

4.2 Experiment Design and Setup for Intact Olfactory Epithelium

Before SCAPE was introduced into this research field, the most common method to image the calcium activity of olfactory sensory neurons was epi-fluorescent imaging on dissociated olfactory neurons. A schematic of the epithelium and the calcium signaling pathway in the OSN are shown in Figure 18. Specifically, olfactory epithelium is obtained from mouse nasal cavity and enzymatically digested. Dissociated olfactory sensory neurons are then cultured directly on concanavalin A-coated cover glasses. In this culture prep, OSNs remain functional within the same day of dissection. In this case, a regular epi-fluorescent microscopy can be used to image the culture dish at a single plane. However, as we know the olfactory epithelium overlies the curved nasal turbinates and the OSNs are stacked together in different layers and project their axons to the olfactory bulb. During the dissociation process, the axonal terminals are damaged, and the

specific layout information of the olfactory epithelium is lost. And also, on the intact olfactory epithelium, there is a mucus layer, which covers the olfactory cilia. This mucus is also damaged in the culture prep which might also affect the OSN response we observed.

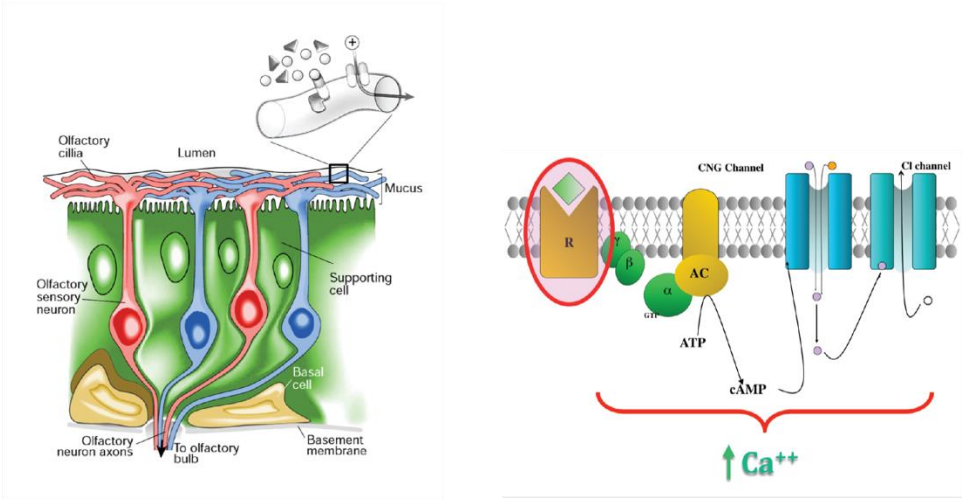

Figure 18 Schematic of the Epithelium and the Calcium Signaling Pathway in OSN. Schematic of mouse olfactory epithelium is on the left, showing the odor compounds are binding with the specific receptors in the olfactory cilia in the mucus layer. As the biggest familiy of GPCR, the sencondary calcium ion involved signaling pathway is shown on the right including calcium dependent ion channel, which is related to the neuron activity.

4.2.1 Sample Preparation for Intact Olfactory Epithelium

Taking advantage of the high-speed volumetric imaging capability of SCAPE microscopy, we would like to overcome the problem of regular dissociated cell perp by imaging the intact epithelium. As mentioned in Chapter 2, there are three important parameters when in SCAPE volumetric imaging: speed, FOV and resolution. When imaging the olfactory sensory neurons to understand the single OSN response property, the tissues/neurons are relatively stable, and what we care about the most is the calcium response level instead of the transient dynamic. So, we do not have to image as fast as 10-20 volume per second, and in our case specifically, 5 VPS or 2

VPS sometime is sufficient to answer the question we asked in our research. In this case, we could expand our FOV to as big as 800-1000μm while keeping a decent spatial sampling density which preserves the cellular resolution for us to identify the single OSN response profile from the staking structure of the epithelium.

In the pilot experiment, we started with a simple prep which is just peeling off the olfactory epithelium from the nasal turbinates and placing it on a glass bottom perfusion chamber. The piece of epithelium was held in position with a nylon mesh. The resolution across the entire piece of epithelium was very promising where we could see the cilia knobs on the surface and OSNs stacked together underneath. However, since we were using the mesh to hold the tissue, it wasn't stable enough in the perfusion chamber, the tissue was moving with the perfusion flow and also slowly drifting over time. By manually aligning the 3D volumes we acquired, we were able to get the first set of OSN responses to a few different odors we delivered through the perfusion system. However, this method would also damage OSNs when removing the epithelium from the nasal cavity, though to a less extent than dissociated neurons.

We then started to consider imaging OSNs in a more intact state. Hence, we came up with a hemi-head prep, where we cut open the head sagittally and removed the septum to expose the surface of the olfactory turbinates. This way we preserved the axonal projections as well as mucus layers, keeping the OSNs in a healthiest status. The biggest challenge to use this kind of prep in the past was that the turbinate surface is curved and the OSNs are distributed across different depths, which makes 2D imaging method difficult to focus on a specific layer with many OSNs. However, this is no longer an issue with SCAPE-based volumetric imaging.

To image the hemi-head prep, we custom designed and 3D printed a glass bottomed perfusion chamber to mount the sample. The perfusion chamber was also designed to constrain

the perfusion flow in the nasal cavity with the inlet at the nostril and the outlet at the throat (Figure 19, blue trace, arrows). A small amount of light-cured dental composite (Tetric EvoFlow®, Ivoclar Vivadent) was applied to adhere the tissue to the chamber. The dental composite holds the sample stable in the perfusion chamber for hours with perfusion. Before mounting, the tissue was put in cold modified Ringer's solution (mM: 113 NaCl, 25 NaHCO3, 5 KCl, 2 CaCl2, 3 MgCl2, 20 HEPES, 20 Glucose, pH 7.4) for 20min.

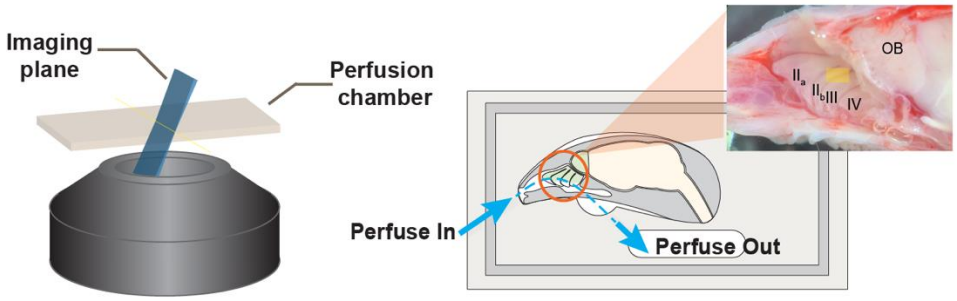

Figure 19 Schematic of intact olfactory epithelium imaging platform for SCAPE microscopy. The SCAPE microscope objective is configured in an inverted layout. A custom-designed glass bottom perfusion chamber was placed above the objective with water immersion. The right half of mouse head was mounted in the perfusion chamber, with olfactory turbinates exposed. The perfusion chamber was designed to control the perfusion flow through the nasal cavity with the inlet at the nostril and the outlet at the throat (blue arrows). Depending on the tissue condition, the field of view typically covers the ventral half of either turbinate IIb or III, and some of the neighboring turbinates (yellow rectangle).

Using this hemi-head, intact in-vitro preparation we are able to image the activity of olfactory sensory neurons in mice expressing the genetically encoded Ca^{2+} indicator GCaMP6f under the OSN specific OMP promoter (OMP-GCaMP6f). This preparation enabled a variety of odor stimuli to be perfused over the intact tissue while recording the simultaneous response of a large number of olfactory neurons layered within the epithelium of the curved turbinates (Figure

20, Movie 10). Mature OSNs express only one allele of an odor receptor gene [48-52], and therefore the response of a single neuron should represent the response of its receptor.

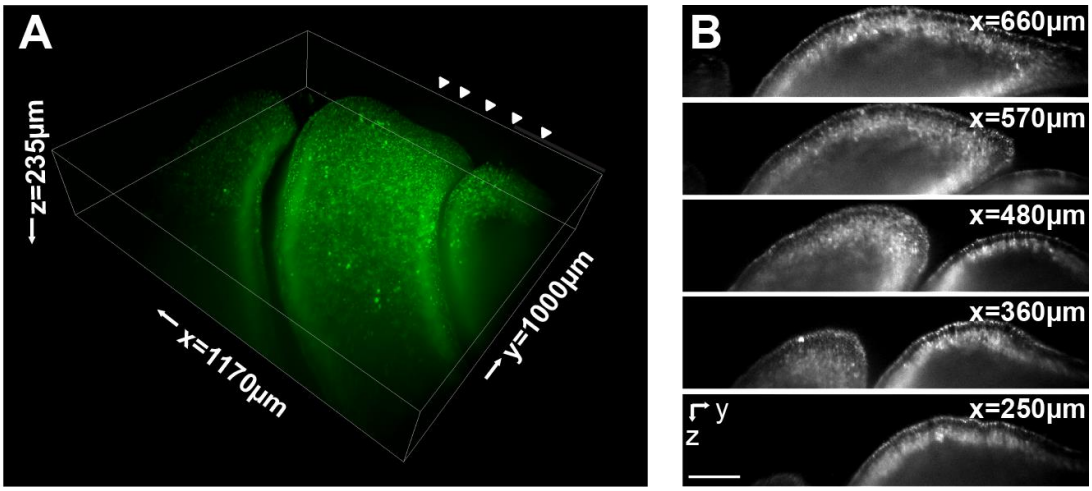

Figure 20 SCAPE Imaging of Olfactory Epithelium with 3D Rendering and Depth Sectioning. (A) 3D volumetric rendering of SCAPE data acquired on the intact olfactory epithelium using our sample prep, showing a field of view of 1170µm×1000µm×235µm. The same volume was imaged for more than an hour at 5 volumes per second (VPS) in the perfusion chamber during sequential odor delivery. (B) 5 different y-z' SCAPE image sections across the volume in (A) with arrowhead pointing. The x-direction scanning step size is 3.6µm. Cellular resolution is achieved and both knob and soma can be resolved across the whole volume. Scale bar = 100µm.

4.2.2 Olfactory Stimulus and Experiment Design

With the sample preparation method described above, we were able to keep the epithelium health for imaging over hours. However, a proper perfusion system which could deliver multiple different odorants to the tissue, with the flow rate stable enough is also needed for the long-term imaging. After trying different perfusion system, we decided to use Agilent 1260 Infinity HPLC system with isocratic pump and auto sampler in the inlet path and a two-way peristaltic pump from Gilson as the outlet path. This perfusion system should offer a relatively stable perfusion flow through the chamber, as well as the ability to automatically deliver different odorant in the perfusion flow.

To test the performance of the perfusion system, we used a fluorescent dye diluted in Ringer's solution as our odor delivery indicator, which was then visualized using SCAPE microscopy. We also had a hemi-head sample mounted in the perfusion chamber, and all the imaging parameters were set to the same as normal imaging experiments. We imaged a 1000x800x220μm FOV at 5 VPS. During the test, we were able to see the exact timing of the dye reaching the sample as well as the washout process post chemical delivery. After trying different odor injection parameters, we set our injection volume of each odor at 100μL, ejection speed at 200μL/min and flow rate at 0.75mL/min. We then synchronized the HPLC with the SCAPE acquisition computer with a hand shack signal to precisely control the timing of odor delivery and image acquisition. In a typical experiment, each imaging trail is 75s long with odorant delivered around 30s. This way we could see both onset and offset of the odor response in the recording.

The odorants used in our study were first diluted in DMSO to make stock solutions, then subsequently diluted in modified Ringer's solution to the desired concentrations, with DMSO concentration at 1-2‰. Most OSNs did not respond to DMSO alone at this level, but we still add a DMSO alone injection at the beginning of all our imaging trials to make sure that the activities we observed is indeed from the odor diluted in DMSO. For the odor mixtures, we always set the concentration of each odor the same as the single compound odor injection. At the end of each imaging session, the adenylate cyclase activator forskolin (50μM, Sigma-Aldrich) was applied to assess the viability of OSNs.

Using this odor delivery protocol, we were able to image the intact epithelium for hours with more than 20 different odor injections including a few structural scans as well. We were able to design different odor sequences for different purposes, including dose-dependent activities and pairwise comparisons.

4.3 Large Scale Volumetric Data Analysis

Using SCAPE microscopy, we were able to image a large volume of intact epithelium at as high as 5 volumes per second, which contains tens of thousands of OSNs in a single acquisition area. The huge improvement of the scanning throughput also came with a huge increase of the volumetric imaging data size, which gave us two challenges in data analysis. For example, for a 75s imaging trial, the raw SCAPE camera spooling data is about 20GB, and for a typical 15 odor injections protocol session, the overall data size is 300GB, which makes it impossible to analyze the data set in traditional ways.

4.3.1 3D Volume Registration

The first challenge we faced was how to properly register all the 3D images we acquired such we could compare the activity of the same neuron across multiple odor injections for the hour-long imaging session. The intact epithelium we imaged was living tissue attached on the surface of delicate turbinates. We realized that during imaging session, the tissue will slowly drift and deformed non-rigidly. In this case, normal 3D drift correction algorithm failed to properly register the data. Therefore, a non-rigid 3D correction algorithm was needed. At the meanwhile, we found that the sample displacement and deformation was very small and neglectable within each trial, we could just take one volume template from each trial and only register across trials, then we could apply the transform function for each template to all frames in each trial separately. This strategy helps us to simplify the large-scale registration problem into a computationally less expensive one.

To resolve the non-rigid registration, we first tried several pre-existing image processing plug-ins in ImageJ, but none of them worked very well. One reason was that the tissue deformation

happens mostly locally, which will easily fail the registration with overfitting. The other reason was that we were using the volumetric images of GCaMP instead of static GFP signal for registration, and the spontaneous activity of OSNs made it very hard to automatically register the volumes with different set of "landmarks" found in each volume. Therefore, we turned to a Matlab based non-rigid motion correction package called NoRMCorre[53]. Based on this package, we developed a semi-automatic motion correction pipeline with manual correction, which works very well for our large scale 3D data.

4.3.2 Neuron Segmentation and Calcium Signal Extraction

The second challenge we faced was how to properly extract the calcium activity from the volumetric GCaMP imaging, since the GCaMP label we used in this study was not receptor specific, the activities of OSNs that overlay might be mixed together. To solve this problem, we utilized constrained nonnegative matrix factorization (CNMF)[54] as our source extraction tool to extract the calcium activity for each OSN.

First, we tried the 3D-CNMF algorithm to handle a small volume after the registration of the concatenated trials which contains 10-15 trials. The algorithm did output the extracted calcium signal of single neuron responding to different odor injections, however, it also extracting out a lot of non-somatic GCaMP signal. Because the GCaMP label we have express in OSNs in not soma or unclear localized but cytosolic GCaMP, such we are also getting GCaMP signal from the cilia knob. And more importantly, the 3D algorithm is very slow which take a long time to analysis the huge volume we acquired.

Taking a step back, the initial main idea of CNMF is to properly separate the neuronal calcium signal from the overlapping neurons as long as they have different temporal activity

profiles in 2D. Though the data we have it real 3D volume, we could also convert it into multiple 2D set to simplify the analysis. Then for each imaging session, after the supervised registration, each 75s trial was then concatenated over time and reduced into multiple 2D projections over 7μm thick depth sub-stacks. 2D constrained nonnegative matrix factorization (CNMF) was then applied to each sub-stack time-series to extract single-cell calcium time-courses and cell locations for each responding neuron [55]. To verify the accuracy of the 3D-2D CNMF result, we compared the extracted calcium activity time course with the raw imaging data by manual ROI selection. The result shown not noticeable difference. Also, we compared the signal of multiple OSNs located at different positions of the volume by manual ROI selection before and after the registration, which help us to validate the registration algorithm as well. An example of the extracted GCaMP signal is shown in Figure 21. Signals from each neuron were then analyzed in the context of their responses to all combinations of odors. In this example, it is immediately clear that responses to mixtures of odors are not a simple linear addition of the responses to the individual odors that compose the blend. To quantify this effect, we define a ratiometric index factor $I_{mod} = (d_2-d_1)/d_2$, where d_1 is the linearly regressed magnitude of peak response to the mixture of all 3 odors and d_2 is the magnitude of the peak response to a pure odor. This index factor could be used for quantification analysis for the cross-odorant modulation in the future.

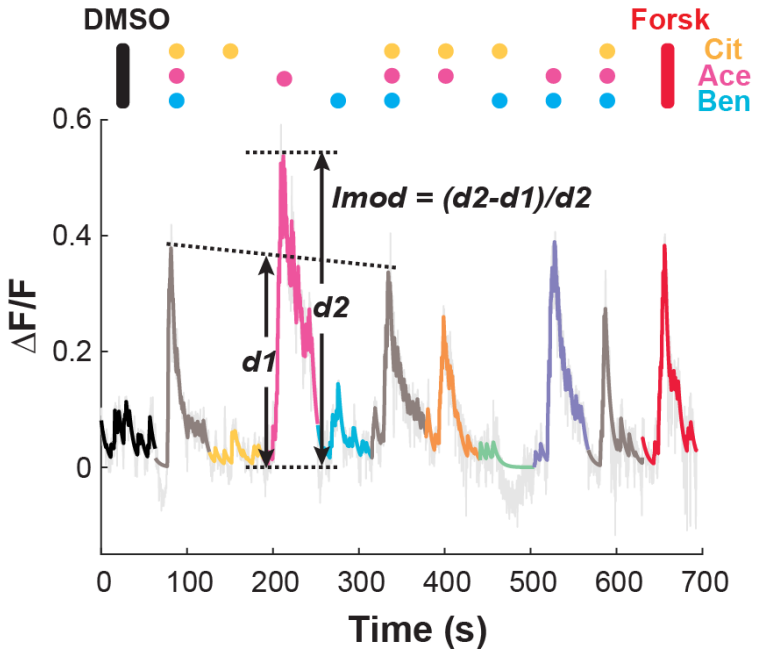

Figure 21 Example Time Course of Single OSN Response to Odor Seqence. Representative GCaMP fluorescence time course of an individual OSN extracted from SCAPE data. Colored and grey traces represent the fitted and raw unmixed ΔF/F from the CNMF algorithm, respectively. The time course consists of 11 concatenated trials. A 30s-long stimulus was delivered in each trial, with a 3.5min time interval (not shown) between each. Odor stimuli combinations are denoted by colored dots at the top. For neurons that were most responsive to one odorant (acetophenone in this case), a modulation index (Imod) was calculated as (d2-d1)/d2, where d2 was the response magnitude to the single odorant, and d1 was the response magnitude to the mixture linearly corrected based on responses to the 2nd and 6st mixture stimuli.

4.4 Non-linear Modulation of Odor Mixture in Peripheral Olfactory System

To test OSN responses to odor blends, we designed two odor sets: odor set 1 contains citral, acetophenone and benzyl acetate, each at 100μM. These odors are common ingredients in perfumery but possess different nuances: citral is described as citrus; acetophenone, the simplest aromatic ketone, often described as almond or mimosa, and benzyl acetate is described as possessing a floral and jasmine scent. Thus, the three components of the mixture are chemically

(Figure 22) and perceptually distinct. All three odors have medium to high odor intensity, which ensures that each of them can recruit a large number of neurons for analyses. Odor set 2 is a specific formula well known to perfumers as a "woody accord" and contains 148μM dorisyl, 48μM dartanol and 127μM isoraldeine. It was chosen both because it is a common blend with a singular perception, and it is chemically quite different from mixture 1. Stimuli were pseudo-randomly presented as the total mixture, each component singly and in the 3 possible binary pairs.

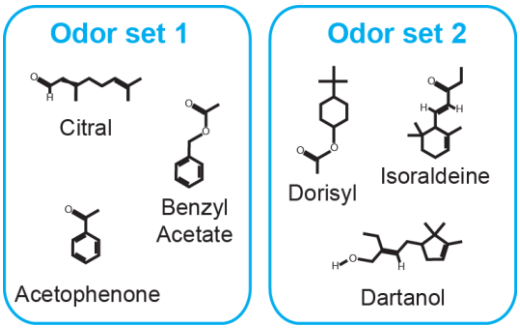

Figure 22 Chemical structures of each component in odor set 1 and 2

4.4.1 Modulation Effects for Odor Blend 1 and 2

Using the method above, we were able to extract the cellular response from more than 10,000 neurons for single recording volume in each mouse. Figure 23 shows data from more than 10,000 cell responding to odor blend 1 among 5 mice. Peak responses of neurons were normalized and plotted in a heat map format. Each row represents the response of a single cell and each column represents an odor stimulus condition. The data were then sorted into 8 subgroups based on response patterns. Here we focused on subgroups II-IV, in which neurons dominantly activated by one of the three individual odors. The neurons in the top rows within these subgroups showed smaller response to the mixture compared to individual odor. This shows clear evident of cross

odor inhibition effect in OSNs. More complex modulation effects could also be observed in the binary odor pairs in different columns of the heat map, as well as in other subgroups.

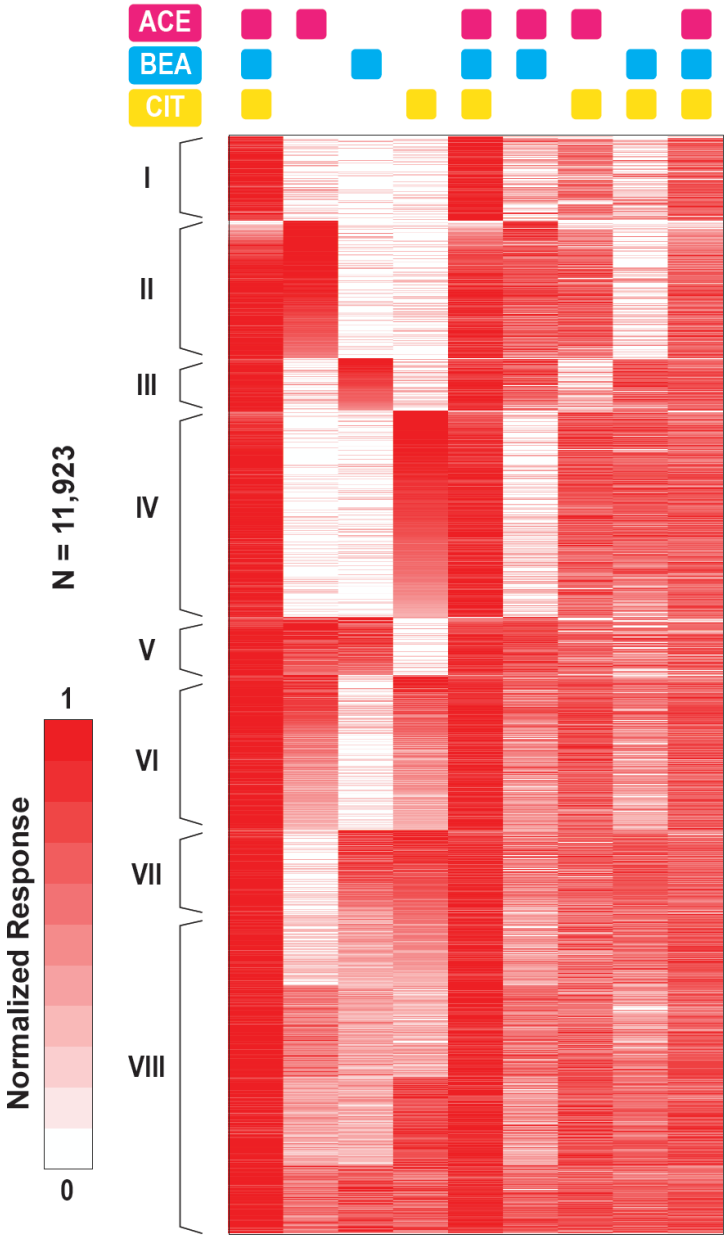

Figure 23 Response profile of odor blend 1. Heatmap of normalized peak responses (N = 11,923, 5 mice) to odor mix 1. Odor stimuli (columns) were given in a pseudo-stochastic manner for each mouse and re-aligned for this presentation. OSNs (rows) were clustered into 8 subgroups (I-VIII). Odor stimuli combinations are denoted by the colored squares at the top.

Similar to odor blend 1, Figure 24 shows data from more than 1,300 cell responding to odor blend 2 among 3 mice. Peak responses of neurons were normalized and plotted in a heat map format. Each row represents the response of a single cell and each column represents an odor stimulus condition. The data were then sorted into 8 subgroups based on response patterns. Similar modulation effects could also be observed on the neurons responding to odor blend 2. The neurons in the top rows within subgroups II-IV showed smaller response to the mixture compared to individual odor. The results showed that this cross-odor modulation effect in OSNs level could possibly be a more generalized mechanism for olfactory response to complex odor mixture.

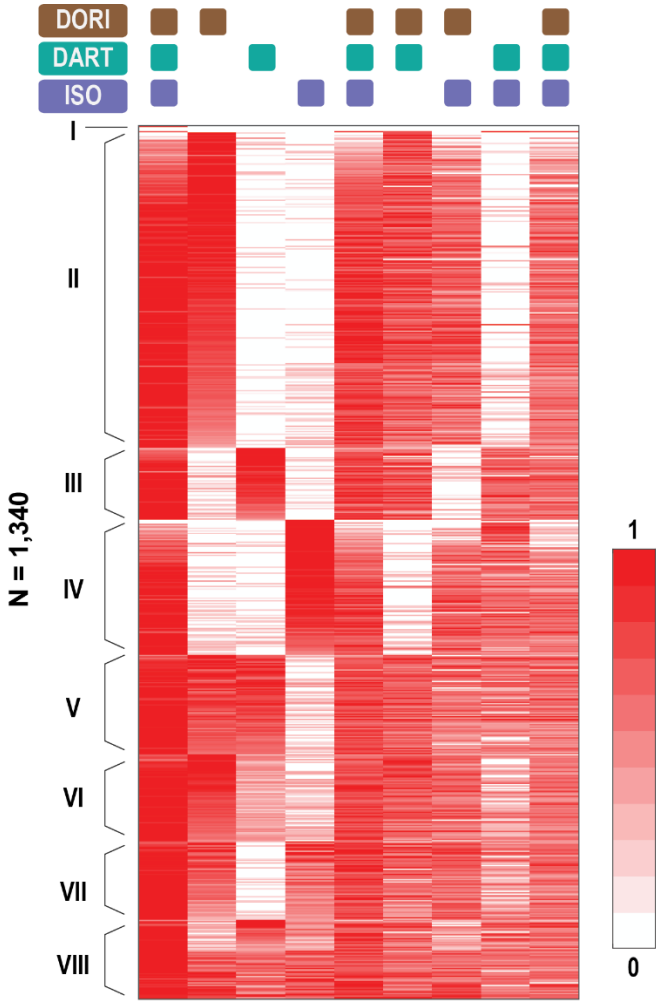

Figure 24 Response profile of the odor blend 2. Heatmap of normalized peak responses (N = 1,340, 3 mice) to the odor mixture 2. Odor stimuli (columns) were given in a pseudo-stochastic manner and re-aligned for presentation clarity. The 8 groups were determined in the same manner as for Odor mix 1.

4.4.2 Dose Dependent Modulation

We interpret these results as evidence for receptor mediated antagonism or partial agonism. Even among binary pairs of molecules within the 3-component mixture, we found significant degrees of suppression as shown in **Error! Reference source not found.**. We thus performed dose response analysis using one of these binary pairs of odors as shown in Figure 25. 648 neurons were found to respond to at least one component of the binary mixture, of which 57 were not activated by

citral. From these neurons, we identified 23 cells that did not respond to 100 µM citral alone, but which did show larger responses to increasing concentrations of acetophenone. Despite evoking no response when applied alone, citral was found to block or reduce the response of these cells to low concentrations of acetophenone. At higher concentrations of acetophenone however, the maximal response level was the same as in the absence of citral. Figure 25A shows example traces. Figure 25B shows aggregate suppression ratios for the 23 cells exhibiting dose-dependent suppression. This result is consistent with a mechanism of dose dependent competitive antagonism. Although these results do not rule out the possibility that allosteric interactions may in some cases be responsible for the observed effects, these interactions are known to be rare among Class A GPCRs and are thus unlikely to underlie the suppression effects observed across all cells and odor mixes tested here.

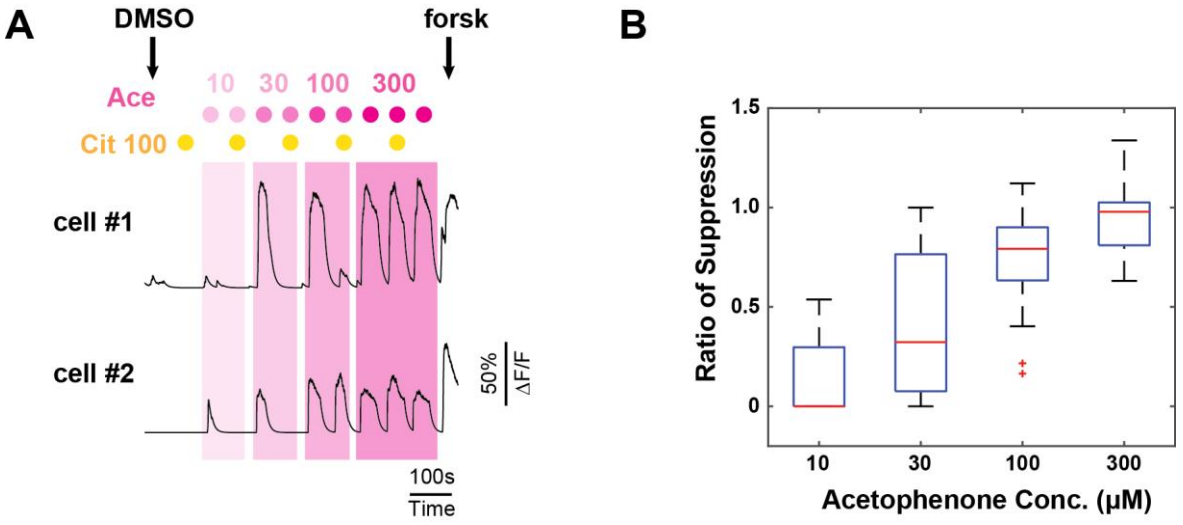

Figure 25 Dose-dependent modulation effect on acetophenone-responsive cells. OSNs were stimulated by increasing concentration of acetophenone (from 10 to 300µM) with or without 100µM citral. 57 OSNs (out of 648 neurons which responded to at least one component of the binary mixture) were not directly activated by citral; among those, 23 exhibited suppression of the response to acetophenone in the presence of citral. (A) Representative time courses of suppressed neurons. (B) Boxplot of concentration-dependent ratio of suppression. For each of the 23

suppressed cells, a suppression ratio at each concentration of acetophenone was calculated as the peak magnitude of the response to the acetophenone/citral mix over acetophenone alone. One-way ANOVA test showed significant difference between groups ($p=5.06\times10\text{-}17$). At 10μM, the median (red line), the third quartile (bottom of the box) and the lowest datum still within 1.5 IQR (bottom whisker) overlapped at 0.

4.5 Discussion

Odor suppression has been well documented in psychophysical study, however, the neural mechanisms underlying these effects remain obscure. Using monomolecular odors as stimuli could help understand the ligand-receptor relations and maps of odor sensitivity in certain specific condition, however, it is limited when natural stimuli is presented with complex blends or mixtures of orders. By screening widespread cell-specific responses to more realistic blends of odors in our study, we demonstrate here that the OSNs themselves are engaged in antagonist and partial agonist interactions with odor molecules, before any further processing of the stimulus at higher levels.

We utilized SCAPE microscopy as a high-throughput 3D imaging and screening method to investigate responses of many intact neurons simultaneously, stimulated with multi component odor blends. This enabled us to screen a much larger number of neurons to reveal this inhibition or antagonism mechanism beyond single receptor level [42, 45-47]. These results revealed a complex interaction of mixtures of odors at the peripheral sensory level, which differs from the commonly accepted idea of a simple combinatorial encoding of odors at this level.

I this study, we only focused on neurons wholes responses to mixture were dominated by one of the three odors within the odor blends. However, more sophisticated analysis could be done based on the response heatmap including modulation between binary pairs and enhancement etc. In addition, more complex experiment with more odorant stimuli could be designed which could

help understanding the molecular mechanism of this modulation effect. Together with the recent work in piriform cortex suggesting a lack of topographical representation [56].

Here, we also demonstrated the new vison brought by SCAPE imaging method when a much larger number of neuronal activities could be observed simultaneously within the intact tissue. The recording throughput was improved dramatically in the order of hundred with better or equivalent temporal resolution, which allows us to observe the neuronal activity at a statistically convincing level without sampling error due to the limited recording bandwidth from the imaging method. The SCAPE imaging and data analysis platform we developed here could also be used to imaging other live tissue or perform a larger scale drug screening.

Chapter 5

WHOLE BRAIN IMAGING OF HEAD FIXED WALKING ADULT DROSOPHILA WITH OLFACTORY STIMULUS

It is an attractive topic to understand functional neuronal circuits across the whole brain. However, from both theory and data analysis perspectives, to acquire and analyze all the neuronal activity in the adult *Drosophila* brain containing about 150 thousand neurons remains a big challenge. Taking advantage of the highly developed *Drosophila* genetic technology and the SCAPE microscopy developed in our lab, we were able to take the first step to understand the cellular activity across the intact adult fly brain. In collaboration with Dr. Richard Axel's lab and working closely with Dr. Evan Schaffer and Neeli Mishra, a postdoctoral fellow and graduate student from Axel lab, we developed an experiment and data analysis platform including an olfactory stimulus and behavior monitoring, which could be used to understand sensorimotor integration by imaging the whole adult fly brain at a high temporal resolution with the ability to extract cellular level calcium activity. The imaging platform and data analysis methods developed for this project could be easily extended to cover more diverse research topics.

5.1 Whole Brain Monitoring of Behaving Adult Drosophila

The neural circuits responsible for a wide variety of computations in the arc from sensation to action involve neurons both distributed throughout the brain and potentially interconnected in recurrent loops. Thus, the ability to simultaneously observe the activity of neurons distributed throughout the brain in a behaving animal, and to do so with sufficient temporal resolution to reveal interactions between these neurons, is essential to understanding the neural basis of these processes. Although great progress has been made in the development of techniques for whole-brain imaging, the ability to do so in a behaving animal has been limited [57], and instead has often relied on fictive behavior in which movement intent is inferred from motor neuron activity in an immobilized animal [58, 59]. The lack of techniques for imaging the entire brain with single-cell resolution in an adult animal engaged in complex behaviors limits the questions that can be asked and the precision with which we can understand the function of neural circuits.

The small size of the *Drosophila* brain makes the study of complete neural circuits possible, from the encoding of sensory input through internal computation to motor output [60]. Moreover, the rich repertoire of well characterized behaviors in the fly make it an ideal model in which to study the neural basis of complex behavior [61]. However, efforts to monitor neural activity distributed throughout the fly brain have been limited in either spatial or temporal resolution. Some approaches were able to achieve a near-whole-brain imaging for adult *Drosophila* by trading off the spatial resolution such as light-field microscopy [62] for head-fixed preparation and wide field tracking microscopy [63] for freely walking *Drosophila* with optical window on the dorsal head. Some other approaches with traditional point scanning method could achieve cellular resolution throughout the whole brain but with poor temporal resolution due to the pixel rate limit of this method [64]. I have previously demonstrated the ability of SCAPE, a novel single-objective variant

of light sheet microscopy, for fast volumetric imaging in larval *Drosophila* and in mice. Here, I demonstrate the application of SCAPE microscopy for volumetric imaging of an intact brain in behaving adult *Drosophila* at single-cell resolution and at rates exceeding 10 volumes per second. These rates allow us to monitor neural dynamics occurring on the time scale of hundreds of milliseconds. By studying the well-known neural circuit such as early olfactory system with SCAPE, we were able to first validate the spatial resolution of this new imaging method. Then further study on the higher-level olfaction related memory, study and sensorimotor integration could be conduct with the same experiment platform and data analysis pipeline. Furthermore, more sophisticated study such as the hidden brain state and global modulation circuit could be achieved with high speed whole brain imaging using SCAPE microscopy.

5.2 Experiment Design and Setup for Head-fixed Adult Drosophila

My goal of this project is to image the brain wide calcium activity of the adult *Drosophila* with proper odor delivery and behavior monitoring. To achieve this, 3 submodules are needed which are: a head plate and proper sample mounting system for the head-fixed adult prep; an odor delivery system which is synchronized with SCAPE microscopy and could be used to delivery different odorant during the imaging; an air-suspended ball tracking system for the fly to walk on during the imaging, which is also compatible with the head plate and the odor delivery system. The odor delivery system and the fly walking system could be controlled by Arduino which could be easily integrated with the current SCAPE controller software with serial communication as shown in Figure 26.

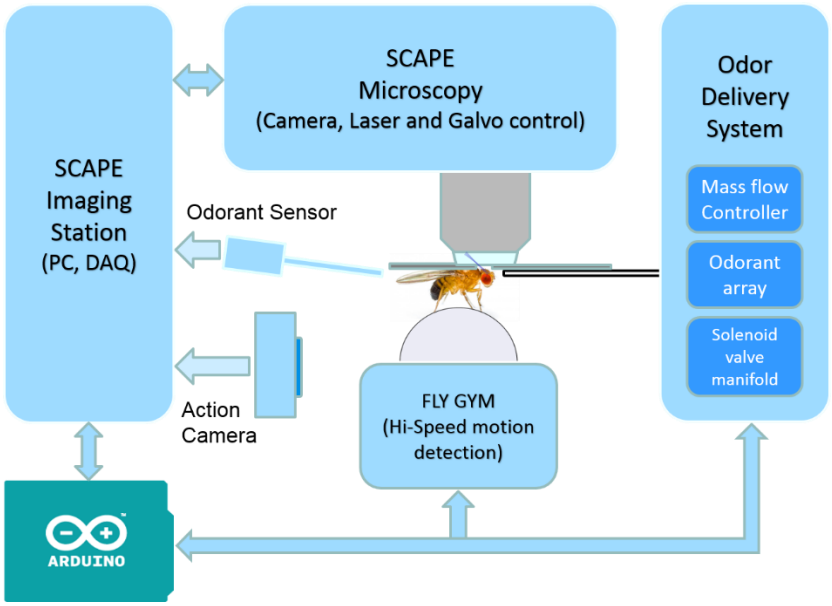

Figure 26 Schematic of the Close-loop Fly Experiment Setup. In the experimen setup, the fly is mounted head-fixed undernerth the SCAPE microscopy which the brain is exposed for imaging. A odor delivery tube is postion in front of the fly which delivers a constant air flow to the fly and deliver different odor to the fly during the imaging session. A air suspended plastic ball with tracking system is positioned below and fly properly for the fly to walk on. Both the ball moving trajectary and the odor delivery are controlled and recorded by Arduino which communicated to the SCAPE PC. A separate high-speed IR camera is also positioned around the fly to record the locomoton during the SCAPE imaging.

5.2.1 Head-fixed Fly Preparation

Before I started to design a customized head plate to image the adult fly using SCAPE microscopy, I tried the standard head-fixed adult fly prep, which is used in electrophysiology and two-photon imaging. To achieve the best accessibility and visibility of the brain, it is very important to know how the fly head should be positioned under the SCAPE objective and how much of the cuticle of the fly head needs to be removed during our surgery. It is also important to check whether we could resolve the cellular level calcium activity and what is the depth limit for our single photon excitation in the scattering fly brain.

In the regular imaging prep, the adult fly is mounted on a tape-bottom petri dish and the head is fixed and hold in position by another thin layer of tape. A small window is opened through the top of the head and the cuticle is removed to expose the brain. The fat and the trachea over the brain is removed for better optical accessibility and the brain is bathed in standard *Drosophila* extracellular saline as shown in Figure 27. Muscle 16 is cut to reduce the brain motion during the imaging.

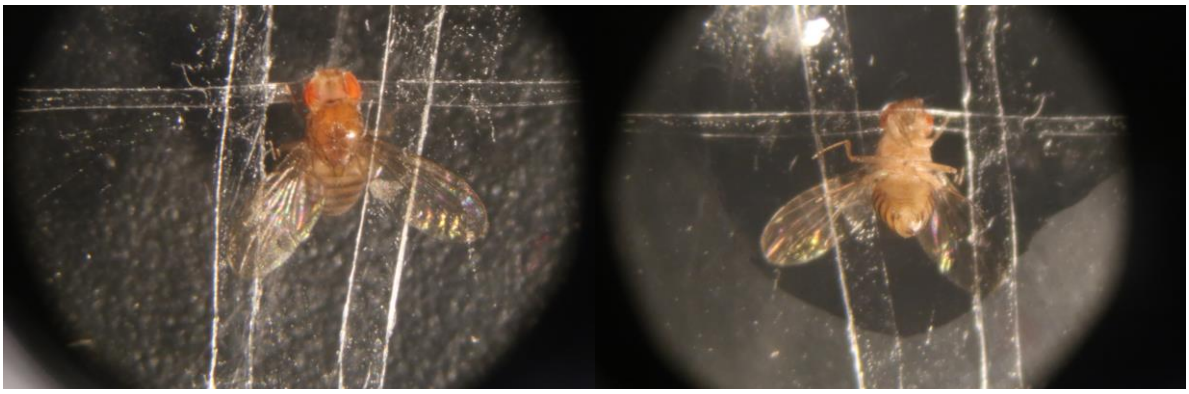

Figure 27 Image of the Traditional Imaing Prep. The top view is on the left showing the exposed brain and the bottom view is on the right showing the fixated head with un-constrained legs.

The fly we used in the pilot experiment is a pan-neuronal GCaMP6 labelled with static dsRed expressed in all the Kenyon cells of the mushroom body (yw;UAS-GCaMP6f,MB-dsRed;Nsyb-Gal4). With this fly, we were able to check the resolution by looking at the small Kenyon cells in the red channel while checking the deep brain region GCaMP activity in the green channel. By rotating the sample at different angles, I found that having the light sheet entering the brain from the anterior edge of the brain window would give a better penetration depth and the best access to the entire brain except for the optical lobe, which could not be access without removing the retina from the dorsal side of the animal. Because the light sheet of SCAPE is oblique, it is better to have a slightly wider opening above the region of interest. It is much easier to clear the anterior region of the brain since we also need that to cut muscle 16. Meanwhile, we would

still need to make the posterior side of the window as big as possible which also helps accessing the calyx which is close to the posterior surface of the brain.

After the preliminary measurements, I started to design, and 3D print the fly head plate. The head plate should be designed to be mounted on a XYZ manipulator which could be used to position the fly on the behavior rig later on. And a low-profile design is preferred to have a better access to record the locomotion using a high-speed camera. After trying with different materials, I finalized the design as shown in Appendix A.3. A mounting adaptor to hold the head palate to the manipulator was also designed and 3D printed at the same time. The head plate can also hold about 2mL of saline which was tested to be sufficient for hours long imaging without perfusion.

With the new head plate, a plastic tape of a metal sheet could be placed on the well and the rest of the surgical process is similar to regular imaging prep except that an extra-large area of cuticle needs to be removed for better optical accessibility.

5.2.2 Odor Delivery System

For the olfactory stimulus, we needed to design and build a simple olfactometer that could be used to deliver different odorants to the fly during the imaging session. There is a special requirement for the olfactometer used for *Drosophila,* the output air flow needs to be constant during the whole delivery period since the fly is very sensitive to the change of air flow and we do not want to induce a second variable during the stimulus input. However, we did not need a sophisticated odor delivery system which could deliver the odor in arbitrary concentration waveform, a multi-channel capability is more important for us to observe the varied activity of olfaction dependent on brain wide activity.

We designed and built an 8 channel olfactometer. To keep the constant flow output, I used two mass flow controllers (Aalborg Compact Gas Mass Flow Controller, 0-200 sccm, and 0-500 sccm) which control the air carrier flow and the odor carrier flow independently. And dummy channel is added in one of the odor channels which keep the odor path on for the whole time. Two sets of 8-way manifold (The Lee Company, 8-way faced mount) with 3-port solenoid valves are used in the odor path before and after the odor bottle, and digitally controlled by Arduino. An extra filter was added at the inlet and outlet port of the odor bottle to minimize the cross contamination. Before using the system, all the odor bottles should be flushed with the odor path air flow. This helps balancing the pressure of all the channels and reduces the sudden pressure change during the channel switch.

The Arduino controls the 16 solenoid valves by switching each channel of the custom designed driving board, 8 channel each. The Arduino is communicating with the SCAPE control software through a USB port and triggering with the camera start signal. The parameters including trial length, odor type, onset time, delivery duration, inter-stimulus interval, trial repeat time and odor type sequence, could be customized by the stimulus editor GUI embedded in the SCAPE control GUI.

A proper odor detector is also necessary for an olfactometer. We used an inexpensive regular carbon monoxide & flammable gas sensor (MQ-9) as the replacement of PID in this case. To test its performance, I custom designed an adaptor which mount the odor sensor right before the PID, as shown in Figure 28, and then compared the recorded signal for different odor deliveries. The result shows that the gas sensor is sufficient to detect both onset and offset time of the odor stimulus while showing poorly performance to detect the odor concentration profile due to its big time constant, for both raising and falling edge, and different odor does activate the sensor at

different amplitude. This is sufficient for the experiment in which the timing of the odor stimulus is critical while the concentration profile is less important. The full part list is available in Appendix A.2.1.

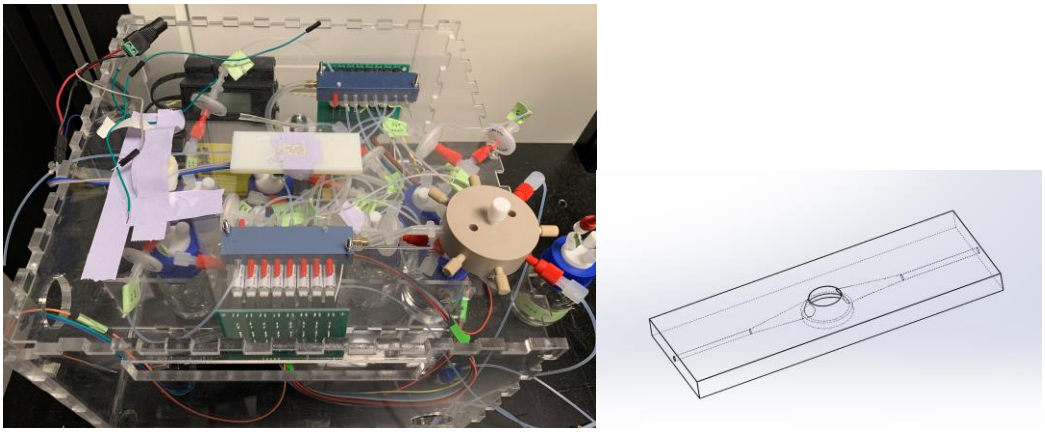

Figure 28 8-way odor delivery system and the Odor sensor adaptor for PID.

5.2.3 Fly-Gym: Air-suspended Ball Tracking and Locomotion Monitoring

The standard way to monitoring the adult fly walking behavior is to use an air-suspended ball for the fly to walk on and then precisely tracking the motion of the ball to get the walking trajectory of the fly walking. Despite the demonstration of prior Fly-walker systems, the common solutions are large, difficult to implement, and incompatible with a number of imaging and electrophysiology configurations. They can also be challenging and cost-prohibitive for labs to construct. Therefore, there is a demand for an inexpensive and simple closed-loop experimental setup capable of delivering stimuli and tracking behavior to investigate the neuronal circuits in *Drosophila* melanogaster. Working with the research assistant Katie Yang in the lab, we were able to develop a compact, low-profile, Arduino-based open source platform for monitoring locomotive behavior of a fly walking on a floating ball for less than $100. The platform is compatible with various stimulus delivery systems. The most important part in this system is how to track the motion of the ball precisely. We used the ADNS-9800 LaserStream gaming sensor (Avago

Technologies), which offers adjustable resolution up to 8200 counts per inch (cpi) and high update rate up to 12000 fps. Also, the firmware for Arduino is freely available as open source resource. The Arduino communicates with the imaging acquisition workstation with a Matlab based GUI, which is used to record the sensor readout and display the walking trajectory in real-time.

To keep this system easy to assemble and utilize, we minimized the number of components needed. Most of the parts can be easily purchased online, the treadmill holder is 3D printed and the acrylic box is laser cut. All the parts are designed to be self-aligned, which makes it easy to assemble as shown in Figure 29. The overall cost of the system is less than $100.

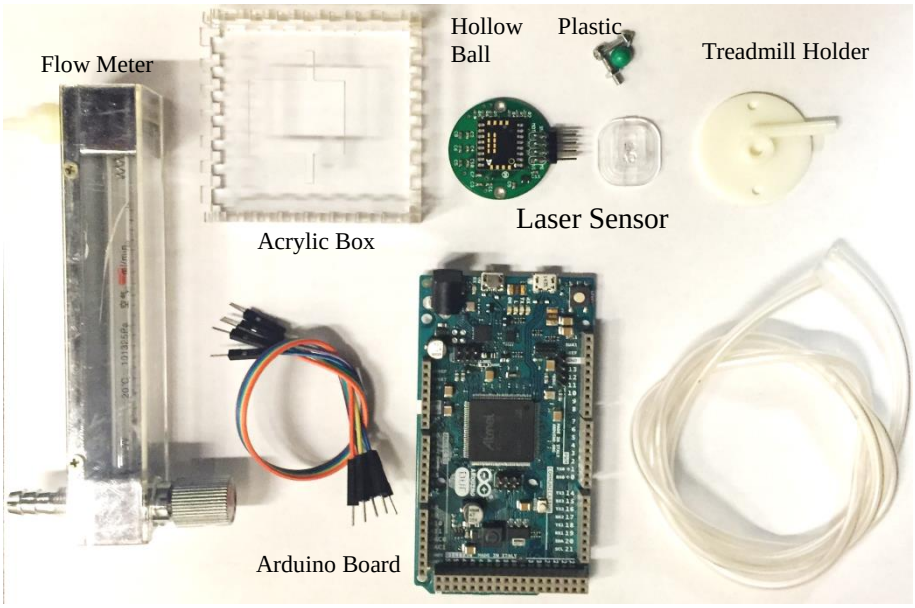

Figure 29 Assembly Parts for the Fly-Gym

A 6 mm diameter hollow plastic ball (weight about 90 mg) is supported on a cushion of air brought in through external tubing in Figure 30. The conical shape of the treadmill holder's central chamber ensures that the ball floats undisrupted without noticeable vortex interruption. The mount is screwed onto a PCB with an IR emitter/sensor pair that serves to track the motion of the ball. As the holder rests on the lens of the IR sensor, the system is inherently self-aligning. To test

whether the ball is suspended well enough for fly walking, we positioned a tethered fly on top of the ball. The fly was able to walk as normal and we were able to trace the trajectory as well.

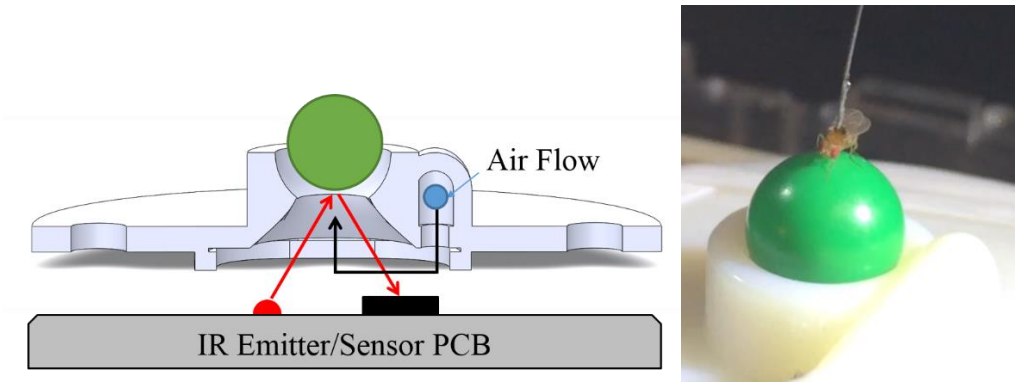

Figure 30 Longitudinal View of Ball Holder and the Photo of Fly Walking on the ball

As the ball holder sits directly under the lens, no extra alignment is needed for the system, but a proper calibration is still needed to get a precise readout of the walking trajectory. Accurate calibration requires proper alignment of the ball to the ball holder at the same time as the air-suspended condition. To do so, we also designed a separate holder for calibration purposes, shown in Figure 31, that used a stepper motor to apply controlled rotation to the plastic ball. This allowed us to find an accurate conversion factor between the counts on the sensor and the distance that the ball rolled. We tested the system with different motor speeds to get a calibration factor to convert the count readout from the sensor to real distance. Also, we tested the system with different height displacements and counts per inch (CPI) which indicates that the system is robust to slight misalignments of the assembly.

The height of the assembled system is less than 24mm including the floating hollow ball, allowing it to fit onto most commercially available microscope stages. The sampling rate of the high-speed laser sensor can go up to 12000 Hz with 8200 counts per inch precision.

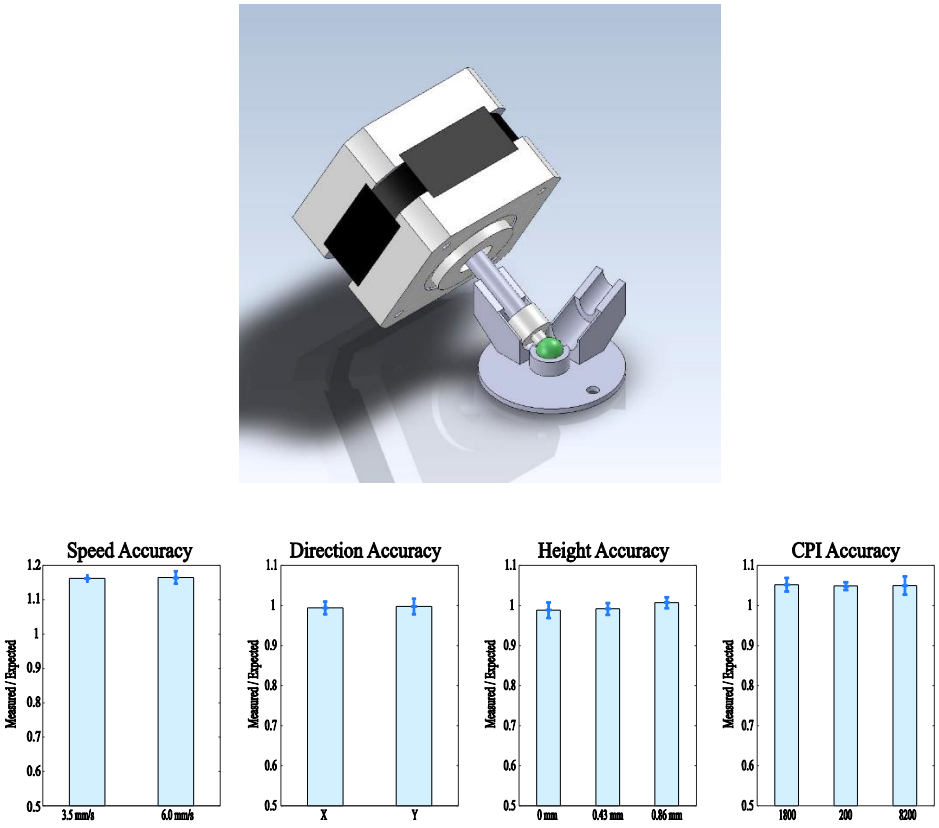

Figure 31 Schemetic of the Calibration Setup and the Calibration Results.

In addition to the ball tracking system, we also set up a high-speed camera close to the fly to record the potential locomotion of fly during the imaging. A long working distance micro lens was mounted in front of the camera which allowed us to put the camera away from the fly. An IR filter was used to block the blue excitation light, which work with a separate IR LED as a light source of the camera. The camera is triggered and synchronized with the SCAPE control software as well and it spools the data directly to the imaging acquisition workstation. The full part list is available in Appendix A.2.2.

5.3 Optimization and Characterization of Whole Brain Imaging

A Having designed and built the restrain and the odor delivery systems it was time to characterize the performance of SCAPE microscopy for whole fly brain imaging. First of all, I chose two dual color sparse label fly lines with the fine dendritic and axonal terminals labelled, which could be used to characterize the resolution. The two fly lines are *Mz19-Gal4; UAS-GFP, MB027B-dsRed* and *85e04-Gal4; UAS-GFP, MB027B-dsRed*. We also used the confocal atlas to perform a direct comparison of the imaging resolution as shown in Figure 32. The cellular resolution was achieved while the axon terminal projection can also be observed with sufficient resolution at both channels. The 3D rendering shows the unique ability of SCAPE to image the whole 3D volume. The field of view in this image is 450x265x180um and the acquisition time is less than 0.1s for the entire volume, using SCAPE, which is much faster than for standard confocal imaging.

The second test I performed for resolution characterization was to use the denser nuclear localized fluorescent label which could help us understand whether we have enough resolution to resolve the activity of neighboring cells as well as in the deep brain region. The fly line we used for this purpose was *UAS-GCaMP6f; UAS-RedStinger, Fru-Gal4,* in which GCaMP6f and nuclear-bound dsRed are expressed within the male-specific fruit fly neuronal subset consisting of 2% of the male nervous system. I first performed the imaging in vivo using our customized head plate and then made a dissected brain slice and imaged the same sample at SCAPE microscopy and confocal microscopy to be able to compare side by side. The imaging results are shown in Figure 33 and Movie 11. In the SCAPE-confocal comparison, depth-encoded color projection is used to represent the depth information in a 2D image. Both images show cellular resolution for neuropil and nuclei label throughout the whole volume with the field of view of 800x420x120μm, while acquisition times using SCAPE were much shorter. The 3D rendering shows the in vivo images of

the same fly line, where the single cell resolution can be achieved in the intact scattering tissue as well as across a big portion of the brain.

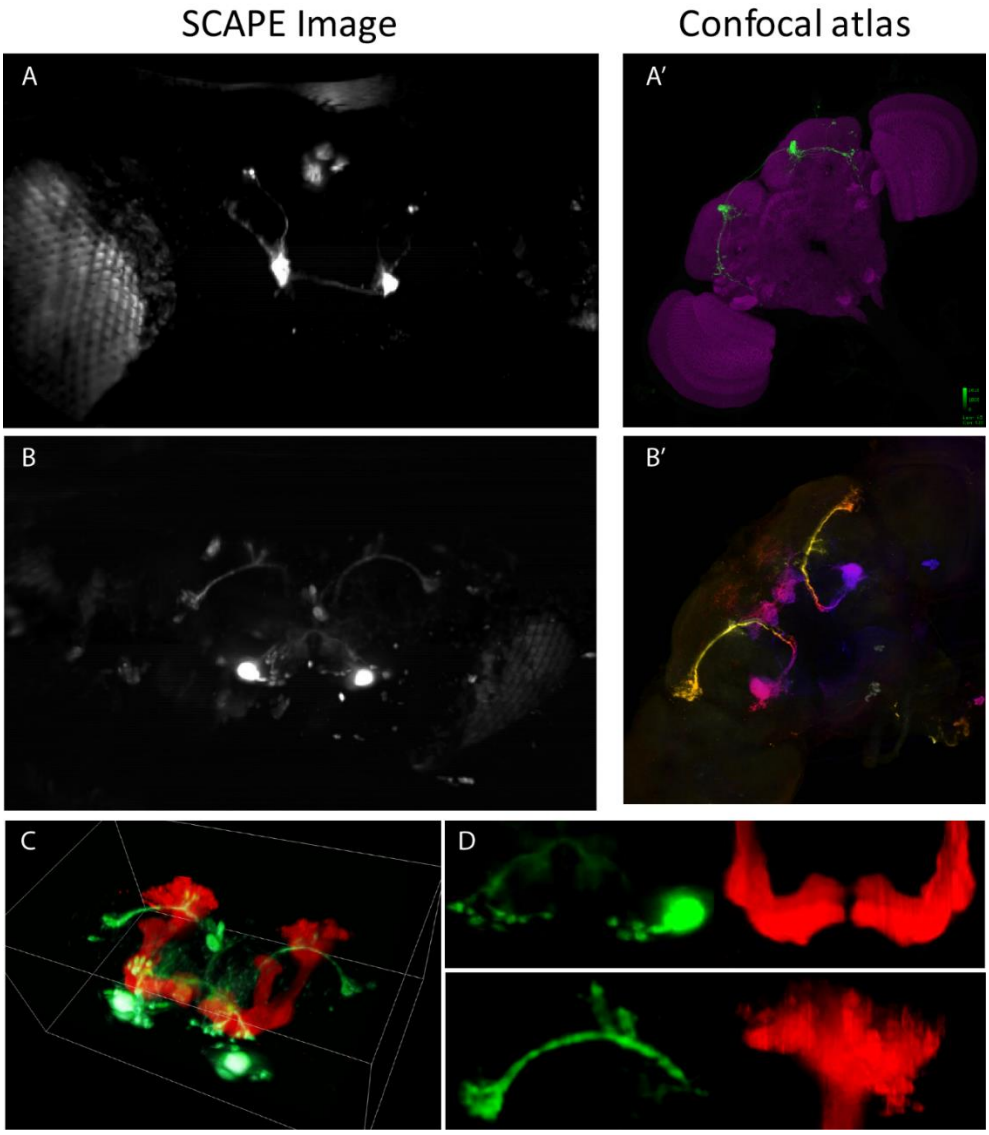

Figure 32 SCAPE Imaging of Sparsly Labelled Fluorescent in Adult Fly Brain. (A, A') Comparison of the maxiumun intensity projection between SCAPE imaging and confocal atlas scan in green channel for fly 85e04-Gal4; UAS-GFP, MB027B-dsRed, where 6 neurons are labelled with GFP and the kenyon cells in the mushroom body is labelled with dsRed. (B, B') Comparison of the maxiumun intensity projection between SCAPE imaging and confocal atlas scan in green channel for fly Mz19-Gal4; UAS-GFP, MB027B-dsRed, where projection neurons in two glomeruli are labelled with GFP and the kenyon cells in the mushroom body is labelled with dsRed. (C) Dual color 3D Rendering

of whole-brain SCAPE data in (B). The field of view of 450x265x180um was acquired using SCAPE microscopy in 0.1 sec. (D) Maximum Intensity Projections of Green/Red Channels in smaller ROI. In green channel, the soma of olfactory projection neurons, glomeruli and axonal projections can be seen. In red chanel, β/γ lobes of the mushroom body, and Kenyon cells in calyx can also be resolved.

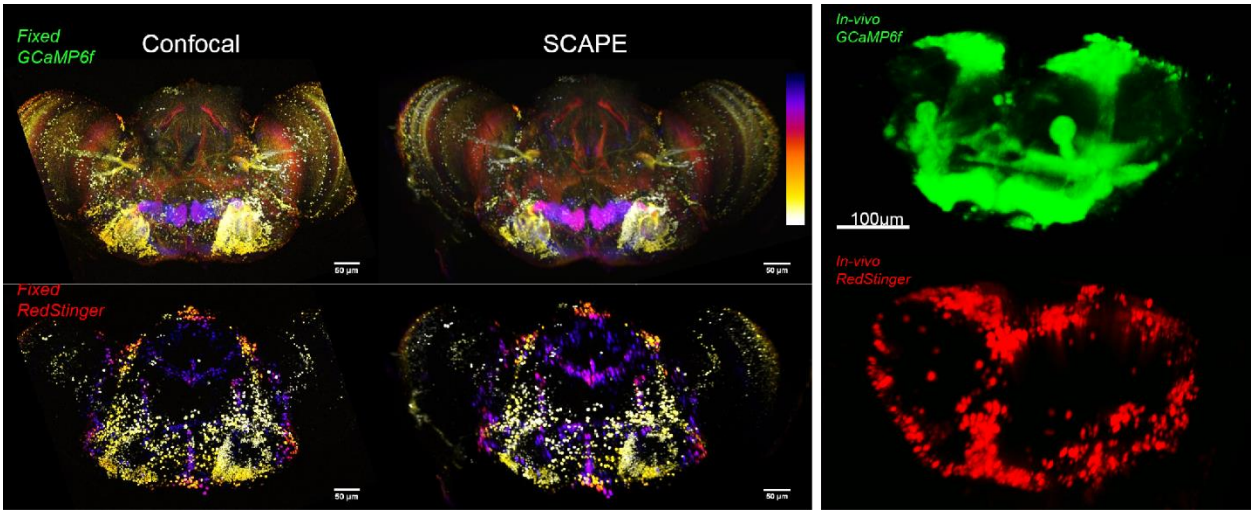

Figure 33 SCAPE Imaging of Nuron Subset In Adult Fly. Depth-encoded color projection is used to compare between confocal and SCAPE imaging of the dissected brain slide of *UAS-GCaMP6f; UAS-RedStinger, Fru-Gal4*. In the left panel, the dissected brain was image using Zeiss confocal microscopy in about 2 minutes. In the middle panel, the same sample was imaged using SCAPE in less than 1 second. Both images show cellular resolution for neuropil and nuclei label throughout the whole volume with the field of view of 800x420x120µm. On the right panel, the 3D rendering of the same fly line imaged in vivo is shown in green and red channel separately.

5.4 Large Scale Data Analysis for Whole Brain Drosophila Imaging

After characterizing the resolution of whole brain in-vivo imaging of adult fly, we were able to start imaging the fly with the olfactory stimulus and monitoring the walking behavior at the same time. However, as with all the other SCAPE microscopy experiments, we had to face the challenge of data analysis. The two biggest challenges for analyzing the whole brain functional SCAPE data being motion correction and GCaMP activity extraction.

5.4.1 Motion Correction for Dual Color 3D Data

Unlike the 3D volume registration problem which we had with the mouse olfactory epithelium data, the motion artifact of the fly brain data involves a much higher frequency component. We could see that the brain was moving within the field of view during the whole the experiment and at a rate of a 0.5-2 Hz. Although the cuticle structure of the head is fixed steady on the tape mounting surface, the brain itself could still move a bit since the adult fly brain is not fixated at any solid supporting structure and is just covering by the cuticle inside the head. Especially when the fly is walking on the ball, all the movement from the body will also affect the brain which induces motion artifacts. Based on our tests we calculated that to capture the motion artifact, we would need more than 8 volume per second imaging speed. To properly correct the motion artifact in the huge 3D volumetric time series data, we tried once again NoRMCorre.

We normally imaged the flies in two colors with fluorescent labels in the same or different sets of neurons. Most of the time, the red channel was used to image static fluorescence like dsRed or RedStinger. We tried to use the NoRMCorre algorithm for both green and red channel at first, and we did realize that the red channel worked much better than the green GCaMP channel. The reason might be the dynamic changes in fluorescence from the GCaMP channel failed the algorithm when we performed the registration in the frequency domain, while the red channel is much more stable. Because the two fluorescent channels are co-aligned with each other, we could apply the same motion correction translation from the static red channel to the green channel. However, even the correction based on the red channel was still not perfect since there was also quite a lot of auto fluorescent signal in the images. Auto fluorescence tends to be quite noisy, so I applied thresholding for the red data we fed into the NoRMCorre algorithm, which got rid of most of the auto fluorescent background as well as some dim fluorescent signal from the neurons. But

the threshold is carefully set to keep the landmark signal across the whole brain region, otherwise we would not be able to correct the region which is completely thresholded to 0. Then we applied this correction translation to both channels and got the corrected volumetric SCAPE data, which is ready for further analysis.

5.4.2 Dimensionality Reduction and Calcium Activity Analysis

Analyzing the very sparsely labelled functional data in the adult fly brain is trivial, since the resolution we have shown in Section 5.3 makes it straightforward to get the GCaMP dynamic at cellular level. To take the full advantage of the SCAPE microscopy, we would like to image a much larger number of neurons across the whole brain which could actually help understand the functional connectivity of the adult fly brain.

First of all, to have a general idea of how the whole brain responds to our olfactory stimulus, we tried imaging the pan-neuronal labeled cytosolic GCaMP3.1 fly line, *yw122; UAS>>GCaMP3.1; Nsyb-Gal4*. The whole brain was imaged at 10 volumes per second over a field of view of 625x282x165 μm. Each volume was acquired in 0.1 sec with 90 steps taken across the volume with a step size of ~1.8 μm. The volumetric GCaMP imaging data is shown in Figure 34. We are able to circle the ROI in 3D space based on the anatomical map of the fly brain and to extract the activity of different brain region of neuropil. Taking advantage of the high temporal resolution, we could also resolve the onset timing difference between different brain regions. After extracting the $\Delta F/F$ across the whole 3D volume and across the whole imaging period, we were able to render the active region responding to the stimulus and then map to the anatomical map of the adult fly brain to identify the corresponding region as shown in Figure 35.

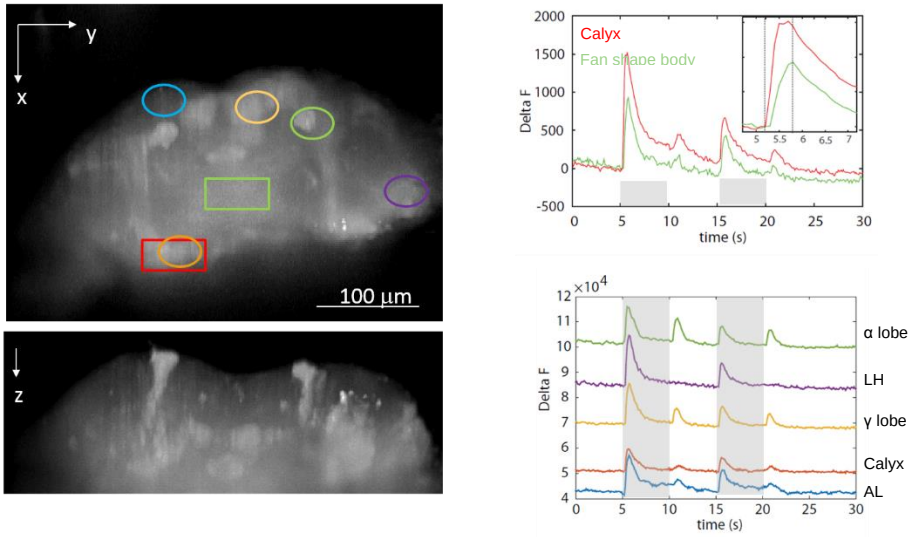

Figure 34 SCAPE Imaging of Pan-neuronal Labelled GCaMP Activity and Example of Time Course in Different ROI. Topview and sideview maximum intensity projection of the whole brain volumetric imging after the presence of odor stimulus. The colored ROI is mannually selected based on the prior annotomical knowledge and the corresponding time course across the 30s imaging peiod with two 5 second octonal stimulus delivered at 5s and 15s.

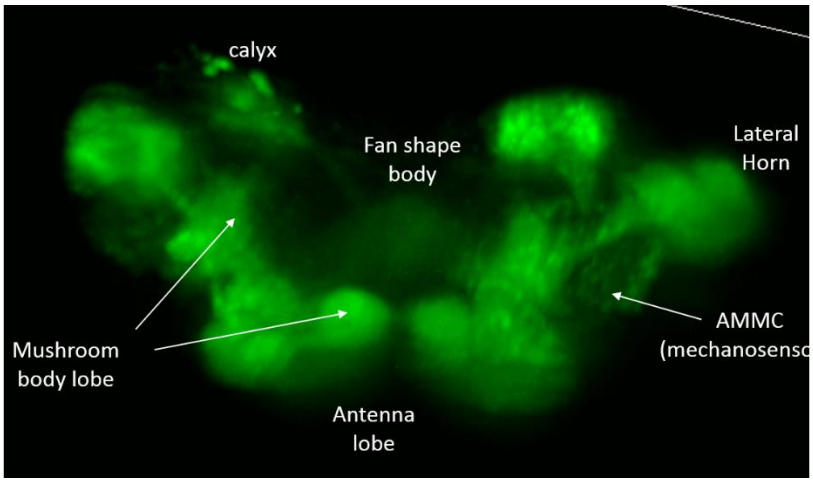

Figure 35 3D Rendering of the Active Brain Region during the Olfactory Stimulus. The ΔF/F is calculated across the whole volume and the time porjection is applied for the stimulus period to get the reaponse 3D map, which is then renered in Amira. Different responding region could be also regonized based on the annotomical map.

Though we are able to pull out the calcium activity directly through the SCAPE acquired data itself, we were not able to extra the cellular level neuronal activity by simply picking up the ROI. To pick up the cellular level we would need also properly correct any motion artifact, otherwise the motion itself might be treated as fluorescence change of the GCaMP activity. For this reason, the flies used after the preliminary experiment all co-expressed static red fluorescence.

In the experiments with proper odor delivery and data analysis the line used is the same one we used for the resolution characterization, *UAS-GCaMP6f;UAS-RedStinger,Fru-Gal4*, which expresses GCaMP6f and nuclear-bound dsRed within the Male-specific fruit fly neuronal subset consisting of 2% of the male nervous system. During imaging, 2 stimuli were delivered over a 40 second run: a 3 second octonal pulse at 5 seconds and a 3 second male specific pheromone pulse at 25 seconds. About 50 male flies were kept in a bottle as the pheromone source. The imaging field of view is 450x340x150μm and the 3D volume was imaged at 10 VPS. After motion correction using the nuclear localized red fluorescent signal, we were able to start analyzing the GCaMP data. Compared with the pan-neuronal GCaMP data, the Fru-GCaMP data looks much sparser, so I thought to try CNMF, which is used to analyze the mouse olfactory epithelium data (see Section 4.3.2). The 3D rendering of both the green and red channel is shown in Figure 36, together with the analysis result. When I first used the CNMF algorithm, the 3D version wasn't working well initially, which might be due to the size of the data. Then using a similar trick to the one used for the mouse epithelium, I made 2D projection of the GCaMP data and applied the well-established 2D CNMF algorithm to it, which work out very well. More than 100 components were extracted, and we did find stimulus correlated neuronal activity across the brain while the components can also be found and match when checking with the 3D volumetric GCaMP imaging.

Among the components I found, some were odor specific neurons which could lead to further experiments to understand this male specific circuit.

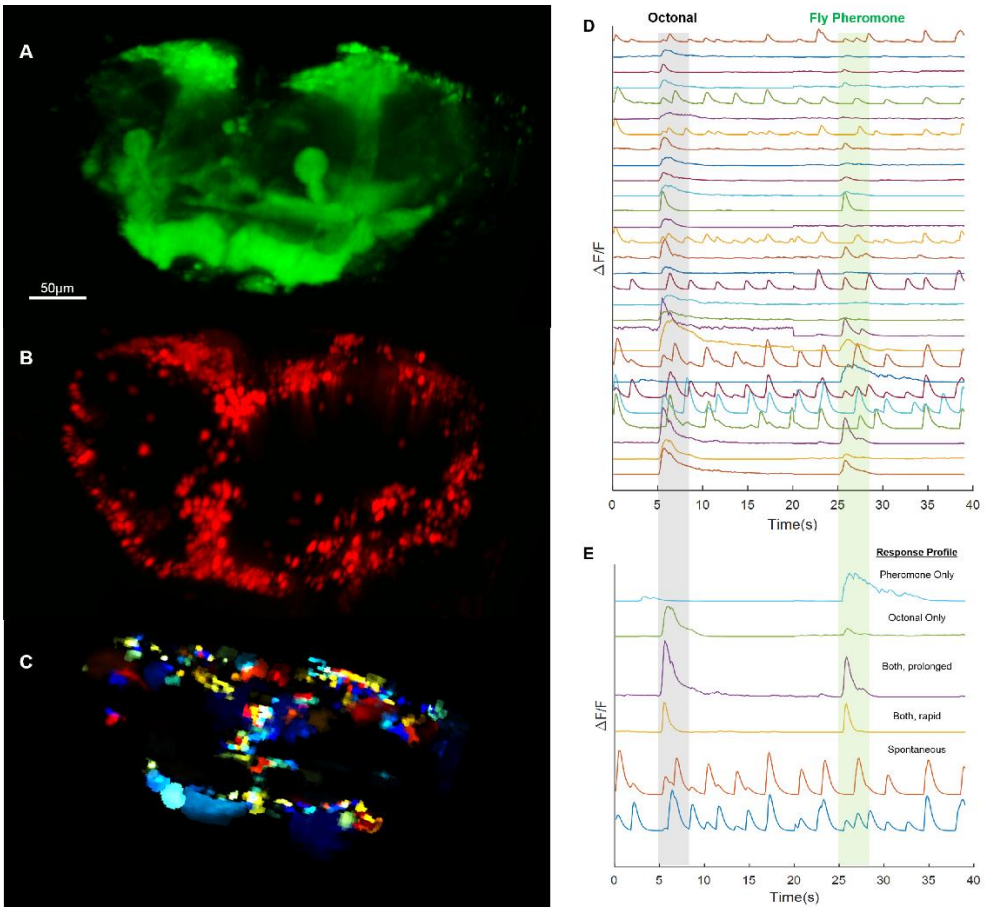

Figure 36 SCAPE Imaging of Fru-GCaMP-RedStinger and CNMF Based Analysis. GCaMP6f and nuclear-bound dsRed are expressed within the Male-specific fruitless neuronal subset consisting of 2% of the male nervous system (UAS-GCaMP6f; UAS-RedStinger,Fru-Gal4). A field of view of 450x340x150µm was imaged at 10 VPS. (A,B): Both green and red channels are rendered in 3D with Amira. (C) CNMF source extraction was used in the projection view to isolate single neuron activity. The red nuclear marker can be used to localize the soma of every labelled neuron and help separate the GCaMP signal at the soma. (D) 2 stimuli were delivered over a 40 second run which is indicated with color bar in the time course. 29 randomly picked neural time courses from the source extraction algorithm are shown. (E) We show a subset of the 29 neuronal responses shown in (C). As expected, different neurons have different odor response profiles. The speed at which cellular-specific activity is acquired can allow identification based on a number of parameters (ex: onset, phase and frequency response).

However, as shown in the figure above, CNMF failed to pull out the neuropil activity since they are much bigger in space which broke the segmentation constrains set in the algorithm, so we started thinking what the next step in our experiment could be. On the one hand, we could completely ignore the neuropil dynamic for now and focus on the soma level calcium dynamic, which could be achieved by using nuclear localized GCaMP labelling. On the other hand, since the neuropil dynamic is a critical computational module in *Drosophila* brain and contains a lot of information which could not be resolved based on the somatic signal only, we should still work on other data analysis methods or try a modified version of the CNMF algorithm.

It is quite straightforward to image the nuclear localized GCaMP since it is similar to the nuclear localized RedStinger we used previously to test the spatial resolution aspect. With help from the Axel lab, we were able to construct a fly line with Nuclear-localized GCaMP6s and RedStinger co-expressed with the synaptobrevin driver (*UAS-NLS-6s, UAS-RedStinger, nSyb-Gal4*). After extracting ΔF/F across the whole volume and perform the time projection during the Stimulus period, we were able to see the odor specific response directly, using 3D rendering or 2D projection as shown in Figure 37. Also, for the single odor trial, we try PCA analysis across the whole volume which gets the pixel wise components correlated with the stimulus onset. Interestingly, delayed and anti-correlated components could also be found with this analysis which might related to down-strain neuronal circuit or inhibitory circuit. We are also working very close with the Flatiron institute to optimize the 3D CNMF algorism to work efficiently in our large scale SCAPE imaging data.

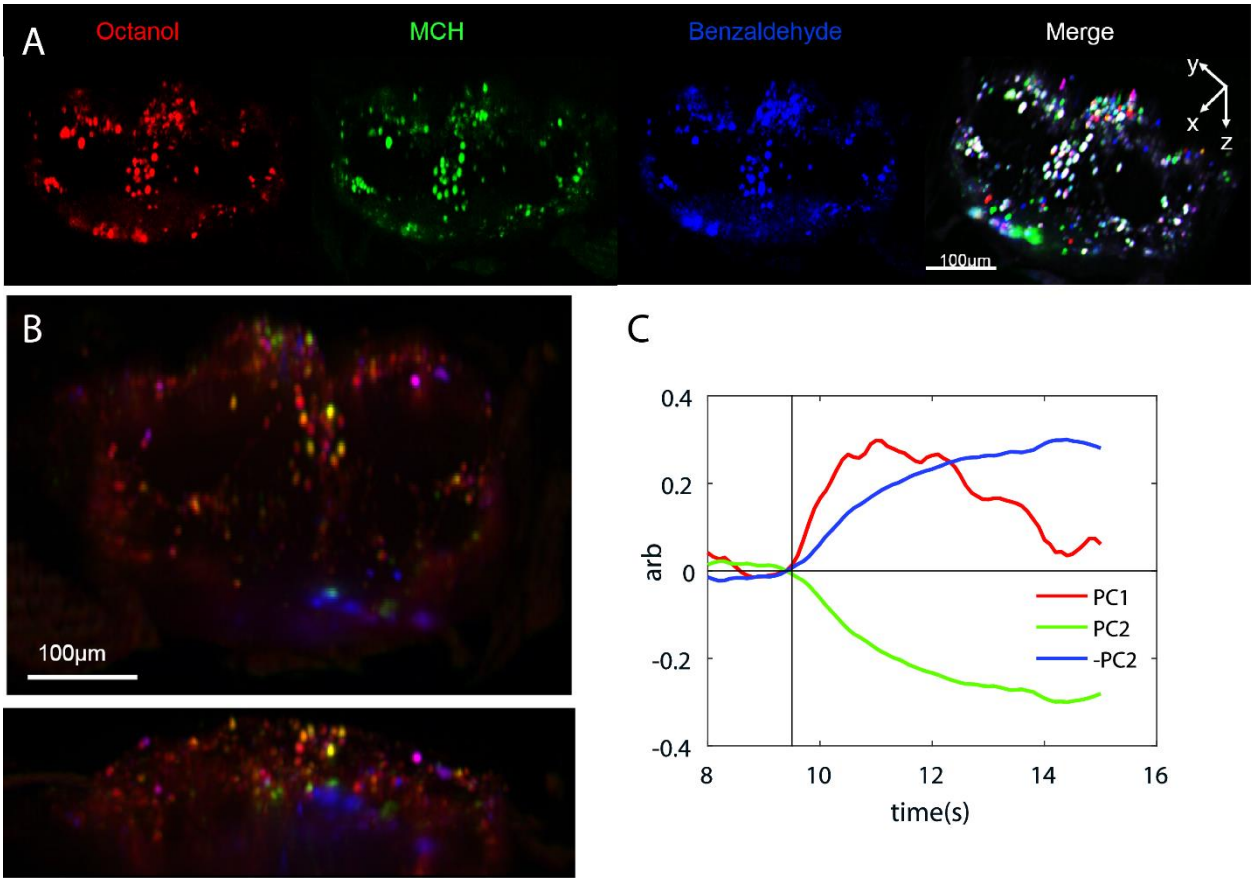

Figure 37 SCAPE imaging of Pan-neuronal Nuclaer Localized GCaMP and Analysis. Nuclear-localized GCaMP6s is expressed with the synaptobrevin driver (UAS-NLS-6s, nSyb-Gal4). (A) Three different odor stimulus was given during imaging, different/sparse cellular level response can be identified based on dF/F. Different odor stimulus is coded in RGB color. 3D rendering of the three odor driven map is also shown on the right side. (B) Maximum intensity projection of three response maps. (C) Single trial analysis for 10% octanol stimulus using PCA. Odor stim was delivered at 9.5s. PCA was applied for the whole 3D volume. The first positive component showed a cell-specific response (red), but the second component revealed both negative (green) and positive cell responses (blue). These three components are color coded and merged.

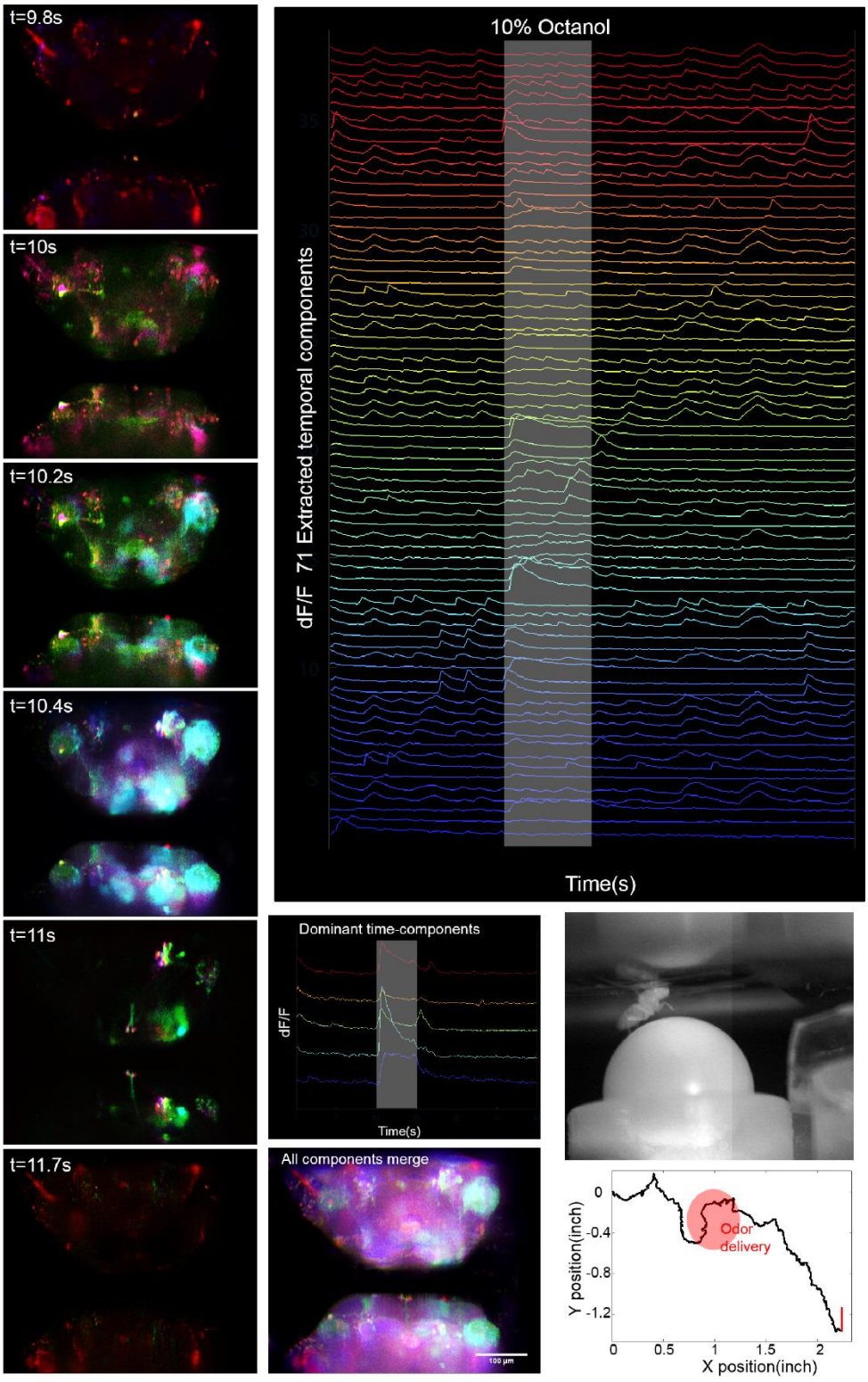

Figure 38 SCAPE Imaging Analysis with NNLS with Behavior Analysis. (A) Odor response onset progression was shown vertically. Colors represent spatial components from least squares non-negative fit to time-courses

shown to the right (5 dominant time-components plotted together below). 10% octanol was delivery from 10 to 15s. Images show progression of response starting in antennal lobes and its projection to lateral horn. And then the mushroom body, including the calyx and other output and inter neurons and then other sensory motor regions. (B) Most of the components can be recognized based on the know structure of fly anatomy. An all components merge projection in top and side view is shown below. (C) A high speed IR camera was used to record the fly walking and other behavior at 100Hz and the fly walking trajectory is reconstructed based on the Fly-Gym sensor readout. The odor stimulus period is circled in red, which can used to correlate the brain activity in the further analysis.

To analyze the regular cytosolic GCaMP volumetric data, I tried other spatial temporal unmixing method called non-negative least squares fit (NNLS) as shown in Figure 38 and Movie 12. After applying the algorithm based on the seeded temporal components, we were able to separate a lot of neuronal circuits-like spatial components which actually match the anatomical structure of the adult brain with different specific functional circuits. Here we also analyze the behavior observation data recorded with Fly-Gym. That information can be used for further analysis but is not presented here. Together with our collaborators, we are also testing other methods, like modified CNMF for further analysis and we are trying to create a standard analysis pipeline for this kind of pan-neuronal labelled whole brain GCaMP data.

5.5 Discussion

SCAPE microscopy is a single-objective light sheet imaging technique capable of acquiring a field of view as large as the *Drosophila* brain with cellular resolution at rates exceeding 10 Hz. The imaging geometry of the system permits increasingly complicated closed-loop experimental paradigms to simultaneously probe sensorimotor systems at the whole-brain and single-cell level. The value of large volumetric imaging of the fly brain has been shown in recent study using traditional light-sheet microscopy with limited access to the brain [65]. The near-whole-brain

imaging field of view and higher spatial resolution offered by SCAPE microscopy makes it possible to observe a complete neuronal functional circuit within a behavior animal. This unique ability also permits identification of known and unknown brain region or cellular level functional circuit together with structural characteristics offered by EM scan.

Furthermore, the ability to observe the global neuronal activity at cellular level of the behaving brain offers a unique opportunity to study brain state variables and hidden neuronal modulation circuits. Together with the genetic tool for *Drosophila*, we might be able to identify different neuronal circuit perform as internal state indicator and modulator. And with the development of sequencing technology, more specific neurotransmitter might be identified related to the global modulation.

While at the same time, large scale 3D data analysis is still a major challenge and bottleneck for the further study and application. For example, to monitor the longer time scale internal brain state change across the whole brain, one single trail data might exceed a few hundred GB, which makes it impossible to deal with the data without proper per-processing and dimensionality reduction. And better segmentation and spatial temporal unmixing algorithm is also needed to deal with densely labelled pan-neuronal GCaMP imaging data. We are currently collaborating with several different groups to create a better data analysis pipeline to make the process of information extraction from the large scale volumetric data easier and accessible by neuroscientists.

Chapter 6

EXPERIMENT DESIGN FOR THE OTHER MODEL ANIMIALS

In projects described in the previous chapters, I worked closely with our collaborators to use SCAPE microscopy as the main imaging method to understand the problem for larval and adult *Drosophila* and mouse olfactory epithelium. In addition to that, I also worked closely with other collaborators within and outside Columbia University, including imaging of the immobilized larval zebrafish brain, beating larval zebrafish heart, and immobilized and freely moving *C. elegans*. In these pilot experiments, I developed and optimized the sample preparation and work closely with Venkata Voleti in our lab to adjust and improve the SCAPE microscopy, adapted our imaging system in the model animals, and helped our collaborators to start using SCAPE independently.

6.1 Imaging the Neuronal System of Immobilized Larva Zebrafish

Larval zebrafish is one of the most popular model animals for in-vivo volumetric imaging with light-sheet microscopy in neuroscience and developmental research due to its optically transparent body and small size. It has been demonstrated that brain-wide neuronal calcium activity in zebrafish larvae could be captured using traditional light-sheet microscopy [58]. However, the volumetric speed of regular light-sheet microscopy offered for the whole brain imaging of zebrafish larvae is only at about 1-2 VPS, and the limited light-sheet excitation geometry makes it nontrivial to design the experiment. Taking advantage of the single objective lens layout and high-speed volumetric imaging capability of SCAPE, we were able to push this volumetric imaging speed up to 10VPS for whole brain imaging and more than 30 VPS when a smaller brain volume is sufficient for the research.

6.1.1 Whole Brain Imaging of Pan-Neuronal Labelled Larva Zebrafish

When imaging the zebrafish larva with SCAPE microscopy, we are able to use the traditional zebrafish sample preparation for two-photon or confocal structural imaging. The 3 to 7 days post fertilization zebrafish larva is positioned on a glass bottom petri dish or perfusion dish and then embedded with a small drop 1.5% low gelling point agarose made using E3 fish water. The fish is then positioned in the agarose properly as straight and horizontal. After the agarose is solidified, extra fish water is added in the dish to keep the fish alive. In this prep, we were able to keep the fish alive for days or we could take the fish out of the agarose mount after the imaging to imaging the at different developmental stage or for other research purpose. Also, the agarose around the tail of the zebrafish larva could be removed which allows the fish to perform swim attempts. Though in this case, extra motion artifact might be induced, taking advantage of the high

volumetric speed we could achieve, motion correction could be applied, or we could tolerance a few frame drops without missing the calcium dynamic too much. If paralysis of the fish is acceptable for the study, some neuromuscular decoupling drug could be used to eliminate all the motion artifact which simplify the post process by a lot.

In the past few years, we were collaborating with experts in this field to try optimizing our system for better whole brain imaging of zebrafish larvae, including Dr. David Schoppik, Dr. Misha Arhens, Dr. Ed Boyden and Dr. Michael Orger. With their help, we were able to image among the most popular pan-neuronal labelled calcium indicator for whole brain imaging, including membrane bound GCaMP6, nuclear localized GCaMP5G, GCaMP6 and somatic GCaMP6. With different genetic labelled calcium indictor, we were able to observe different neuronal activity and use the proper ones in different research project. For example, with the nuclear localized pan-neuronal label (Figure 39), we are able to easily isolate the neurons across the whole brain volumes and extract the calcium activity by simply selecting the ROI within the 3D volume, or using more sophisticated analysis methods like 3D-CNMF etc. When imaging the regular membrane bound GCaMP6f labelled fishes, we were able to see the dendritic and axonal projection of the neuron, and the neurons can also be easily identified by looking at the non-fluorescent nuclei at the center of each neuron as shown in Figure 40. In the meantime, during pilot experiments we had with zebrafish whole brain imaging, we were able to lower our laser power at the sample down to 100μW while 4-6 VPS could still be achieved. In this case, we could easily apply the vision stimulus even using the cellphone screen or mini projector, even though the excitation blue light is visible to the fish. The depth color coded sliding windows difference videos of both nuclear localized and cytosolic pan-neuronal GCaMP whole brain imaging are shown in Movie 13 and 14. Taking advantage of the single objective lens layout, we were able to design

more complex experiment with different kind of stimulus and behavior monitoring assets which is helpful to dissect the functional circuit better with whole brain imaging.

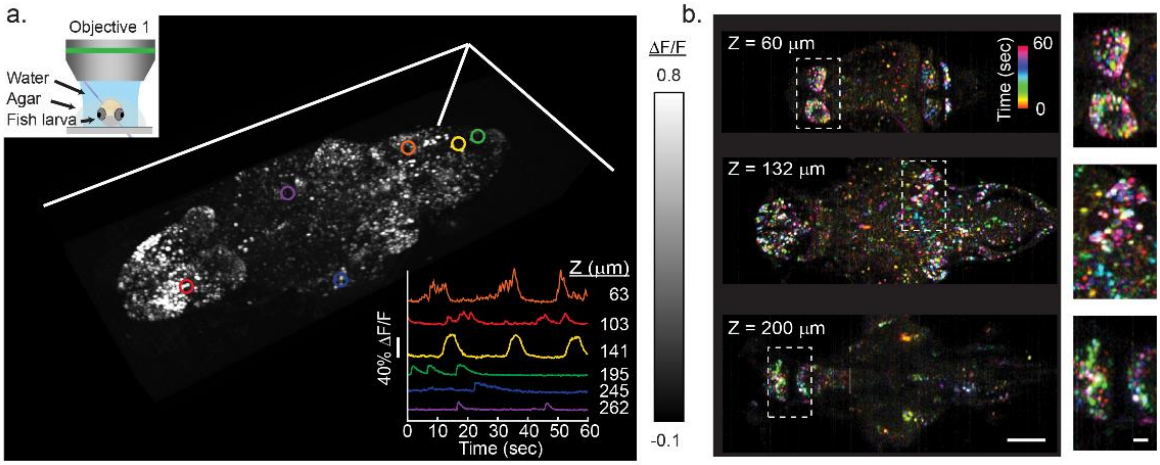

Figure 39 SCAPE imaging and Analysis of the whole brain of larval zebrafish with nuclear localized GCaMP. Data acquired at 6 VPS, with the FOV of 820x380x260 μm **a)** 3D rendering of maximum intensity projection taken over all 360 time points over a 1 minute run with spontenious activity. Time series extracted from 6 neurons drawn from locations within the brain at 6 depth planes within the fish. The schematic of the fish prep under the SCAPE objectives is shown in top left. **b)** Time-encoded color projection of 3 depth planes showing spontaneous activity over a range of brain regions. Insets show ~2x close ups of indicated regions. Scale bars are 100 μm and 20 μm.

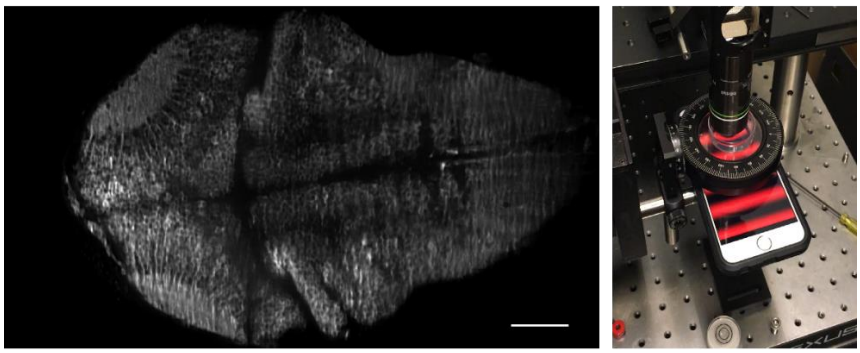

Figure 40 SCAPE Imaging of Membrane Bounded GCaMP, Single Plane Example. (Left) A single XY plane from a SCAPE image of a larval zebrafish expressing panneuronal membrane bounded GCaMP6f.. The nuclei in individual neurons can be clearly visualized at the center of each neuron. In this case, we can also see the activity in neuropil. (Right) Example of vision stimulus using a cellphone screen. Scale bar is 100 μm.

6.1.2 Imaging the Vestibular System of Larva Zebrafish

As mentioned in the Chapter 2, we are able to achieve a much higher volumetric speed by scanning through a smaller FOV. In some specific research field, there is not an urgent need to image through the entire brain and observe the neuronal activities of all the neurons, while getting a better spatial and temporal resolution is more important to resolve the functional dynamic of a specific pre-defined local neuronal circuit, for example the vestibular system in the larva zebrafish. Working closely with Dr. David Schoppik and his post-doctoral fellow Dr David Ehrlich, we were able to develop a new imaging method based on SCAPE microscopy, which enables us to image the vestibular circuit while the fish is sensing different vestibular stimulus.

To image the vestibular neuronal activities, we would like to image the fish in different body orientation and also let the fish be able to sense different acceleration. This could be achieved by tilting the whole microscope together with the fish [66]. In our case, we used a different approach which only moves the fish while keep the SCAPE microscope stationary. We mounted the fish on a galvo mirror embedded in agarose, while the tail was exposed by removing the agarose around it as shown in Figure 41. By moving the galvo mirror at different speed and angle during the imaging, we were able to capture the vestibular activity of the fish responding to the body positioning angle change and observe the swimming attempt at the same time as shown in Movie 15. Since the circuit we are interested in located at a smaller brain region, we are able to achieve a volumetric speed above 30, which allows us to resolve the transient response of the vestibular neurons. Or on the other hand, we could image a bigger FOV which covers the fish in different positioning angle within the 3D imaging field, so we able to imaging more different neuronal behavior by designing different galvo moving pattern and track the neurons which the 3D volume for the better functional characterization of the interested neurons. Or we could use a higher

magnification SCAPE system which offers a better spatial resolution and allows us to characterize the functional dynamic of the dendritic and axonal terminal in the vestibular system.

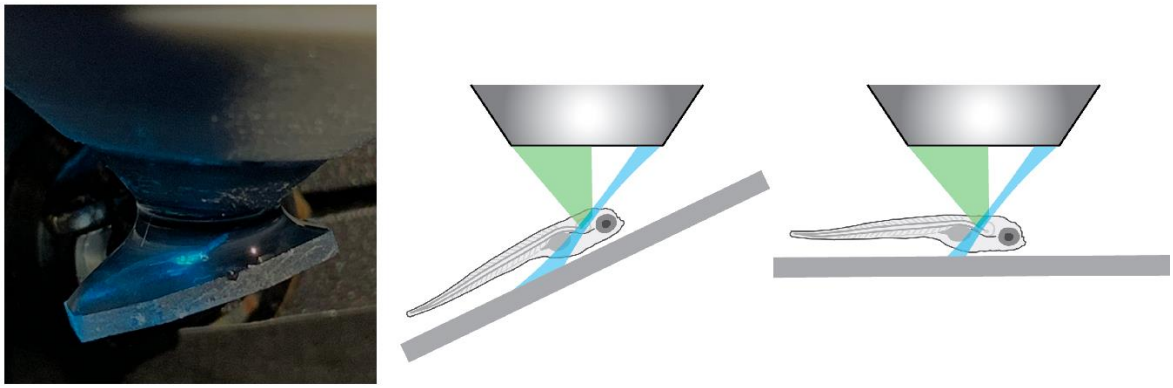

Figure 41 Zebrafish Larva Mounted on Galvo Mirror, Prep Photo and Schematic. Example of zabrafish-on-galvo prep and the schemeatic of SCAPE imaging when the fish is rotated to different body positioning angle.

Taking advantage of the single objective lens layout, we were also able to setup a projector for vision stimulus and a high-speed camera easily, which could be used to build a close-loop experiment asset by synchronizing the vision/vestibular stimulus and detect the swimming attempt in real-time, which helps understanding the multi-sensorimotor integration during the larval zebrafish development.

6.2 Imaging the Cardiac System of Immobilized Larva Zebrafish

Not only a great model animal for whole brain function imaging, larval zebrafish are also a well-known model for cardiac system research. Studies of the larval zebrafish heart provide insights into the way that the vertebrate heart develops, as well as the influence of genetic and environmental factors on structural and functional heart development. Multiple cardiac system disease models have been established and could be used for researchers to understand the

development of the heart defects and ultimately to the methods to detect and treat structural and conduction abnormalities from this genetic defect.

Today, light-sheet microscopy has been widely used to image the larval zebrafish heart [67], however, the high cardiac rhythm (2-3 beats. second), makes it also impossible to capture the whole 3D beating heart in real-time. A time-gated reconstruction method was used to reconstruct the beating behavior by imaging each plane separately for a longer sequence, then synchronized and reconstruct the volumetric imaging of the beating heart. However, this method is also quite limited, because the basic principle behind the reconstruction algorithm is the heart is beating in a fixed pattern, which is not true for genetic defected heart and also drug treated heart. Also, to capture the cardiac transduction within the heart, a higher temporal resolution is necessary.

Collaborating with Dr. Kimara Targoff, we were working to develop a new imaging method without using the time-gated reconstruction to acquire the real-time volumetric imaging of the beating larval zebrafish heart. Using the similar sample preparation as the brain imaging described previously, the fish is mounted in the 1.5% low gelling point agarose and submerged in the fish water and we image through the cover glass on the bottom. The fish was positioned in the agarose with the head pointing down with an angle, which varies with the developmental stage of the fish. By tiling the fish, we are able to have the heart horizontally positioned above the objective. The petri dish is also mounted on a two-axis rotation stage on top of the XYZ-translation stage. By rotating and tiling the sample, we are able to use the minimum amount of imaging depth to achieve the maximum camera frame rate and at the same time, scanning through the smallest FOV, which together help us achieve the highest volumetric speed with the resolution to resolve the different beating pattern between different genetic defeat during the development stage. When

imaging with both green and red fluorescent channel simultaneously, we were also able to visualize endothelial cells on the heart as well as the red blood cells as shown in Figure 42.

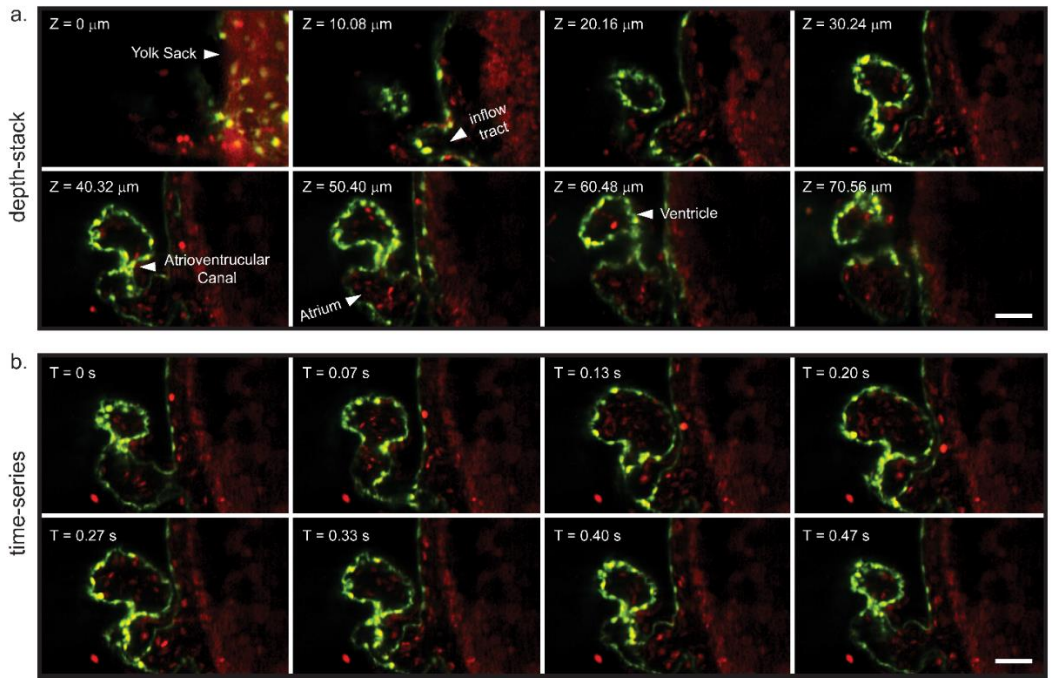

Figure 42 Dual-color imaging of beating zebrafish heart using SCAPE. (a) Depth stack of a single volume acquired in 0.066 sec (b) Time series of a single depth plane at 37 μm below the surface of the sample over the course of one heartbeat, starting with atrial contraction and ending with an atrial dilation. Scale bar – 50 μm Fish were expressing GFP within their endothelial cells and dsRed within the red blood cells (Tg(flk:GFP)(gata1:dsRed)). Images were acquired at 15 volumes/sec.

The need for better spatial temporal resolution pushes us to develop newer version of SCAPE microscopy. Our volumetric speed increase from 15VPS to 50VPS and now up to 300VPS with the latest system configuration and camera, which enables us and our collaborators to perform a lot of experiments which is not possible in the past including cell-to-cell calcium transduction in real time, 3D red blood cell tracking and the real time drug effect to the cardiac system. An example of 100 VPS SCAPE imaging of larval zebrafish heart with GFP labelled endothelial cells and dsRed in red blood cells is shown in Movie 16.

6.3 Imaging the Immobilized and Freely Moving C. Elegans

Previously we have demonstrated the ability of using SCAPE microscopy to image the freely moving *Drosophila* larva to study its proprioceptive system. Then we were wondering whether it is also possible to use SCAPE to image *C. elegans*, which has a much simpler nerve system and fully established connectome. Working with a few worm labs within and outside Columbia, we started to characterize the performance of imaging the *C. elegans* with SCAPE.

To characterize the resolution of the imaging performance with *C. elegans*, we would like to try with an immobilized prep or highly constrained prep where the worm can only move slowly. With the help from our collaborators, I developed a simple worm preparation procedure. Similar to the preparation we used to for the *Drosophila* larva arena, a ~100μm think 10% agarose pad is made on a glass slide and a small drop of water is add to the surface to moisturize it. Then the worm is positioned at the center of the agarose pad with a drop of 25mM tetramisole added to immobilize the worm for the imaging. A platinum wire is used to gently position the worm at the center of the agarose pad before the cover glass is positioned on top. The last step is to seal the cover glass with Valap wax (1:1:1 mix of lanolin, paraffin and Vaseline), so the agarose and the worm could be kept moist and ready for image for hours.

The preliminary results using the standard SCAPE microscopy showed that the resolution is not enough to resolve the cellular level details of *C. elegans*. Because the current system is optimized its resolution for *Drosophila*, fish and mouse imaging, with the cell dimeters between 3-10μm. However, the neurons in *C. elegans* are much smaller which is less than 1μm, also they are very densely pack together in some region. So, a further improvement in resolution is necessary to be able to image the cellular level neuronal activity of *C. elegans*.

During the past few years, our lab has continued developing the SCAPE system to push the resolution limit for the worm imaging, and we were able to achieve a good sub-micro resolution for the smaller FOV and slower volumetric speed as shown in Figure 43. Until recently, with the camera and objectives in the market, we were able to push the resolution to image the whole nerve system of *C. elegans*. We were able to image the immobilized worm at 6VPS for more than 10 minutes at its head region which contain more than 100 neurons which is part of its central nerve system. And the resolution allows us to properly extract the calcium dynamic of every single neuron.

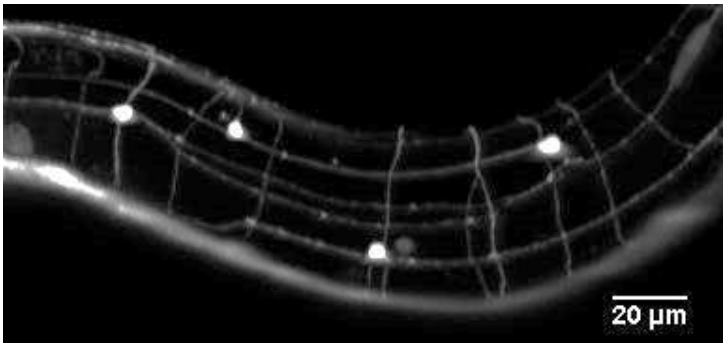

Figure 43 High Resolution Imaging of C. Elegan with Pan-neuronal Labelled GFP

After successfully imaging the immobilized worm, we turned to another more challenge task, which is to image the freely moving worm as we did for the *Drosophila* larva. I then made similar prep for worm, but it is much smaller and harder to manage. The worm is positioned within a small 300x500µm water-filled arena that was manually etched from a 60µm thick layer of 10% agarose pad on a glass slide. A glass cover glass is then placed on top of the arena and sealed with Valap wax. With this prep, we are able to image the worm moving inside the arena from above, since the thickness of the agarose pad is close to the worm itself, we could observe the worm crawling behavior but not swimming. We are able to achieve the volumetric speed of more than 25VPS across the whole arena while preserve the submicron resolution to resolve the cellular level

calcium activity in the freely behaving worm. Dual color image is also achieved by imaging the nuclear localized GCaMP and dsRed together, which helps the cell tracking and extract the ratiometric calcium activity to avoid the motion artifact in the green GCaMP channel as we discuss in Chapter 3. More results are available in our recent publication [68].

Chapter 7

DISCUSSION AND FUTURE WORK

This thesis demonstrates a range of different scientific applications using SCAPE microscopy and also shows how high-speed volumetric imaging offers a brand-new angle for biological research. The flexibility of the SCAPE system makes it possible to be used in a much wider field. However, there are still a lot improvement that could be done on SCAPE to improve both optical performance and ease to use, which includes integrating the optogenetics modules, a zoom module, extra color channels etc. Also, developing better data analysis pipelines and visualization methods would also be very helpful to allow more researcher to use SCAPE independently for their own research.

7.1 All-optical Functional Neuron Imaging and Manipulation

To understand neuronal circuits, we would always want to know how the neuron respond to specific input stimulus. However, in the real world, it is almost impossible to get a pure or fully controlled input to a specific neuronal circuit from the external stimulus during in vivo experiments. Because the brain is working as a complete network and there are also a lot of currently unknown internal states beyond the neurons we observe. In this case, when we design the experiment, we always want to eliminate external variables as much as possible to get a more reliable response

from our designed experiments. Today, with the fast developing optogenetic technology and a huge amount of work to develop different optogenetic sensors, we can precisely control neuronal activity by genetically expressing light-sensitive ion channels in specific channels which can reliably stimulate neuronal circuits with precise control. Also, with the development of the structural illumination with 2 photon lasers, we are now able to genetically and spatially control neuronal activity in 3D space.

The single objectives layout of SCAPE microscopy makes it much easier to integrate a patterned illumination module into the existing imaging system compared with other light-sheet approaches, since the only moving component in our system is the galvo mirror and the objectives and the sample are relatively stationary. By simply replacing the prism mirror before the objectives with a dichroic mirror, we would be able to install an optogenetic module into the pre-existing SCAPE system. By doing this, we could observe and manipulate a much larger number of neurons reliably. Extra stimulus and behavior asset could still be used when imaging together with the optogenetic tool, which allows us to design a much more sophisticated experiment to explore, understand and verify the neuronal circuit with light.

7.2 Data Processing Pipeline for Large-scale 5D Imaging Data

Big data handling is right now one of the most popular research topics for numerous different fields. The volumetric imaging data acquired with SCAPE microscopy is a good example of a realistic problem set for big data questions. We acquired hundreds of TB of data using SCAPE microscopy in the past few years, and we are even planning to record the activity of all the neurons in the small model animal in a much larger time scale. We need a better tool to help us extract the useful information out from this enormous volumetric imaging data we have. Also, the data

analysis requirement for high-speed volumetric functional data is different from the traditional 2D imaging data most people are familiar with due to the image size and 3D spatial constrain, a lot of well-established analysis method for 2D imaging also cannot applied to the 3D data. We will need a standard and automatic data processing pipeline for people to understand this form of data and then be able to work on these data by their own.

We have now worked with a lot of different model animals with different experiment conditions and research questions, and we do have a general idea of how to convert the data into a more accessible and easier-to-understand format for our collaborators based on their different problem sets and requirements. Extra work is needed to build a standard pipeline so we can spend more time thinking about how to understand the information than how to get the information. Meanwhile, it might also be worth investigating some GPU based computation algorithms to further speed up the processing, as the time we spent on just waiting the analysis to be done is also one of the biggest limiting factors for high-speed 3D data analysis.

7.3 SCAPE 3.0 and Further

The development of the SCAPE system should not stop as well, there is always a need to image smaller features with bigger fields of view at higher speed. Our lab is continuing to push the performance limits of SCAPE in these directions. As for now, in addition to standard configuration SCAPE microscopy for most of the current research, we also have hi-res SCAPE, motorized SCAPE, multiphoton SCAPE, meso-SCAPE and zoom SCAPE. There is also a lot more can be done based on the basic layout. How to make different types of system interchangeable? How to make it modular? How to minimize the size of the whole system? And more importantly, how to use SCAPE in more places and help us to understand how our brain work a bit more. SCAPE

microscopy shows a new vision for the neuroscience community and now it is time for us to use this fantastic tool to solve the scientific questions within the amazing three dimensional world.

References

1. Masse, N.Y., G.C. Turner, and G.S.X.E. Jefferis, *Olfactory Information Processing in Drosophila.* Current Biology, 2009. **19**(16): p. R700-R713.
2. Couto, A., M. Alenius, and B.J. Dickson, *Molecular, anatomical, and functional organization of the Drosophila olfactory system.* Curr Biol, 2005. **15**(17): p. 1535-47.
3. Kim, A.J., A.A. Lazar, and Y.B. Slutskiy, *System identification of Drosophila olfactory sensory neurons.* J Comput Neurosci, 2011. **30**(1): p. 143-61.
4. Aso, Y., et al., *The neuronal architecture of the mushroom body provides a logic for associative learning.* Elife, 2014. **3**: p. e04577.
5. Honegger, K.S., R.A. Campbell, and G.C. Turner, *Cellular-resolution population imaging reveals robust sparse coding in the Drosophila mushroom body.* J Neurosci, 2011. **31**(33): p. 11772-85.
6. Denk, W., J.H. Strickler, and W.W. Webb, *Two-photon laser scanning fluorescence microscopy.* Science, 1990. **248**(4951): p. 73-6.
7. Seelig, J.D. and V. Jayaraman, *Neural dynamics for landmark orientation and angular path integration.* Nature, 2015. **521**(7551): p. 186-91.
8. Keller, P.J., et al., *Fast, high-contrast imaging of animal development with scanned light sheet-based structured-illumination microscopy.* Nat Methods, 2010. **7**(8): p. 637-42.
9. Pitrone, P.G., et al., *OpenSPIM: an open-access light-sheet microscopy platform.* Nat Methods, 2013. **10**(7): p. 598-9.
10. Bouchard, M.B., et al., *Swept confocally-aligned planar excitation (SCAPE) microscopy for high speed volumetric imaging of behaving organisms.* Nat Photonics, 2015. **9**(2): p. 113-119.
11. Hillman, E.M., et al., *High-speed 3D imaging of cellular activity in the brain using axially-extended beams and light sheets.* Curr Opin Neurobiol, 2018. **50**: p. 190-200.
12. Vaadia, R.D., et al., *Characterization of Proprioceptive System Dynamics in Behaving Drosophila Larvae Using High-Speed Volumetric Microscopy.* Curr Biol, 2019. **29**(6): p. 935-944 e4.
13. Pulver, S.R., et al., *Imaging fictive locomotor patterns in larval Drosophila.* J Neurophysiol, 2015. **114**(5): p. 2564-77.
14. Ghannad-Rezaie, M., et al., *Microfluidic chips for in vivo imaging of cellular responses to neural injury in Drosophila larvae.* PLoS One, 2012. **7**(1): p. e29869.
15. Chhetri, R.K., et al., *Whole-animal functional and developmental imaging with isotropic spatial resolution.* Nat Methods, 2015. **12**(12): p. 1171-8.
16. Lemon, W.C., et al., *Whole-central nervous system functional imaging in larval Drosophila.* Nat Commun, 2015. **6**: p. 7924.

17. Royer, L.A., et al., *Adaptive light-sheet microscopy for long-term, high-resolution imaging in living organisms.* Nat Biotechnol, 2016. **34**(12): p. 1267-1278.

18. Finlayson, L.H. and O. Lowenstein, *The structure and function of abdominal stretch receptors in insects.* Proc R Soc Lond B Biol Sci, 1958. **148**(933): p. 433-49.

19. Grueber, W.B., L.Y. Jan, and Y.N. Jan, *Tiling of the Drosophila epidermis by multidendritic sensory neurons.* Development, 2002. **129**(12): p. 2867-78.

20. Merritt, D.J. and P.M. Whitington, *Central projections of sensory neurons in the Drosophila embryo correlate with sensory modality, soma position, and proneural gene function.* J Neurosci, 1995. **15**(3 Pt 1): p. 1755-67.

21. Grueber, W.B., et al., *Projections of Drosophila multidendritic neurons in the central nervous system: links with peripheral dendrite morphology.* Development, 2007. **134**(1): p. 55-64.

22. Heckscher, E.S., S.R. Lockery, and C.Q. Doe, *Characterization of Drosophila larval crawling at the level of organism, segment, and somatic body wall musculature.* J Neurosci, 2012. **32**(36): p. 12460-71.

23. Cheng, L.E., et al., *The role of the TRP channel NompC in Drosophila larval and adult locomotion.* Neuron, 2010. **67**(3): p. 373-80.

24. Suslak, T.J., et al., *Piezo Is Essential for Amiloride-Sensitive Stretch-Activated Mechanotransduction in Larval Drosophila Dorsal Bipolar Dendritic Sensory Neurons.* PLoS One, 2015. **10**(7): p. e0130969.

25. Hughes, C.L. and J.B. Thomas, *A sensory feedback circuit coordinates muscle activity in Drosophila.* Mol Cell Neurosci, 2007. **35**(2): p. 383-96.

26. Meltzer, S., et al., *Epidermis-Derived Semaphorin Promotes Dendrite Self-Avoidance by Regulating Dendrite-Substrate Adhesion in Drosophila Sensory Neurons.* Neuron, 2016. **89**(4): p. 741-55.

27. Kim, M.E., et al., *Integrins establish dendrite-substrate relationships that promote dendritic self-avoidance and patterning in drosophila sensory neurons.* Neuron, 2012. **73**(1): p. 79-91.

28. Schrader, S. and D.J. Merritt, *Dorsal longitudinal stretch receptor of Drosophila melanogaster larva - fine structure and maturation.* Arthropod Struct Dev, 2007. **36**(2): p. 157-69.

29. Corty, M.M., J. Tam, and W.B. Grueber, *Dendritic diversification through transcription factor-mediated suppression of alternative morphologies.* Development, 2016. **143**(8): p. 1351-62.

30. He, L., et al., *Direction Selectivity in Drosophila Proprioceptors Requires the Mechanosensory Channel Tmc.* Curr Biol, 2019. **29**(6): p. 945-956 e3.

31. Hallem, E.A. and J.R. Carlson, *Coding of odors by a receptor repertoire.* Cell, 2006. **125**(1): p. 143-60.

32. Buck, L. and R. Axel, *A Novel Multigene Family May Encode Odorant Receptors - a Molecular-Basis for Odor Recognition.* Cell, 1991. **65**(1): p. 175-187.

33. Young, J.M., et al., *Different evolutionary processes shaped the mouse and human olfactory receptor gene families.* Human Molecular Genetics, 2002. **11**(5): p. 535-546.

34. Zhang, X.M. and S. Firestein, *The olfactory receptor gene superfamily of the mouse.* Nature Neuroscience, 2002. **5**(2): p. 124-133.

35. Zhang, X.M., et al., *Odorant and vomeronasal receptor genes in two mouse genome assemblies.* Genomics, 2004. **83**(5): p. 802-811.

36. Niimura, Y., A. Matsui, and K. Touhara, *Extreme expansion of the olfactory receptor gene repertoire in African elephants and evolutionary dynamics of orthologous gene groups in 13 placental mammals.* Genome Research, 2014. **24**(9): p. 1485-1496.

37. Cain, W.S., *Odor Intensity - Mixtures and Masking.* Bulletin of the Psychonomic Society, 1974. **4**(Na4): p. 244-244.

38. Gillan, D.J., *Taste-Taste, Odor-Odor, and Taste-Odor Mixtures - Greater Suppression within Than between Modalities.* Perception & Psychophysics, 1983. **33**(2): p. 183-185.

39. Laing, D.G., et al., *Quality and Intensity of Binary Odor Mixtures.* Physiology & Behavior, 1984. **33**(2): p. 309-319.

40. Kay, L.M., T. Crk, and J. Thorngate, *A redefinition of odor mixture quality.* Behav Neurosci, 2005. **119**(3): p. 726-33.

41. Cashion, L., A. Livermore, and T. Hummel, *Odour suppression in binary mixtures.* Biological Psychology, 2006. **73**(3): p. 288-297.

42. Chaput, M.A., et al., *Interactions of odorants with olfactory receptors and receptor neurons match the perceptual dynamics observed for woody and fruity odorant mixtures.* Eur J Neurosci, 2012. **35**(4): p. 584-97.

43. Holekamp, T.F., D. Turaga, and T.E. Holy, *Fast three-dimensional fluorescence imaging of activity in neural populations by objective-coupled planar illumination microscopy.* Neuron, 2008. **57**(5): p. 661-72.

44. Turaga, D. and T.E. Holy, *Organization of vomeronasal sensory coding revealed by fast volumetric calcium imaging.* J Neurosci, 2012. **32**(5): p. 1612-21.

45. Araneda, R.C., A.D. Kini, and S. Firestein, *The molecular receptive range of an odorant receptor.* Nature Neuroscience, 2000. **3**(12): p. 1248-1255.

46. Oka, Y., et al., *Olfactory receptor antagonism between odorants.* Embo Journal, 2004. **23**(1): p. 120-126.

47. Cruz, G. and G. Lowe, *Neural coding of binary mixtures in a structurally related odorant pair.* Sci Rep, 2013. **3**: p. 1220.

48. Chess, A., et al., *Allelic inactivation regulates olfactory receptor gene expression.* Cell, 1994. **78**(5): p. 823-34.

49. Malnic, B., et al., *Combinatorial receptor codes for odors.* Cell, 1999. **96**(5): p. 713-723.

50. Ishii, T., et al., *Monoallelic expression of the odorant receptor gene and axonal projection of olfactory sensory neurones (vol 6, pg 71, 2001).* Genes to Cells, 2001. **6**(6): p. 573-573.

51. Clowney, E.J., et al., *Nuclear Aggregation of Olfactory Receptor Genes Governs Their Monogenic Expression.* Cell, 2012. **151**(4): p. 724-737.

52. Lyons, D.B., et al., *An epigenetic trap stabilizes singular olfactory receptor expression.* Cell, 2013. **154**(2): p. 325-36.

53. Pnevmatikakis, E.A. and A. Giovannucci, *NoRMCorre: An online algorithm for piecewise rigid motion correction of calcium imaging data.* J Neurosci Methods, 2017. **291**: p. 83-94.

54. Pnevmatikakis, E.A., et al., *Simultaneous Denoising, Deconvolution, and Demixing of Calcium Imaging Data.* Neuron, 2016. **89**(2): p. 285-99.

55. Pnevmatikakis, E.A., et al., *Simultaneous Denoising, Deconvolution, and Demixing of Calcium Imaging Data.* Neuron, 2016. **89**(2): p. 285-299.

56. Roland, B., et al., *Odor identity coding by distributed ensembles of neurons in the mouse olfactory cortex.* Elife, 2017. **6**.

57. Nguyen, J.P., et al., *Whole-brain calcium imaging with cellular resolution in freely behaving Caenorhabditis elegans.* Proc Natl Acad Sci U S A, 2016. **113**(8): p. E1074-81.

58. Ahrens, M.B., et al., *Whole-brain functional imaging at cellular resolution using light-sheet microscopy.* Nat Methods, 2013. **10**(5): p. 413-20.

59. Kato, S., et al., *Global brain dynamics embed the motor command sequence of Caenorhabditis elegans.* Cell, 2015. **163**(3): p. 656-69.

60. Clowney, E.J., et al., *Multimodal Chemosensory Circuits Controlling Male Courtship in Drosophila.* Neuron, 2015. **87**(5): p. 1036-49.

61. Robie, A.A., et al., *Mapping the Neural Substrates of Behavior.* Cell, 2017. **170**(2): p. 393-406 e28.

62. Aimon, S., et al., *Fast near-whole-brain imaging in adult Drosophila during responses to stimuli and behavior.* PLoS Biol, 2019. **17**(2): p. e2006732.

63. Grover, D., T. Katsuki, and R.J. Greenspan, *Flyception: imaging brain activity in freely walking fruit flies.* Nat Methods, 2016. **13**(7): p. 569-72.

64. Mann, K., C.L. Gallen, and T.R. Clandinin, *Whole-Brain Calcium Imaging Reveals an Intrinsic Functional Network in Drosophila.* Curr Biol, 2017. **27**(15): p. 2389-2396 e4.

65. Yang, Y., et al., *Chromatin remodeling inactivates activity genes and regulates neural coding.* Science, 2016. **353**(6296): p. 300-305.

66. Migault, G., et al., *Whole-Brain Calcium Imaging during Physiological Vestibular Stimulation in Larval Zebrafish.* Curr Biol, 2018. **28**(23): p. 3723-3735 e6.

67. Weber, M. and J. Huisken, *In vivo imaging of cardiac development and function in zebrafish using light sheet microscopy.* Swiss Med Wkly, 2015. **145**: p. w14227.

68. Voleti, V., et al., *Real-time volumetric microscopy of in-vivo dynamics and large-scale samples with SCAPE 2.0.* Nature Method, 2019. **In Revision**.

Appendix A: System Configuration and Part List

A.1 Imaging Acquisition Workstation

Parts	Model
CPU	2×Intel Xeon E5-2643 v3, 6 cores, 3.4GHz, 40×PCIe lanes
RAM	12×16GB DDR4-2133
Motherboard	Supermicro X10DRC-T4, onboard 10GbE, onboard 3108 raid controller with 2GB RAM
SSD	1×Samsung 852 Pro 512GB, 1×Intel DC P3500 2TB
HDD	8×Seagate Enterprise Capacity 6TB Hard Drive
Case	Supermicro SuperChassis CSE-745BTQ, redundant power supply
Graphic Card	Nvidia Quadro M4000

Table 4 System Specification of SCAPE Imaging Acquistion Workstation GEN. 2. The system specification used the new Xeon with high frequency which offered better computation performance for imaging processing. 192GB RAM is pre-configured for large data analysis. Non-raided PCIe based SSD was used for full speed data spooling with better stability and reliability. More HDD storage was configured for local storage. Professional graphic card is used for better 3D rendering capability. Server grade computer case was used with redundant power supply.

Parts	Model
CPU	2×Intel Gold 6128, 6 cores, 3.4GHz, 48×PCIe lanes
RAM	12×16GB DDR4-2666
Motherboard	Supermicro X11DPH-T, onboard 10GbE
SSD	1×Intel Pro 6000p 512GB, 1×Intel DC P4600 2TB, 4×Samsung 970 Pro 1TB
HDD	8×Seagate Enterprise Capacity 8TB Hard Drive
Raid Controller	Supermicro AOC-S3108L, 2GB onboard RAM, 8 ports HighPoint SSD7101A, 4 NVMe M.2 ports
Case	Supermicro SuperChassis CSE-745BTQ, redundant power supply
Graphic Card	Nvidia Quadro P2000

Table 5 System Specification of SCAPE Imaging Acquistion Workstation GEN. 2.5. This specification is moderate upgrade based on GEN. 2. Latest CPUs and motherboard were used which offer a better processing power and expandability. Faster SSD and bigger HDD were used which improved the disk performance and stability. Secondary NVMe Raid controller is configured for the increasing need for higher data throughput with the new high-speed camera.

A.2 Odor Delivery and Fly-Gym

A.2.1 Odor Delivery System Part List

Mass Flow Controller:

1x Aalborg GFCS-010007 Compact Gas Mass Flow Controller, 0-500 sccm, N2/Air, Aluminum Body

1x Aalborg GFCS-010481 Compact Gas Mass Flow Controller, 0-200 sccm, N2/Air, Aluminum Body

Solenoid Valve:

16x The Lee Company # LHDA1221515H, HDI-FMT-12V-INERT

6x Screw support

18x Mounting screw

Solenoid Valves Driving Board:

2x 8-way 12V driving board with 5V TTL control port, customized

Manifold:

2x The Lee Company # LFMX0510528B, LEE MANIFOLD-8X

Gas Sensor:

1x Carbon Monoxide & Flammable Gas Sensor MQ-9

1x Pololu Carrier for MQ Gas Sensors (Bare PCB Only)

PID:

1x Auroa Scientific 200B miniPID Dispersion Seneor

Controller:

1x Arduino Mega 2560

Power Supply:

1x AC/DC converter 12V 5V 100W

Accessories:

Tubing and connectors; odor bottle; wires for all the electric parts.

A.2.2 Fly-Gym Part List

Laser Sensor:

1x ADNS-9800 with driving circuit board and sensor lens

Controller:

1x Arduino Due

Flow Controller:

1x Needle valve

1x Air flow meter, 0-250ml/min

Ball Holder/Sensor Adaptor:

3D printed, custom designed, shown in Figure 46

Hollow Plastic Ball:

1x Hollow HDPE plastic precision balls, 6mm

A.3 CAD for Different Sample Head Plate

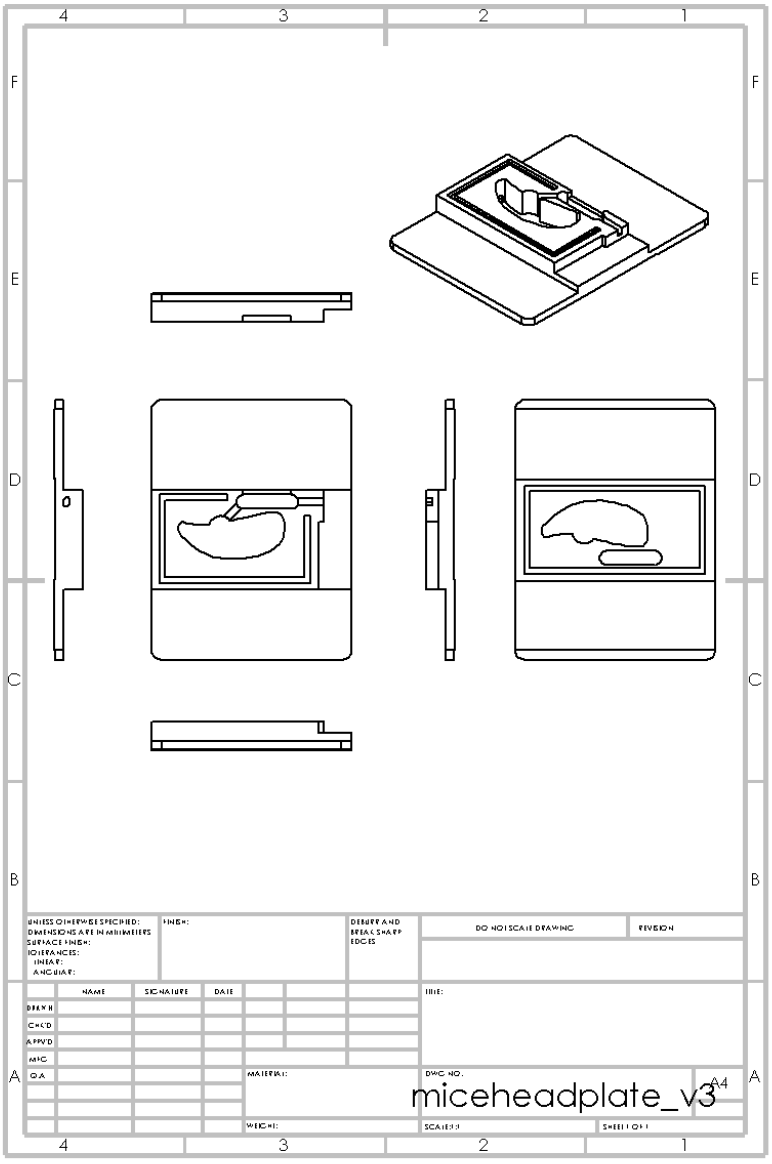

Figure 44 CAD drawing of mouse headplate.

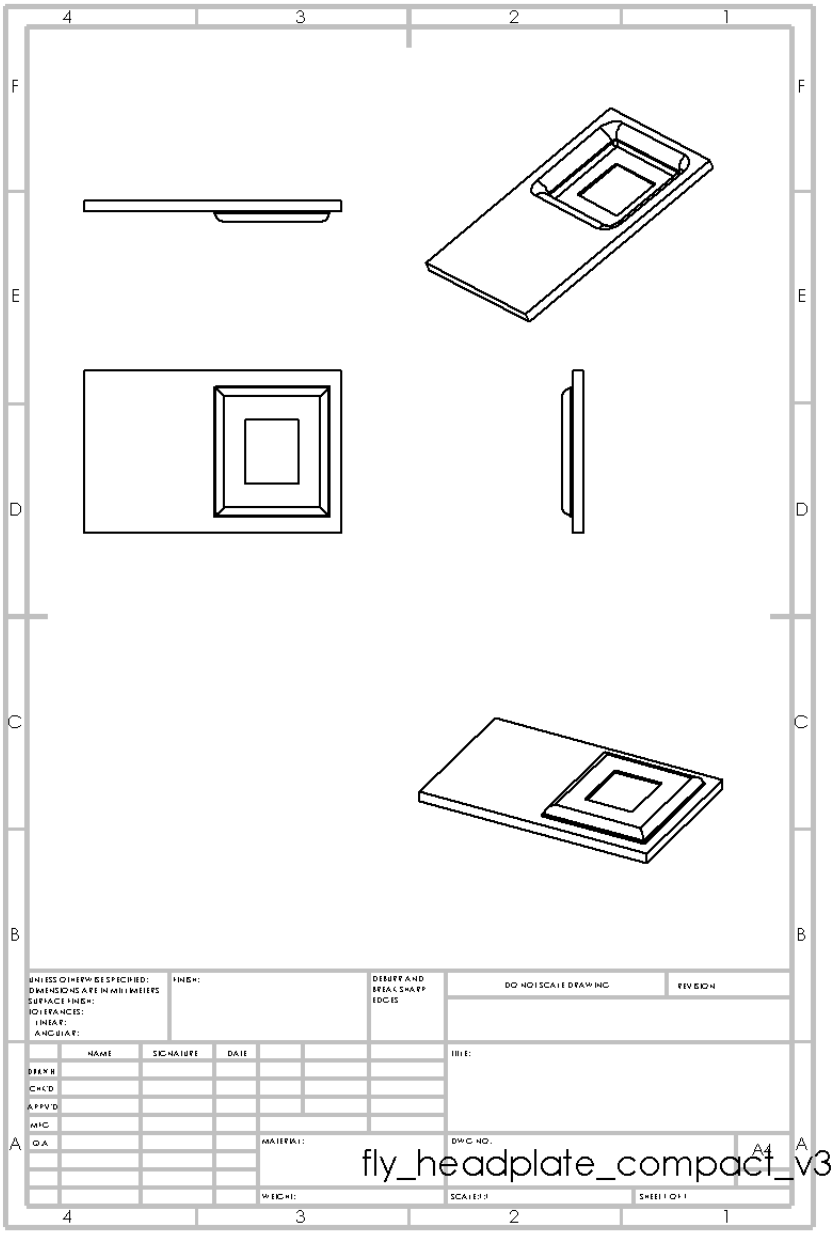

Figure 45 3D drawing of fly head plate.

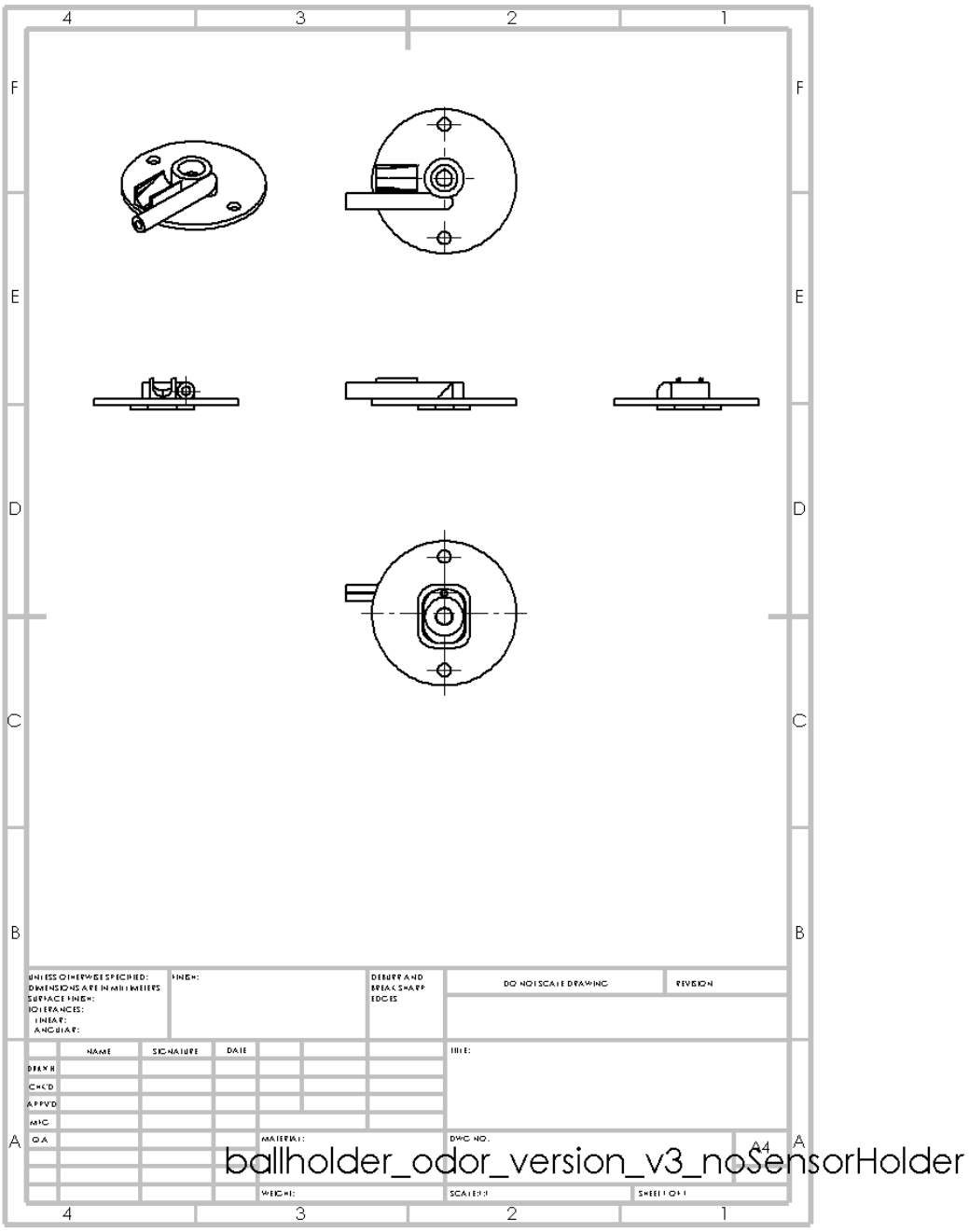

Figure 46 3D drawing of fly-gym ball holder with odor port housing.

Appendix B: Publications and presentations related to this thesis

B.1 Peer reviewed publications

1. Vaadia, R.†, **Li, W.**†, Voleti, V., Singhania, A., Hillman, E. M., & Grueber, W. B. (2019). Characterization of proprioceptive system dynamics in behaving *Drosophila* larvae using high-speed volumetric microscopy. *Current Biology (2019).*
2. Hillman, E. M., Voleti, V. & **Li, W.** (2019).Light-Sheet microscopy in neuroscience. *Annual Review of Neuroscience, Vol. 42, 295-313.*
3. Hillman, E. M., Voleti, V., Patel, K., **Li, W.**, Yu, H., Perez-Campos, C., ... & Galwaduge, P. T. (2018). High-speed 3D imaging of cellular activity in the brain using axially-extended beams and light sheets. *Current opinion in neurobiology*, 50, 190-200.
4. Nguyen, H. D., Ullmann, J. F. P., McLachlan, G. J., Voleti, V., **Li, W.**, Hillman, E. M. C., . . . Janke, A. L. (2017). Whole-volume clustering of time series data from zebrafish brain calcium images via mixture modeling. *Statistical Analysis and Data Mining: The ASA Data Science Journal*. doi:10.1002/sam.11366B.2

B.2 Manuscripts in preparation

1. Voleti, V., Patel, K. B.†, **Li, W.**†, Campos, P. C., Bharadwaj, S., Yu, H., Ford, C., Casper, M. J., Yan, R. W., Liang, W., Wen, C., Kotaro, K.,Targoff, K. & Hillman, E. M. C. (2019). Real-time volumetric microscopy of in-vivo dynamics and large-scale samples with SCAPE 2.0. (In Revision)
2. Xu, L.†, **Li, W.†**, Voleti, V., Hillman, E. M. C. & Firestein, S. (2019). Evidence for Widespread Inhibition in Peripheral Olfactory Coding. (Pending Submission)
3. **Li, W.**, Mishra, N., Schaffer, E. S., Voleti, V., Axel, R. & Hillman, E. M. C. (2019) Whole brain imaging for behaving adult *Drosophila* with cellular resolution using SCAPE microscopy. (In Preparation)

B.3 Conference presentations

1. Next-generation SCAPE microscopes for high-speed neuroimaging

   Hillman, E. M. C., **Li, W.**, Voleti, V., Patel, K. B, Yu, H., Campos, P. C. & Lee, G. S.

   40th International Conference of the IEEE Engineering in Medicine and Biology Society. **Conference Talk**.

   Honolulu, July 2018

2. Implementing and refining SCAPE for imaging small brains and neural populations

   Li, W., Voleti, V., Vaadia, R. Mishra, N., Xu, L.,Schaffer, E. S., Grueber, W. B., … Hillman, E. M. C.

   2018 The BRAIN Initiative Investigators Meeting. **Poster Presentation**.

   Washington D.C., May 2018

3. SCAPE Microscopy for Whole Brain Circuit Identification in Adult *Drosophila*

   Li, W., Mishra, N., Schaffer, E. S., Voleti, V., & Hillman, E. M. C.

   Janelia 2017 Conference: Emerging Tools for Acquisition and Interpretation of Whole-Brain Functional Data, **Poster Presentation**.

   Ashburn, Nov. 2017

4. SCAPE Microscopy for High Speed, 3D Whole-Brain Imaging in *Drosophila Melanogaster*

   Li, W., Voleti, V., Schaffer, E. S., Vaadia, R., Grueber, W. B., Mann, R. S. & Hillman, E. M. C.

   OSA Biomedical Optics, Optics and the Brain. **Conference Talk**.

   Fort Lauderdale, April 2016

5. Swept Confocally Aligned Planar Excitation (SCAPE) Microscopy for the Identification of Neural Circuits in Adult *Drosophila*

   Li, W., Mishra, N., Schaffer, E. S., Voleti, V., & Hillman, E. M. C.

   Society for Neuroscience Annual Meeting. **Poster Presentation**.

   San Diego, Nov. 2016

6. Swept Confocally Aligned Planar Excitation (SCAPE) Microscopy for Largescale Brain Imaging in Adult *Drosophila Melanogaster*.

   Li, W., Voleti, V., Schaffer, E. S., Mendes, C., Mishra, N., Mann, R. S., Hillman, E. M. C.

   Society for Neuroscience Annual Meeting. **Poster Presentation**.

   Chicago, Nov. 2015